NAVAL POSTGRADUATE SCHOOL

MONTEREY, CALIFORNIA

THESIS

THE EFFECTS OF BERING STRAIT FLOW MAGNITUDE ON THE WESTERN ARCTIC OCEAN AND SEA ICE

by

Casey J. Burgener

December 2023

Thesis Advisor: Jaclyn L. Kinney
Second Reader: Younjoo Lee

THIS PAGE INTENTIONALLY LEFT BLANK

REPORT DOCUMENTATION PAGE	*Form Approved OMB No. 0704-0188*

Public reporting burden for this collection of information is estimated to average 1 hour per response, including the time for reviewing instruction, searching existing data sources, gathering and maintaining the data needed, and completing and reviewing the collection of information. Send comments regarding this burden estimate or any other aspect of this collection of information, including suggestions for reducing this burden, to Washington headquarters Services, Directorate for Information Operations and Reports, 1215 Jefferson Davis Highway, Suite 1204, Arlington, VA 22202-4302, and to the Office of Management and Budget, Paperwork Reduction Project (0704-0188) Washington, DC, 20503.

1. AGENCY USE ONLY *(Leave blank)*	**2. REPORT DATE** December 2023	**3. REPORT TYPE AND DATES COVERED** Master's thesis

4. TITLE AND SUBTITLE
THE EFFECTS OF BERING STRAIT FLOW MAGNITUDE ON THE WESTERN ARCTIC OCEAN AND SEA ICE

5. FUNDING NUMBERS

6. AUTHOR(S) Casey J. Burgener

7. PERFORMING ORGANIZATION NAME(S) AND ADDRESS(ES)
Naval Postgraduate School
Monterey, CA 93943-5000

8. PERFORMING ORGANIZATION REPORT NUMBER

9. SPONSORING / MONITORING AGENCY NAME(S) AND ADDRESS(ES)
N/A

10. SPONSORING / MONITORING AGENCY REPORT NUMBER

11. SUPPLEMENTARY NOTES The views expressed in this thesis are those of the author and do not reflect the official policy or position of the Department of Defense or the U.S. Government.

12a. DISTRIBUTION / AVAILABILITY STATEMENT
Approved for public release. Distribution is unlimited.

12b. DISTRIBUTION CODE
A

13. ABSTRACT (maximum 200 words)

This thesis unveils the nuanced influence of Bering Strait flow on Arctic sea ice and ocean properties, challenging initial assumptions. In the western Arctic, while varying Bering Strait flow magnitudes impact sea ice extent, the degree of influence is more moderate than anticipated, with complex interactions involving dynamic and thermodynamic processes. Ocean heat convergence, a crucial factor in ice-melt processes, demonstrates less substantial effects than previously recognized. Unexpected patterns in turbulent heat flux and ice melt dynamics challenge assumptions about the relationship between Bering Strait flow and sea ice retreat. Pan-Arctic effects from Bering Strait flow reveal minimal impact on sea ice extent; however, the pivotal role of ocean heat transport emerges, reshaping understanding of Arctic climate dynamics. The study's implications extend globally, urging proactive measures for climate adaptation and conservation. As the Arctic undergoes rapid transformation, this research serves as a clarion call for continued exploration and collaborative efforts to comprehend and protect this vital region.

14. SUBJECT TERMS Bering Strait, flow variation, Arctic Ocean, ocean heat transport, heat convergence, Chukchi Sea, sea ice	**15. NUMBER OF PAGES** 115
	16. PRICE CODE

17. SECURITY CLASSIFICATION OF REPORT	**18. SECURITY CLASSIFICATION OF THIS PAGE**	**19. SECURITY CLASSIFICATION OF ABSTRACT**	**20. LIMITATION OF ABSTRACT**
Unclassified	Unclassified	Unclassified	UU

NSN 7540-01-280-5500

Standard Form 298 (Rev. 2-89)
Prescribed by ANSI Std. 239-18

THIS PAGE INTENTIONALLY LEFT BLANK

Approved for public release. Distribution is unlimited.

THE EFFECTS OF BERING STRAIT FLOW MAGNITUDE ON THE WESTERN ARCTIC OCEAN AND SEA ICE

Casey J. Burgener
Lieutenant Commander, United States Navy
BS, University of Colorado, 2007

Submitted in partial fulfillment of the
requirements for the degree of

MASTER OF SCIENCE IN METEOROLOGY AND PHYSICAL OCEANOGRAPHY

from the

NAVAL POSTGRADUATE SCHOOL
December 2023

Approved by: Jaclyn L. Kinney
Advisor

Younjoo Lee
Second Reader

Peter C. Chu
Chair, Department of Oceanography

THIS PAGE INTENTIONALLY LEFT BLANK

ABSTRACT

This thesis unveils the nuanced influence of Bering Strait flow on Arctic sea ice and ocean properties, challenging initial assumptions. In the western Arctic, while varying Bering Strait flow magnitudes impact sea ice extent, the degree of influence is more moderate than anticipated, with complex interactions involving dynamic and thermodynamic processes. Ocean heat convergence, a crucial factor in ice-melt processes, demonstrates less substantial effects than previously recognized. Unexpected patterns in turbulent heat flux and ice melt dynamics challenge assumptions about the relationship between Bering Strait flow and sea ice retreat. Pan-Arctic effects from Bering Strait flow reveal minimal impact on sea ice extent; however, the pivotal role of ocean heat transport emerges, reshaping understanding of Arctic climate dynamics. The study's implications extend globally, urging proactive measures for climate adaptation and conservation. As the Arctic undergoes rapid transformation, this research serves as a clarion call for continued exploration and collaborative efforts to comprehend and protect this vital region.

THIS PAGE INTENTIONALLY LEFT BLANK

TABLE OF CONTENTS

LIST OF FIGURES

THIS PAGE INTENTIONALLY LEFT BLANK

LIST OF TABLES

THIS PAGE INTENTIONALLY LEFT BLANK

LIST OF ACRONYMS AND ABBREVIATIONS

CESM	Community Earth System Model
CICE	Community Ice Model
CNO	Chief of Naval Operations
DOD	Department of Defense
ECMWF	European Centre for Medium-Range Weather Forecasts
EEZ	Exclusive Economic Zone
ERA5	ECMWF Reanalysis Fifth Generation
FWC	Freshwater Content
GEBCO	General Bathymetric Chart of the Oceans
IBCAO	International Bathymetric Chart of the Arctic Ocean
LANL	Los Alamos National Laboratory
NSIDC	National Snow and Ice Data Center
OHC	Ocean Heat Content
OHT	Ocean Heat Transport
PIOMAS	Pan-Arctic Ice Ocean Modeling and Assimilation System
POP	LANL Parallel Ocean Program
RASM	Regional Arctic System Model
RVIC	Routing Variable Infiltration Capacity
TED	Thickness and Enthalpy Distribution
TW	Terawatts
SLP	Sea Level Pressure
VIC	Variable Infiltration Capacity
WRF	Weather Research and Forecasting

THIS PAGE INTENTIONALLY LEFT BLANK

ACKNOWLEDGMENTS

Completion of this thesis would not have been possible without help and counsel from many people.

To Dr. Jaclyn Clement Kinney: thank you for your countless hours of guidance, assistance, and encouragement as my advisor.

To Dr. Younjoo Lee: thank you for your invaluable help with programming and in-depth lessons on the Arctic region.

To Dr. Wieslaw Maslowski: thank you for your sharp insights and challenging us all to be better oceanographers.

Additional thanks are owed to Dr. Robert Osinski and Dr. Tony Craig for their support in various phases of this work.

Most important, to my wife Natalie and our three children: thank you for your unending love and support.

THIS PAGE INTENTIONALLY LEFT BLANK

I. INTRODUCTION

A. BACKGROUND ON THE BERING STRAIT

The Arctic, a remote and enigmatic realm encircling the Earth's northernmost pole, is a crucible of environmental extremes and complexity. At its heart lies the Arctic Ocean, a polar expanse that epitomizes the confluence of grandeur and vulnerability (Figure 1). Here, ice reigns supreme, and vast frozen landscapes are perpetually in motion. The Arctic's atmospheric conditions, defined by extreme cold and a strong seasonal cycle of light, sculpt a domain unlike any other on our planet. Amidst this frigid environment, an astonishing array of unique features thrives, from resilient flora and fauna to Indigenous cultures intrinsically connected to their ice-bound homelands. This region, known recently for its susceptibility to a warming climate change, embodies an urgent call for further exploration and understanding. It serves as both a sentinel and an amplifier of global environmental shifts. This thesis will focus on the flow through the Bering Strait and how it impacts the atmosphere, ocean properties, and sea ice of the Chukchi, Beaufort, and East Siberian seas. The sensitivity of this region to varying flow through Bering Strait will be examined using results from multiple coupled simulations of the Regional Arctic System Model (RASM).

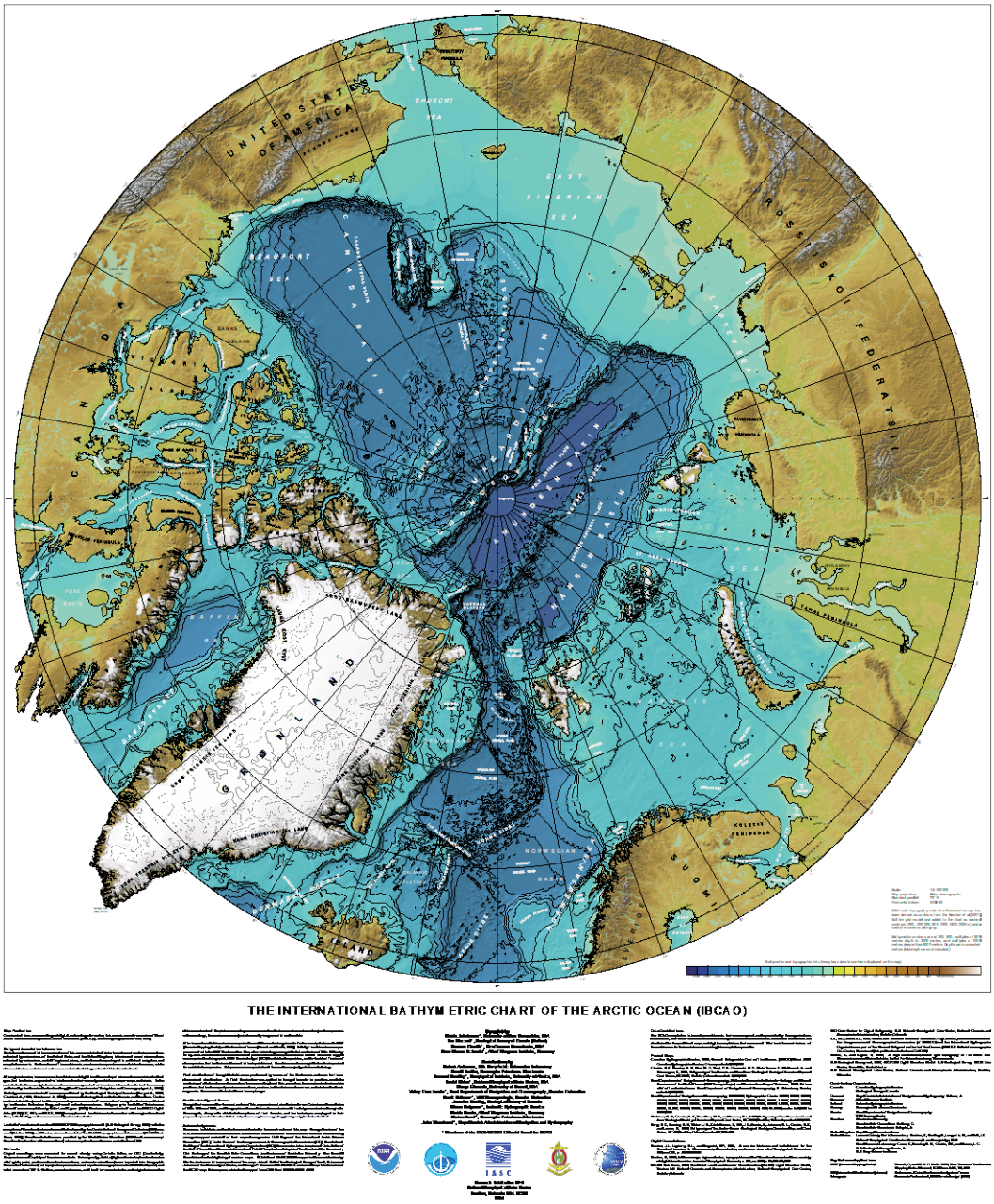

Figure 1 shows Version 4.2 of the International Bathymetric Chart of the Arctic Ocean (IBCAO), developed by an international group of ocean mapping experts. Source: Jakobsson et al. (2020).

Figure 1. Arctic Ocean Bathymetric Chart

1. Arctic Climate and Sea Ice

Characterized by its extreme cold temperatures and unique geographical features, the Arctic region shapes global climate patterns. One of the defining features of the Arctic environment is its extensive sea ice cover, which undergoes significant fluctuations in response to climatic changes.

Historically, Arctic sea ice has acted as a thermal insulator, preventing heat exchange between the underlying ocean and the atmosphere. However, recent decades have witnessed a marked decline in sea ice extent, accompanied by reductions in ice thickness and area (Serreze et al. 2007). This reduction in sea ice cover is reshaping the Arctic's thermal regime and amplifying regional temperature changes, bringing far-reaching consequences for local and global climate systems.

Oceanographic research shows a strong correlation between declining sea ice cover and increased surface air temperatures in the region (Hayden and O'Neill. 2023). The diminished albedo associated with reduced sea ice coverage contributes to enhanced heat absorption by the ocean, thereby accelerating the Arctic's warming trend. This warming trend not only indicates changing local climate conditions but also holds implications for the global climate system, including potential shifts in atmospheric circulation patterns (Blackport and Screen 2020).

The interconnectedness of Arctic climate and sea ice dynamics, focusing on their role in driving regional and global climatic changes, helps explain how the decline in Arctic sea ice has significant ramifications for temperature regimes, ocean-atmosphere interactions, and broader climate dynamics. These insights are particularly relevant when considering the variability of Bering Strait flow and its potential effects on sea ice conditions in the western Arctic. In the subsequent sections, we delve into the specific characteristics of the Bering Strait and its implications for ocean dynamics in the studied regions.

2. The Bering Strait

The Bering Strait, situated between the easternmost point of Russia's Chukchi Peninsula and the westernmost point of Alaska's Seward Peninsula, is a narrow (~85 km

wide at its narrowest point) and shallow (up to ~50 m) water passage that connects the Bering Sea to the Chukchi Sea.

It is the only oceanic portal for exchanging water, heat, salt, nutrients, and other constituents between the Pacific and Arctic oceans. As the critical link between the two oceans, it facilitates the exchange of water masses that shape the hydrography and climate of both regions and plays a pivotal role in shaping the hydrography of the Arctic basin. These properties collectively form a cornerstone in comprehending the hydrographic context that underpins observed changes in the Chukchi, Beaufort, and East Siberian seas, setting the stage for the subsequent exploration of their implications on ocean and ice dynamics in the Arctic region.

3. Bering Strait Hydrography

Atmospheric, oceanographic, and hydrological factors influence the intricate hydrography of the Bering Strait, shaping the volume, composition, and freshwater content of the water masses flowing through this pivotal gateway.

Meteorological forces, such as wind patterns, air temperature, and atmospheric pressure systems, play a fundamental role in driving the flow of water masses through the Bering Strait. These factors directly influence the volume and velocity of the flow, affecting the distribution of heat and salinity in the region. For example, the relatively warmer and fresher Pacific waters passing through the Bering Strait will impact the atmospheric and oceanic conditions in the Arctic environment, including sea ice melt, ocean-atmosphere heat exchange, temperature distribution, and biological productivity (Clement Kinney et al. 2014).

Regional current systems further modulate the flow dynamics. The Alaskan Coastal Current, Anadyr Current, and Bering Shelf Water interact with the flow through the strait and further shape its characteristics (Clement Kinney et al. 2014). The hydrographic characteristics of the Bering Strait, including its flow patterns and properties of water masses, are instrumental in shaping the regional climate, sea ice dynamics, and thermodynamics.

The water masses transported through the Bering Strait contain an essential component of freshwater, contributing to the Arctic Ocean's unique stratification. The influx of cold and relatively fresh Pacific waters through the Bering Strait contributes to maintaining the distinct layers of the Arctic Ocean, particularly the halocline and pycnocline. The halocline, characterized by a rapid increase in salinity with depth, and the pycnocline, marked by a sharp density gradient, serve as critical features in the Arctic's water column. These layers help isolate the relatively fresh surface waters from the saltier, denser waters below, influencing temperature distribution and the availability of nutrients and light in the upper ocean. This stratification is essential for the Arctic's ecosystem, as it creates distinct habitats for various marine species and influences primary productivity.

Continental runoff from Siberian rivers and other rivers also contributes significantly to the freshwater content of the upper Arctic Ocean (Aagaard and Coachman 1975). These freshwater inputs carry a complex mixture of nutrients, sediments, and organic material, further influencing the composition and properties of the Arctic's surface waters. The interactions between riverine inputs and the inflow of Pacific waters are particularly relevant in the nearshore regions of the Arctic, where they affect biological productivity and impact sea ice dynamics.

The interplay of meteorological, oceanographic, and hydrological factors within the Bering Strait is instrumental in shaping the composition and characteristics of the water masses entering the Arctic Ocean. This complex interrelationship extends beyond the strait, influencing the broader Arctic climate system, ecosystem dynamics, and global climate patterns. Understanding these intricate dynamics is paramount for comprehending the Arctic's response to a changing climate and its role as a critical component in the Earth's climate system.

4. Bering Strait Flow Magnitude

The flow through the Bering Strait is not constant but somewhat varies on daily, seasonal, interannual, and decadal time scales. While many factors are at play, the primary drivers of Bering Strait flow are the large-scale sea level pressure (SLP) gradient

and local wind forcing (Woodgate 2018). The varying intensities of the Aleutian Low and Beaufort High cause changes in the strength of the SLP gradient, which appears to be the primary driver of volumetric flow through the strait, with modification caused by the local wind field (Woodgate 2018). Additionally, flow can be influenced by large-scale climate patterns such as the Pacific Decadal Oscillation (PDO) and the Arctic Oscillation (AO), which affect the pressure systems and wind patterns in the region.

Woodgate et al. (2012) comprehensively analyzed Bering Strait oceanic fluxes from the Pacific to the Arctic from 2001 to 2011. Their study provided insights into the temporal trends of these fluxes and their impacts on the Arctic Ocean water column. They observed increased oceanic fluxes through the Bering Strait during the study period. These observations underline the dynamic nature of Bering Strait flow and its sensitivity to regional and larger-scale climatic drivers. Their findings emphasize the Bering Strait's responsiveness to climate fluctuations and hint at its influence on the broader Arctic Ocean environment. However, an assumption regarding flow homogeneity may introduce uncertainty into these observational estimations (laterally and vertically), which has been contradicted by subsequent numerical modeling work (Clement Kinney et al. 2014). In addition, assumptions made regarding the flow of the Alaska Coastal Current, may cause an underestimation of the volume and heat fluxes (Woodgate et al. 2005).

5. Interactions between Oceanic Flow and Sea Ice

A primary goal of this thesis is to discover the effects of Bering Strait flow on sea ice. To do this, it is vital to understand the intricate interactions between oceanic flow and sea ice dynamics. Knowing these interactions and the methods used to study them is crucial for deciphering the mechanisms that govern changes in sea ice extent, area, and thickness.

Laying the foundation for this understanding is a comprehensive modeling approach developed by Zhang and Rothrock (2003) to simulate global sea ice dynamics. Using a 12-category thickness and enthalpy distribution (TED) for ice, their model was coupled with the Parallel Ocean Program (POP) to provide insights into the complexities of sea ice behavior, particularly its growth and melt processes. By accounting for

variations in sea ice thickness and the enthalpy content of ice, their model highlighted the importance of accurate parameterization in capturing the interplay between sea ice and oceanic heat fluxes (Zhang and Rothrock 2003).

Using the numerical model in conjunction with satellite observations, scientists were able to contribute to the understanding of sea ice thinning trends in the Arctic. An analysis spanning several decades indicated a rapid decline in sea ice thickness (Lindsay and Zhang 2005). It revealed the interconnected roles of ocean heat transport and atmospheric circulation patterns in driving these observed changes.

Furthermore, combining submarine records and satellite observations provided additional insights into the temporal trends of Arctic sea ice thickness. A comprehensive assessment of the decline in sea ice thickness over several decades demonstrated the critical role of thermodynamic processes and dynamic interactions with ocean currents in shaping sea ice thickness distribution (Kwok and Rothrock 2009).

Lastly, analysis of climate model projections from the Coupled Model Intercomparison Phase 5 (CMIP5) ensemble attributed multiple air, ice, and ocean processes working together to support rapid ice melt in the Arctic (Notz and Community 2020). These combined processes aid the amplifying effects of Arctic feedback mechanisms, which are partly driven by the diminishing sea ice cover and the associated decline in albedo. This analysis shows the interconnectedness of dynamic mechanisms and emphasizes the potential for a sea ice-free summer Arctic within a few decades (Wang and Overland 2012).

The synthesis of scientific findings up to this point provides a robust foundation for comprehending the complexities of Bering Strait flow variability and its far-reaching impacts on sea ice extent, concentration, and thickness. Coupled modeling techniques, satellite and submarine observations, and Arctic feedback mechanisms underscore the importance of considering local and remote factors to examine sea ice dynamics. The findings from these studies provide hints into how ocean heat transport from Bering Strait flow may be affecting ice melt and growth. As we delve into the specific mechanisms and consequences of Bering Strait flow variability in the subsequent sections, these studies

will serve as pivotal references to contextualize the observed changes in the studied Arctic seas.

B. IMPORTANCE OF BERING STRAIT FLOW

1. Changes in Throughflow Properties

In recent years, observations have indicated increased volumetric flow from the Pacific to the Arctic Ocean through the Bering Strait. This more substantial flow is believed to be linked to changing climate patterns, including rising temperatures and altered atmospheric circulation (Woodgate 2018). The inflowing Pacific water has been observed to be warmer in recent years (Woodgate and Peralta-Ferriz 2021), which could contribute to the overall warming of the Arctic Ocean. In addition, this warmer water has the potential to influence sea ice melt, impacting both the extent and thickness of Arctic sea ice.

2. Significance in the Arctic Context

Observations and modeling studies reveal that shifts in atmospheric circulation patterns, such as the Arctic and Pacific Decadal oscillations, can substantially influence the transport of water masses through the Bering Strait (Woodgate 2018). The Bering Strait's role as a conduit between the Pacific and Arctic oceans is of immense significance in the broader context of the Arctic. These atmospheric-driven changes in Bering Strait flow contribute to the overall warming and cooling of the Arctic, affecting regional climate patterns, ice cover, and ecosystems. Additionally, altered Bering Strait flow can affect global sea level rise by redistributing water masses between the Pacific and Arctic oceans and influencing the distribution of marine species, migration patterns, and primary production in the Arctic Ocean, with cascading effects on the entire Arctic food web (Grebmeier 2012).

3. Relevant Research

Numerous scientific studies and research efforts have been dedicated to understanding the Bering Strait's flow dynamics and consequences. Moorings, buoys, and autonomous underwater vehicles measure water properties, currents, and temperature

in the Bering Strait and provide valuable data for understanding the flow characteristics. Numerical models have been employed to simulate the Bering Strait's flow and its impact on the Arctic, helping researchers explore how changes in flow may influence the Arctic climate. Lastly, historical records, including ship observations and satellite data, have been analyzed to reconstruct past flow conditions and assess long-term trends, providing context for recent changes in Bering Strait flow and Arctic sea ice.

The Bering Strait is a critical component of the Arctic's hydrographic system, bridging the Pacific and Arctic oceans. Changes in its flow properties have profound implications for the Arctic environment, making it a focal point for scientific research and a critical factor in the broader discussions on Arctic climate change and sustainability.

4. Navy Relevance

In addition to scientific research, understanding Bering Strait flow is crucial for resource management, navigation, and policy decisions in the Arctic region, where economic activities are increasing due to declining sea ice.

The Arctic region has garnered increasing attention due to its strategic significance in global security and defense considerations. The White House National Strategy for the Arctic, the Department of Defense (DOD) National Defense Strategy, and the Chief of Naval Operations (CNO) Navigation Plan all recognize and discuss the region's importance. The Bering Strait is a critical maritime gateway with implications for national security and DOD strategies. Notably, the Bering Strait contains the Diomede Islands, which are separated by only 3.8 km. Big Diomede Island belongs to Russia, and Little Diomede Island to the United States. As the Arctic continues to open, each country's Exclusive Economic Zone (EEZ) boundaries and claims could become tumultuous.

The interactions between Bering Strait flow and sea ice directly affect defense operations, particularly in the Arctic. The changing sea ice dynamics influence maritime access, the potential for resource extraction, and the feasibility of deploying naval assets.

Moreover, shifts in sea ice conditions impact the security of remote installations and infrastructure.

The Arctic is home to diverse Indigenous communities whose ways of life are deeply intertwined with the sea ice environment. As Bering Strait flow variability contributes to alterations in sea ice characteristics, Indigenous groups face challenges to their traditional hunting, transportation, and cultural practices. Changes in sea ice will affect the availability of subsistence resources, cultural identity, and the overall well-being of these communities. Recognizing the intricate connections between Bering Strait flow, sea ice, and Indigenous livelihoods, we can help shed light on the broader human dimensions of Arctic change.

We must better understand the dynamics of Bering Strait flow and its impact on sea ice in the Chukchi, Beaufort, and East Siberian seas, as it directly affects the operational environment and security interests of the United States and its allies.

The primary objective of this thesis is to provide an in-depth analysis of the variability in Bering Strait flow and its effects on conditions in the western Arctic seas. By assessing the linkages between Bering Strait flow variability and ocean/ice dynamics, this study aims to enhance both the scientific community and the DOD's knowledge base to make informed decisions about defense posture, infrastructure planning, and resource allocation in the Arctic region.

In the following chapters, this thesis will delve into the intricacies of Bering Strait flow variability and its influence on the conditions of the western Arctic Ocean. It employs a sound methodology that focuses mainly on regional modeling but also uses contributions from historical data and satellite observations.

II. METHODS

A. MODEL DESCRIPTION

This study is based on the Regional Arctic System Model (RASM), a state-of-the-art numerical modeling tool designed to simulate and provide an understanding of the complex interactions within the Arctic system. It has been developed as a collaborative effort over the last 15 years by researchers from multiple institutions with the goal of creating a fully coupled, high-resolution, regional model of the Arctic system.

The configuration of RASM is shown in Figure 2. Topographic pixels (shading) represent single model grid cells on the 50 km atmosphere-land domain and bathymetric pixels represent grid cells on the 1/12° ice-ocean domain. The atmosphere-land domain is bounded in red and includes the Arctic System watershed, with major inland waterways in green. The ocean-ice domain is contained in the white boundary and includes the maximum sea ice zone and connections to both the North Pacific and North Atlantic oceans. The black line outlines the area that represents the relevant central arctic analysis domain for the inter-comparison of RASM results with National Snow and Ice Data Center (NSIDC) observations (Clement Kinney et al. 2020).

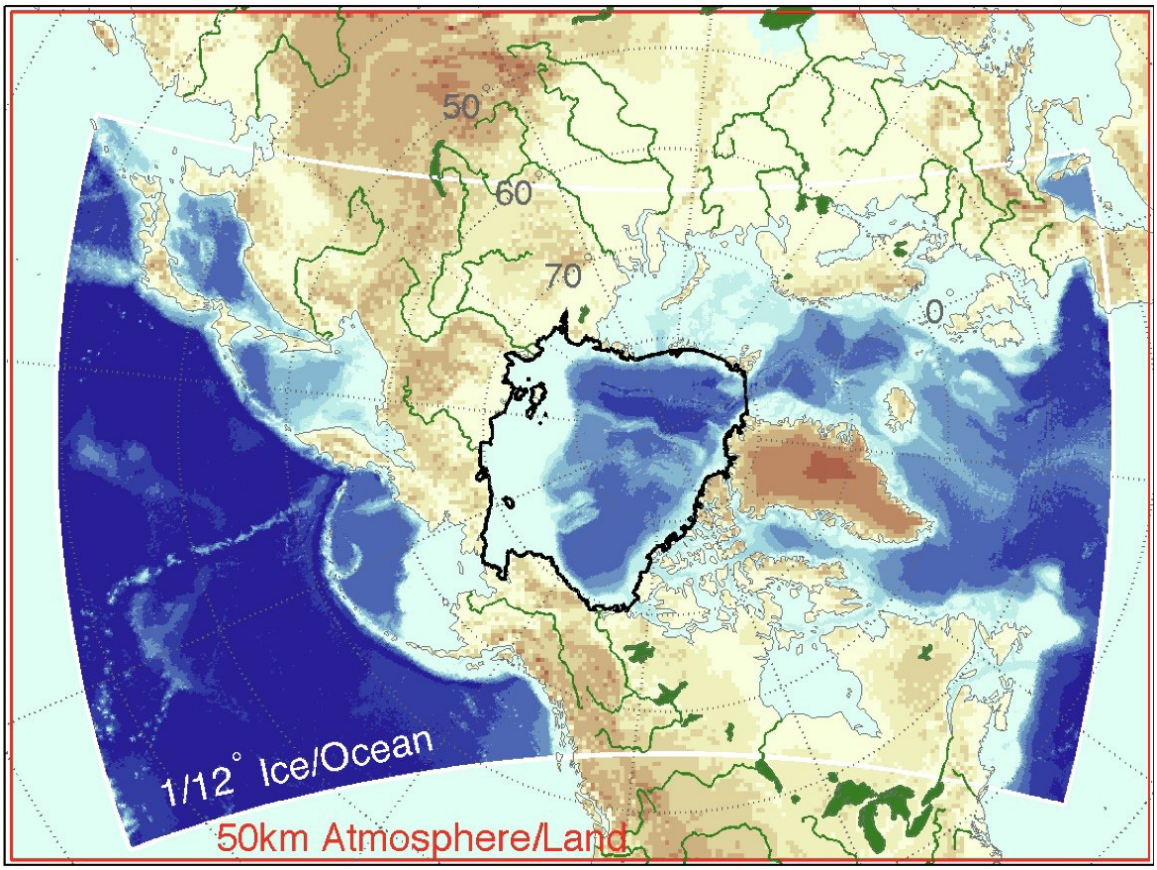

Figure 2. RASM Domains. Source: Clement Kinney et al. (2020).

RASM consists of several interconnected components, each representing a different aspect of the Arctic system. These include ocean, sea ice, atmosphere, marine biogeochemistry, land hydrology, and a river routing scheme. These components are coupled using the flux coupler shown in Figure 3 (Craig et al. 2012). Through high-resolution simulations, RASM offers insights into the spatial distribution of hydrographic properties, ocean currents, atmospheric patterns, and sea ice dynamics.

The Weather Research and Forecasting (WRF) model is the atmospheric component of RASM, configured to a 50km polar stereographic grid. It includes Arctic-specific modifications based on model evaluation used during the development of RASM (Cassano et al. 2017). These help to simulate meteorological variables such as temperature, humidity, wind patterns, and precipitation that are more reflective of the region. WRF's surface layer, radiation, land, and boundary layers have been designed to

facilitate coupling with ocean, sea ice, and land components in RASM, as shown in Figure 3.

The oceanic component in RASM is the Parallel Ocean Program (POP) that simulates the behavior of seawater, including temperature, salinity, ocean currents, and the interaction with sea ice. It uses a high-resolution rotated sphere model grid and has an extended ocean domain that utilizes climatological sea surface temperatures near the boundaries to provide ocean-atmosphere flux data to WRF (Maslowski et al. 2004)

The sea ice component is the Los Alamos National Laboratory sea ice model (CICE) that represents the growth, movement, and melting of sea ice in the Arctic Ocean and marginal seas. It has the same resolution as POP and accounts for the thickness, concentration, and characteristics of sea ice, which are vital for understanding the Arctic's response to climate change. CICE is configured to include anisotropic sea ice mechanics, melt ponds, and mushy-layer thermodynamics, providing much more detailed results in fully coupled sea ice modeling (Cassano et al. 2017).

RASM includes the Variable Infiltration Capacity (VIC) model and the RVIC streamflow routing model that simulate processes occurring on land and rivers, such as snow accumulation and melt, permafrost dynamics, and vegetation growth (Hamman et al. 2017, 2018). While these components are crucial for understanding land-river-atmosphere interactions in the Arctic, they are not a focus of this thesis.

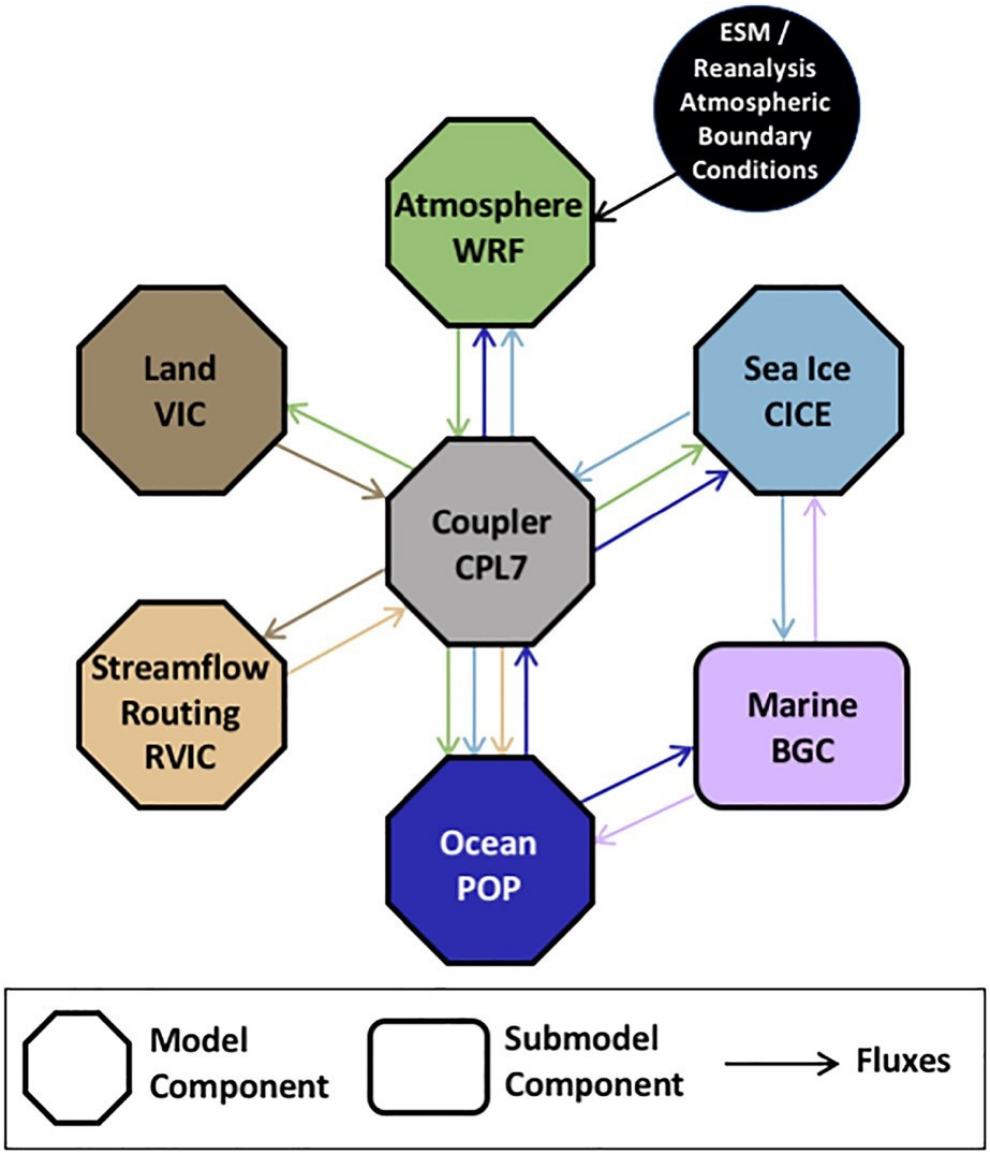

Figure 3. RASM Components. Source: Clement Kinney et al. (2020).

One of the notable features of RASM is its high spatial and temporal resolution. It provides detailed simulations of the Arctic region, allowing us to investigate fine-scale processes that are critical for understanding Arctic climate dynamics. The ocean and sea ice can be configured with a horizontal resolution of either 9 or 2.4km, enabling the model to capture small-scale features like coastal currents, narrow straits, and ice floe movement that are otherwise not seen in models with a coarser resolution.

RASM relies on a range of input data and external forcings for initialization of its simulations. Simulations are initialized with data on the state of the Arctic system at the beginning of the simulation period. This includes information on the state of the atmosphere, ocean, sea ice, biogeochemistry, and land surface. Boundary conditions, established at the edges of the domain shown in Figure 1, are utilized to ensure that simulations are consistent with the larger climate system. This includes information on atmospheric pressure, ocean temperatures, and other external factors.

In summary, RASM is a cutting-edge modeling tool designed to investigate Arctic climate variability, trends, and responses to climate change. Its multi-component approach, high resolution, and integration of various data sources make it an asset for researchers studying the complex interactions within the Arctic system. Additionally, the sea ice component is valuable for predicting sea ice extent, thickness, and distribution, with the potential to aid the Navy and DOD in navigation, resource management, and climate impact assessments.

B. RASM SETUP

RASM was used for this project as it provides a unique opportunity to explore the intricate linkages between Bering Strait flow variability and sea ice dynamics. By coupling ocean circulation, atmospheric processes, and sea ice behavior, we can uncover the mechanisms that connect Bering Strait flow to sea ice extent, ice thickness, heat convergence, and other variables.

Renowned for its high-resolution simulations, RASM is a valuable tool for examining the spatial and temporal distribution of sea ice cover. Leveraging RASM outputs, this study investigates historical trends and seasonal patterns in sea ice extent and concentration. It addresses questions related to the spatial variability of ice cover, the influence of Bering Strait flow variability, and the connection between sea ice changes and larger-scale climate phenomena.

The goal is to discern whether shifts in flow have direct impacts on local sea ice dynamics or if other intervening factors play a more significant role. By employing a

comprehensive modeling approach, we gain insights into the intricacies of sea ice extent and concentration variations within these regions.

All the RASM 9-km cases studied in this section were set up with initial conditions reflecting observations and reanalysis data from September 1979. After an initial 76-year spin-up integration for the ocean and sea ice components, each coupled run was started in September 1979. Results from January 1980 through December 2018 for each of the cases (described below) were used for this study. This timeframe accommodated the atmospheric boundary conditions, which are from the European Centre for Medium-Range Weather Forecasts (ECMWF) Reanalysis V5 (ERA5) data from 1979 through 2018. Forecasted atmospheric conditions tend to be less precise than those obtained using reanalysis from ERA5, which is why the decision was made to initialize the runs from 1979 through 2018. As of this writing, ERA5 data post-2018 is unavailable.

The comprehensive modeling approach utilized three different RASM runs. The first case was set up to represent the historical Bering Strait throughflow. This default case, also known as the "Control Run," was conducted with a mean volumetric flow of 0.7Sv through the Bering Strait, which is similar to historical observational data from moorings within the Bering Strait (Woodgate et al. 2012).

The main motivation for this project was to increase the Bering Strait flow and analyze its effects. As previously discussed, the volumetric flow of the Bering Strait is increasing at a rate of ~0.01Sv per year (Woodgate 2018). Using this rate and a starting volumetric flow of 0.7Sv (as used in the "Control Run"), volumetric flow through the Bering Strait would double in 70 years. We chose to use that value as the flow rate for the next RASM case. Labeled as "2X Flow," this case has a volumetric flow of 1.4Sv through the strait.

Lastly, though the overall volumetric flow through the Bering Strait is increasing, it was deemed valuable to conduct a zero flow RASM run for comparison and to achieve a full spectrum analysis of volumetric flow through the strait. This case, labeled as "Zero Flow," has a volumetric flow of 0Sv through the Bering Strait. This flow rate was

achieved by setting up a gate in RASM that acts as a barrier, allowing no inflow or outflow between the Bering and Chukchi seas. For reference, the three RASM cases are listed in Table 1.

Table 1. RASM Case Names

RASM RUNS	LABEL
R2300aRBRcspi05a	Zero Flow
R2300aRBRcaaa01a	Control Run
R2300aRBRcspi07a	2X Flow

In summary, RASM is a powerful tool for investigating sea ice and ocean dynamics in the Chukchi Sea, Beaufort Sea, and East Siberian Sea. The integration of diverse modeling runs and analysis techniques allow for a holistic examination of Bering Strait flow variability and its implications on sea ice dynamics and the western Arctic Ocean environment. This robust approach will allow for drawing meaningful conclusions about the complex interplay between Bering Strait flow and subsequent changes in Arctic Ocean conditions.

THIS PAGE INTENTIONALLY LEFT BLANK

III. RESULTS

This chapter delves into the results obtained from utilizing RASM to simulate Bering Strait flow variability and its impact on sea ice dynamics in the Chukchi, Beaufort, and East Siberian seas. To comprehend the implications of Bering Strait flow variability on sea ice, it is essential to elucidate the characteristics and capabilities of the numerical model employed.

This thesis draws upon historical observational data, including in-situ measurements and remote sensing products. Oceanographic and meteorological databases provide critical information on hydrographic parameters, flow rates, temperature profiles, and atmospheric patterns. Satellite-derived sea ice data offer insights into sea ice extent, concentration, and thickness, aiding in the quantification of spatial and temporal trends.

A suite of analytical techniques is employed to dissect the complex interactions between Bering Strait flow, sea ice, and ocean dynamics. Statistical methods facilitate the identification of relationships and patterns in the data. Time-series analysis aids in uncovering trends and cyclic variations in flow and ice conditions. These techniques provide a quantitative basis for understanding the temporal coherence between Bering Strait flow variability and sea ice changes.

A. BERING STRAIT CROSS-SECTION

Before delving into the specific effects of Bering Strait flow variability in the Arctic region, it is useful to first look at various fluxes through the strait in the Control Run and 2X Flow cases.

As previously discussed, the net annual mean flow for the Control Run is 0.7 Sv northward (Figure 4). This agrees with mooring data gathered within the Bering Strait (Woodgate 2018). Periodically, slight reversals of the flow (southward) are seen in the monthly mean timeseries.

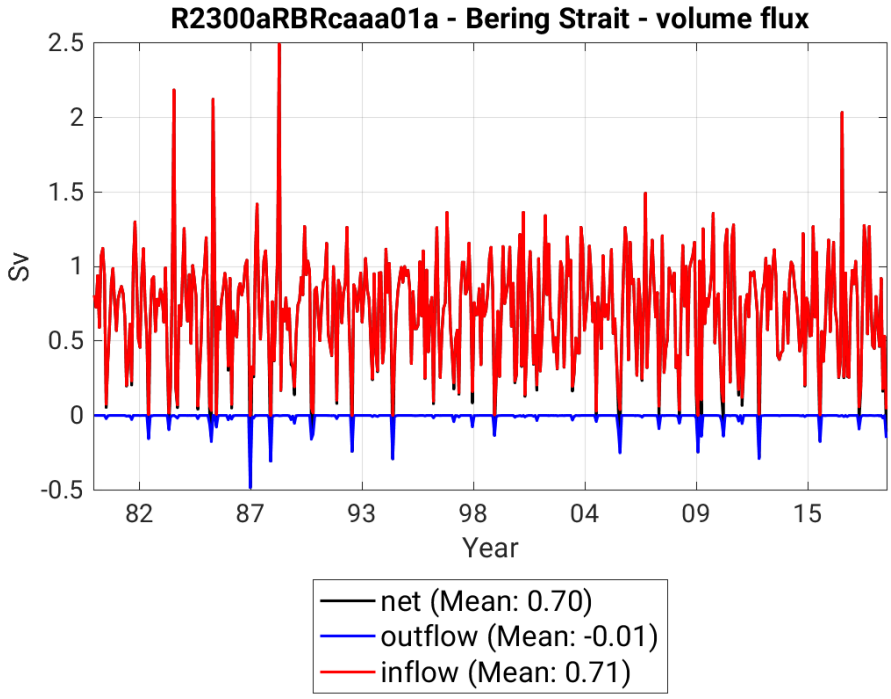

Figure 4. Bering Strait Volume Flux – Control Run

The net flow for the 2X Flow run had a mean of 1.4Sv northward, with a maximum value of 3.3Sv (Figure 5). The flow does not reverse in this case. The Zero Flow case was verified to have zero flow for both inflow and outflow directions and the net flow.

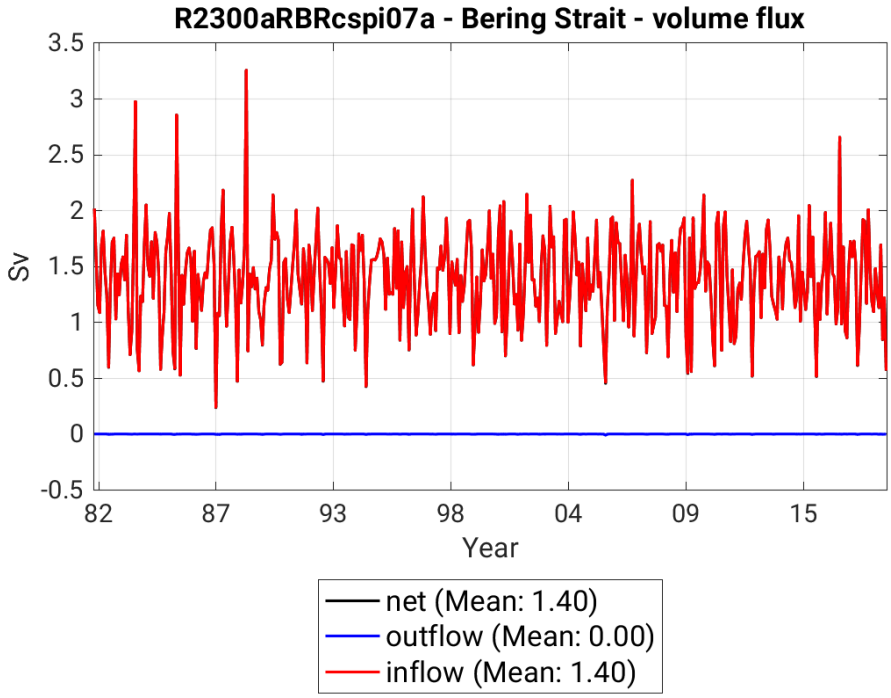

Figure 5. Bering Strait Volume Flux – 2X Flow Run

The Bering Strait cross section for the Control Run and 2X Flow cases is shown in Figure 6. On the far left is temperature (°C), in the middle is salinity, and to the right is velocity (cm/s). The values represent the long-term mean (1980–2018) and positive velocity indicates a northward flow.

The 2X Flow case shows warmer and saltier water than in the Control Run. The velocity structure looks similar between the two cases, speeds in the 2X Flow case are approximately double those of the Control Run, as expected. The Eastern Channel of the Bering Strait (best viewed on the right portion of the "Velocity" graphic of Figure 6) brings warmer, fresher, and rapid flow through the Bering Strait for both cases.

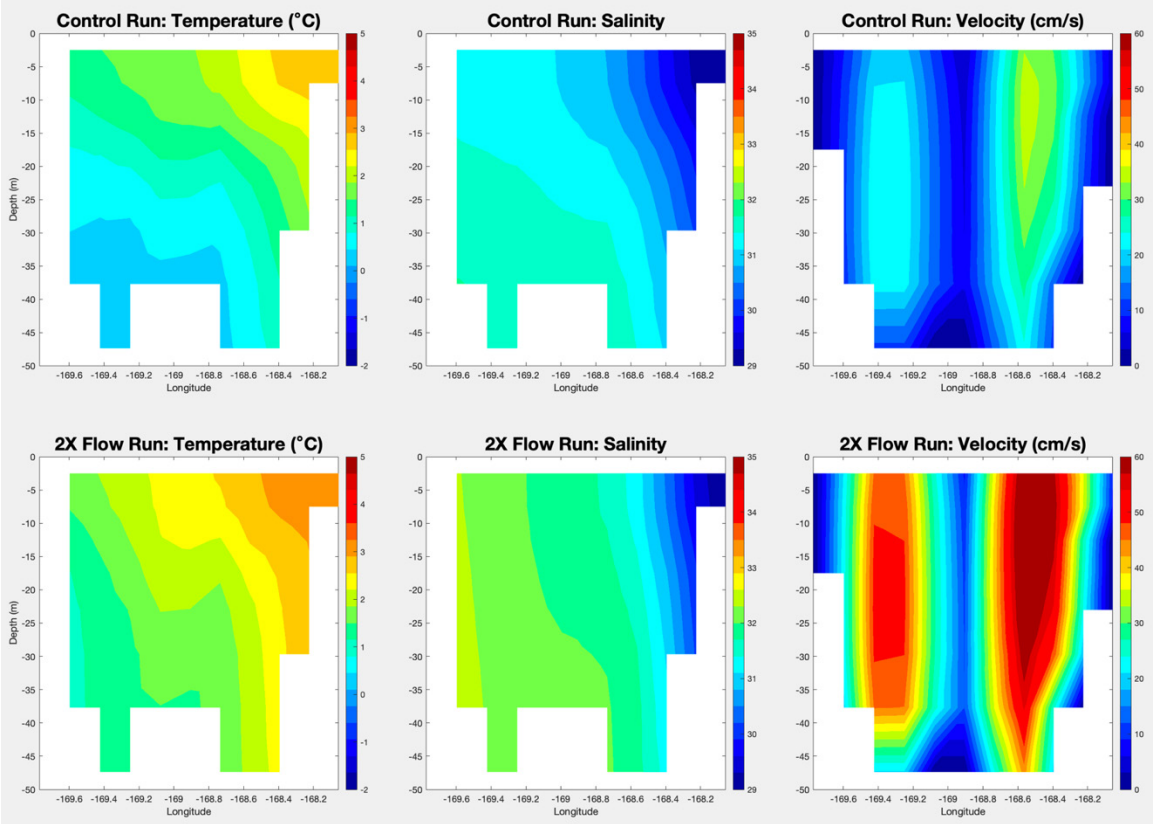

Bering Strait cross section is shown in Figure 6, looking northward. The figure shows a long term mean comparison between the temperature, salinity, and velocity of the Control Run (top row) and the 2X Flow (bottom row).

Figure 6. Bering Strait Cross Section

Monthly mean fields of temperature, salinity, and velocity from the Control Run and 2X Flow were analyzed to see if there were major differences during peak winter and summer conditions near the beginning and end of the RASM runs. We used March to display peak winter conditions (Figure 7), which show the 2X Flow run bringing warmer and saltier water through the Bering Strait. A comparison between March in 1988 and 2018 shows a temperature decrease for the Control Run, but an increase in temperature for the 2X Flow run. The salinity in March decreases over the 39-year model run, while the velocity through the Bering Strait increases by over 10 cm/sec for both the Control Run and 2X Flow cases.

We used August for peak summer conditions (Figure 8), which also show the 2X Flow run bringing warmer and saltier water through the Strait, just as was the case in

March. A comparison between August in 1988 and 2018 shows a temperature increase for both the Control Run and 2X Flow case, but the difference in salinity and velocity are not nearly as pronounced as March. Salinity does not change all that much over the 39-year model run, while velocity in some portions of the strait appears to decrease.

Overall, comparisons between the months of March (peak winter conditions) and August (near peak summer conditions) show an increase in temperature, decrease in salinity, and increase in velocity through the Bering Strait over the course of the 39-year model run (Figures 7 and 8). Note the scales for temperature in March and August have been adjusted to better represent values typically observed for the respective months.

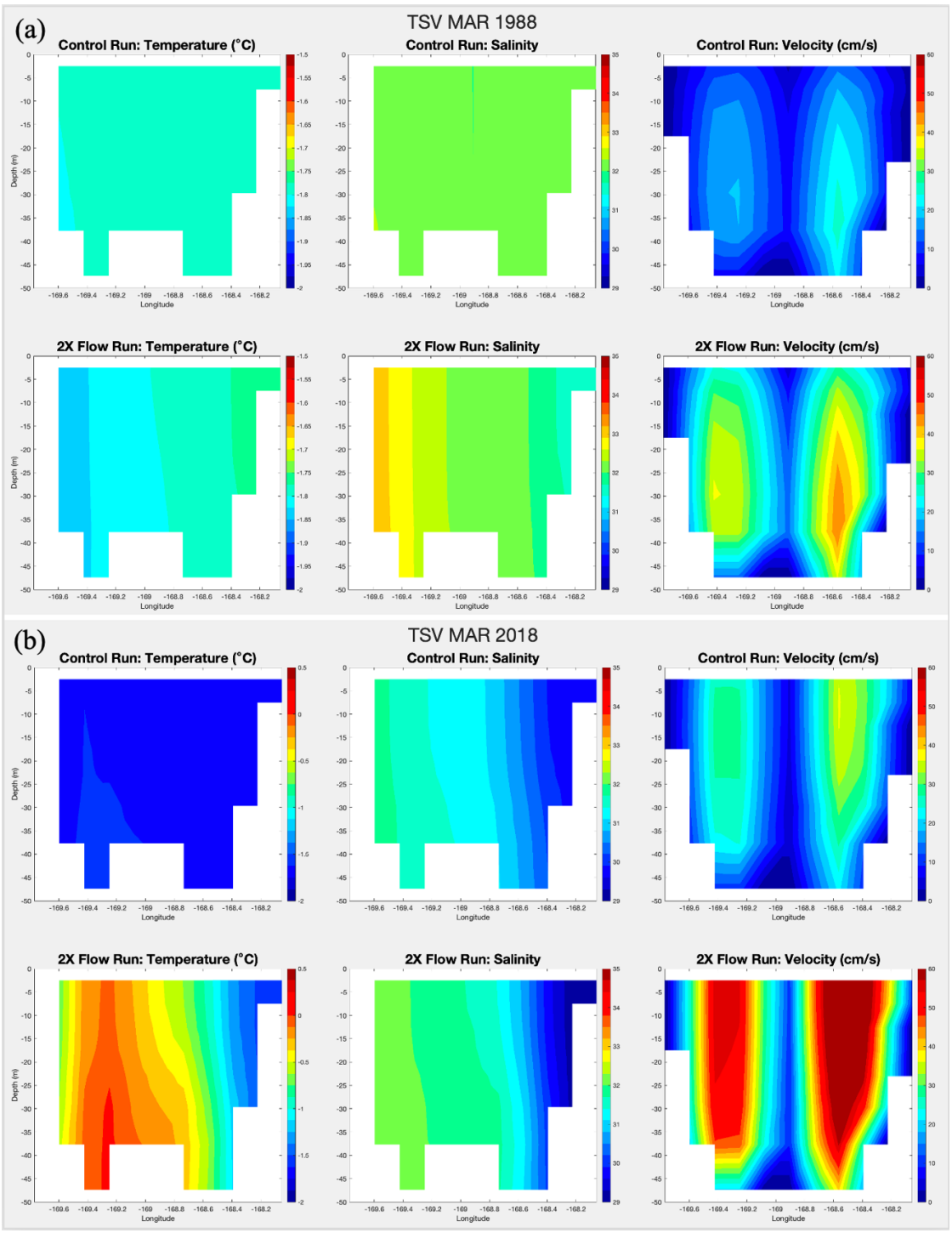

Figure 7 shows a cross section of Bering Strait, comparing temperature, salinity, and velocity fields between the Control Run and 2X Flow cases for March of (a) 1988 and (b) 2018. The Control Run outputs are on the top row for (a) and (b), and the 2X Flow outputs are on the bottom row.

Figure 7. Comparison of Temperature, Salinity, and Velocity Fields at the Bering Strait Cross Section in March 1988 and 2018

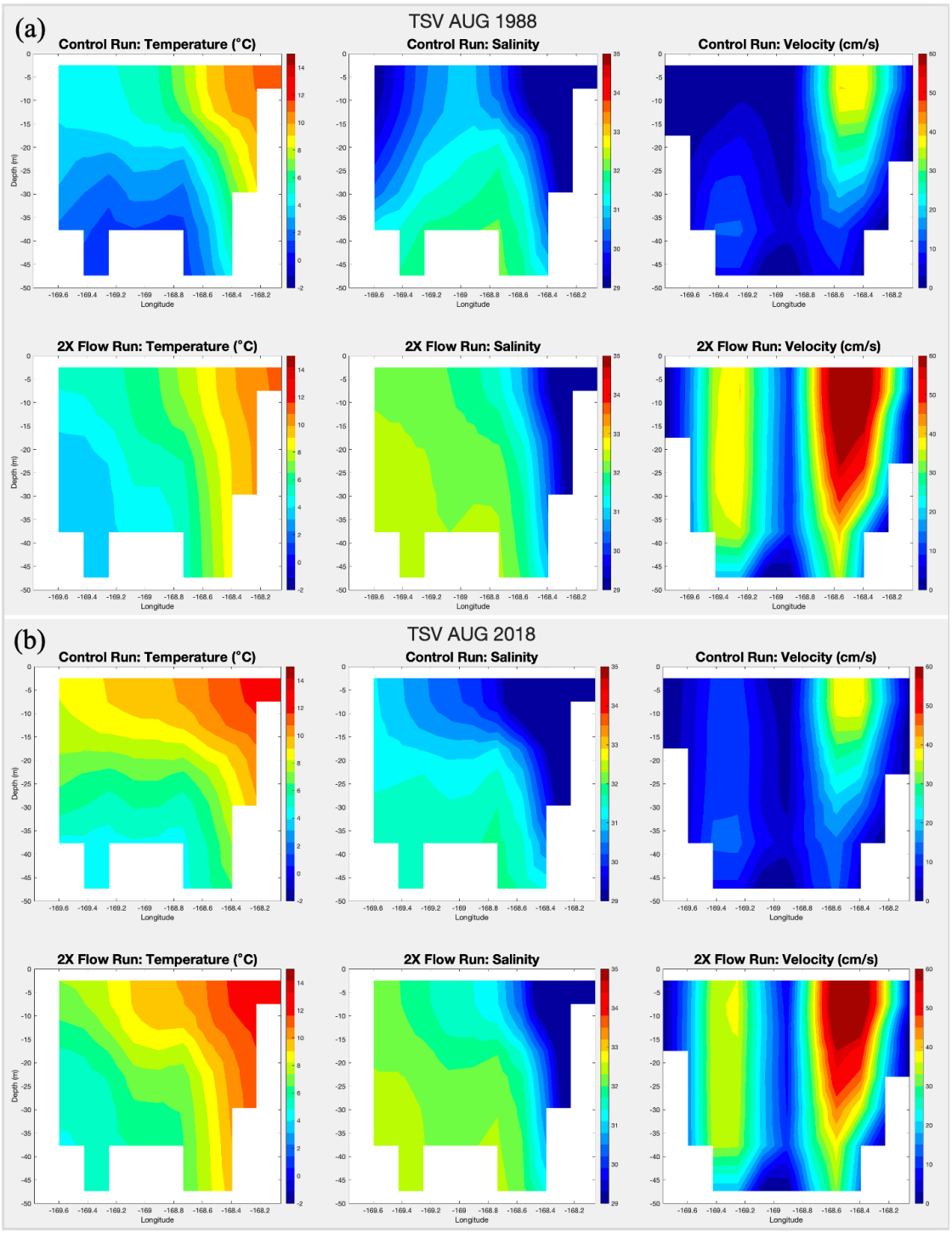

Figure 8 shows a cross section of Bering Strait, comparing temperature, salinity, and velocity fields between the Control Run and 2X Flow cases for August of (a) 1988 and (b) 2018. The Control Run outputs are on the top row for (a) and (b), and the 2X Flow outputs are on the bottom row.

Figure 8. Comparison of Temperature, Salinity, and Velocity Fields at the Bering Strait Cross Section in August 1988 and 2018

B. PAN-ARCTIC

This section examines the temporal trends and spatial patterns of simulated Bering Strait flow variability. We investigate the extent to which changes in Bering Strait flow are related with shifts in sea ice extent, concentration, and thickness within the study area. By assessing these relationships, the section offers insights into the nature of the coupling between Bering Strait flow and sea ice dynamics and elucidates potential feedback mechanisms.

1. Sea Ice

This section discusses the sea ice extent, area, and volume among the three RASM cases.

a. Sea Ice Extent

The skill of the RASM sea ice extent is assessed against available NSIDC data (Figure 9). The sea ice extent for all three RASM cases shows a negative bias when compared with NSIDC data. This negative bias remains in the Zero Flow case but is diminished in the last decade of the Control Run and 2X Flow cases. The mean sea ice extents for the RASM cases are listed in Table 2.

Table 2. Long Term Mean (1980–2018) of Pan-Arctic Sea Ice Extent

Mean Sea Ice Extent (10^6 km^2)	
Zero Flow	9.96
Control Run	10.13
2X Flow	10.08
NSIDC	10.73

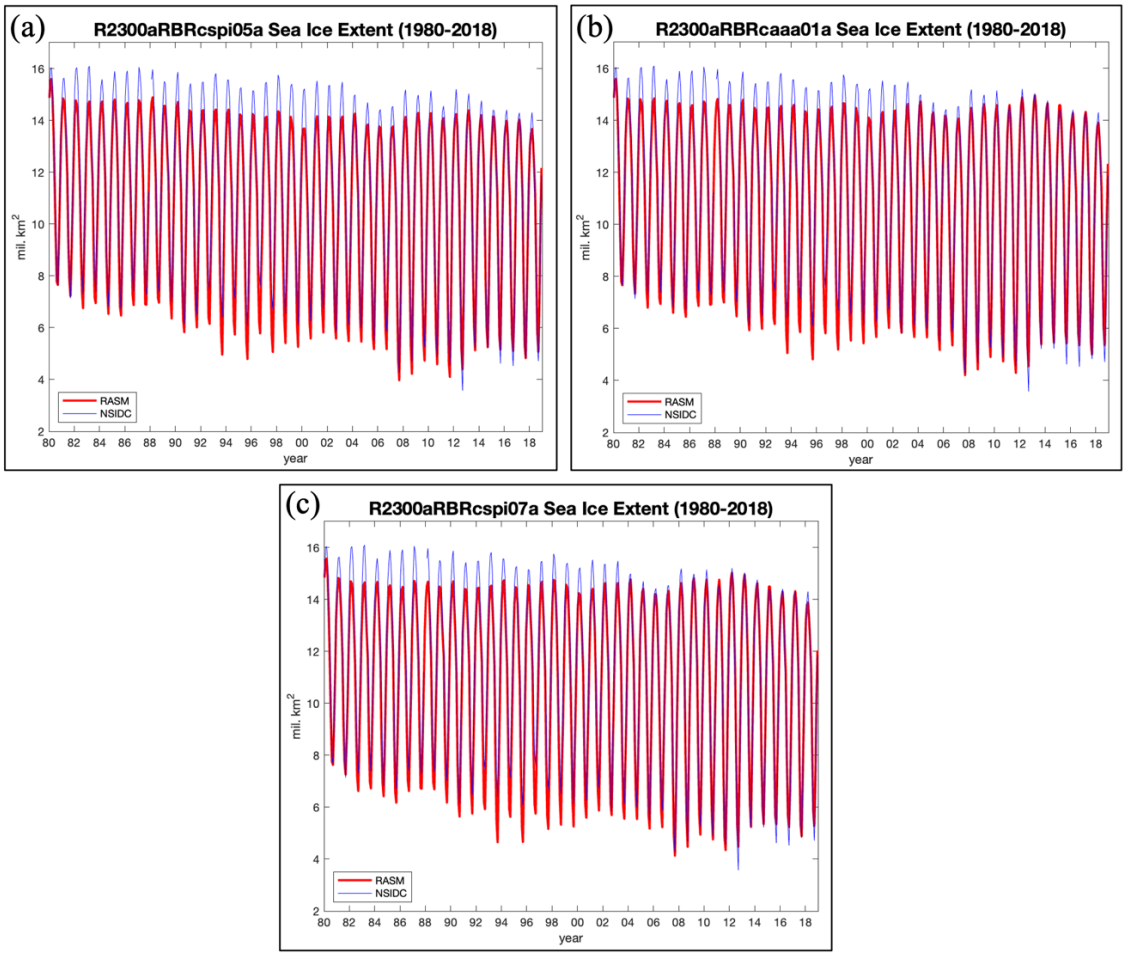

Figure 9 is the monthly time series of pan-Arctic sea ice extent in RASM simulations for the (a) No Flow (b) Control Run and (c) 2X Flow cases. The blue line included in each graphic is the NSIDC monthly time series of pan-Arctic sea ice extent.

Figure 9. Monthly Time Series of Pan-Arctic Sea Ice Extent

b. Sea Ice Thickness

Using the same months and years as sea ice extent for comparison, we see that sea ice thickness has a more dramatic loss in the winter and summer months from 1988 to 2018 (Figures 10 and 11). Both visually and quantitatively, the difference in pan-Arctic sea ice extent among the RASM runs does not seem to differ all that much when the Bering Strait flow is varied from zero to twice the rate, staying approximately within two percent of the annual mean ice extent values.

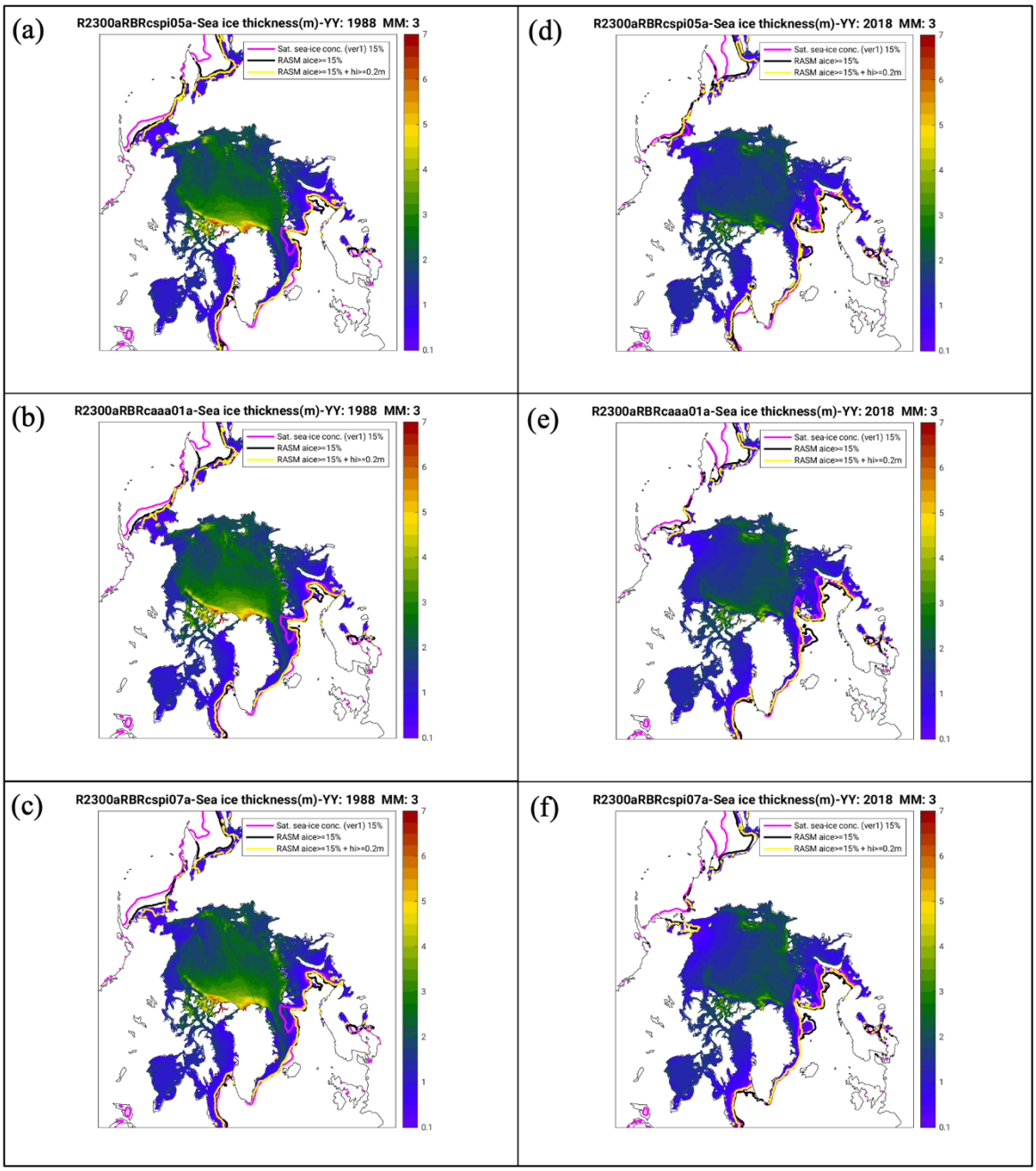

Sea ice thickness comparisons for March of 1988 (a-c) and 2018 (d-f). No Flow case is shown on plots (a) and (d), Control Run is (b) and (e), and the 2X Flow is (c) and (f). The magenta line is outer boundary for NSIDC sea-ice concentration, the black lines are RASM sea ice extent with >15% ice coverage, and the yellow lines are RASM sea ice extent with >15% ice coverage and at least 0.2m ice thickness.

Figure 10. Comparison of Pan-Arctic Sea Ice Thickness Comparison in March 1988 and 2018

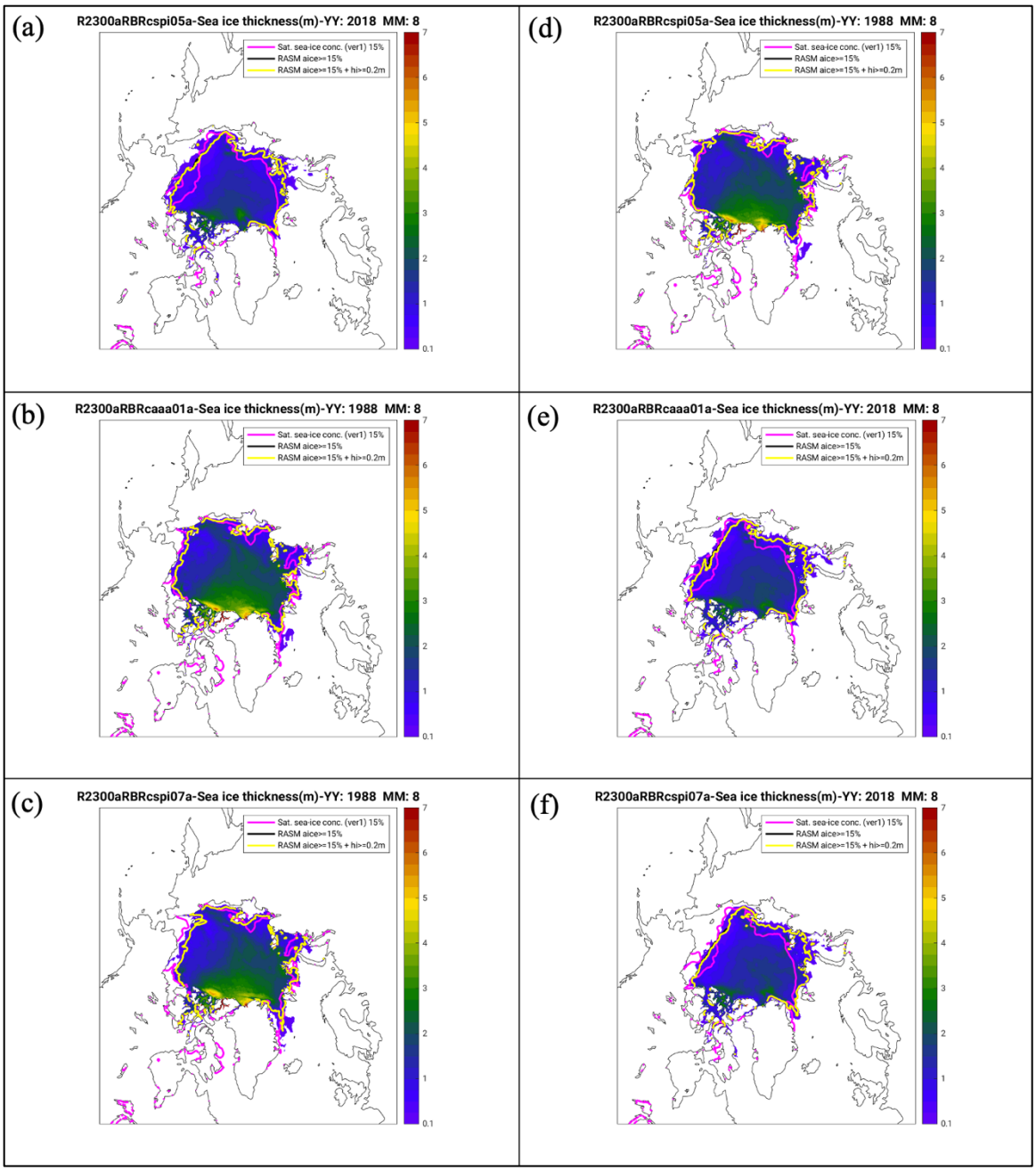

Sea ice thickness comparisons for August of 1988 (a-c) and 2018 (d-f). No Flow case is shown on plots (a) and (d), Control Run is (b) and (e), and the 2X Flow is (c) and (f). The magenta line is outer boundary for NSIDC sea-ice concentration, the black lines are RASM sea ice extent with >15% ice coverage, and the yellow lines are RASM sea ice extent with >15% ice coverage and at least 0.2m ice thickness.

Figure 11. Pan-Arctic Sea Ice Thickness Comparison – August

c. Sea Ice Volume

For sea ice volume, RASM results were compared to pan-Arctic Ice Ocean Modeling and Assimilation System (PIOMAS), a sea ice volume reanalysis product developed by the University of Washington (Zhang and Rothrock 2003; Schweiger et al. 2011). Over the 39-year run, RASM shows a negative bias for all three cases (Figure 12). Again, there is only a small difference in sea ice thickness among the three runs when analyzed on the pan-Arctic scale.

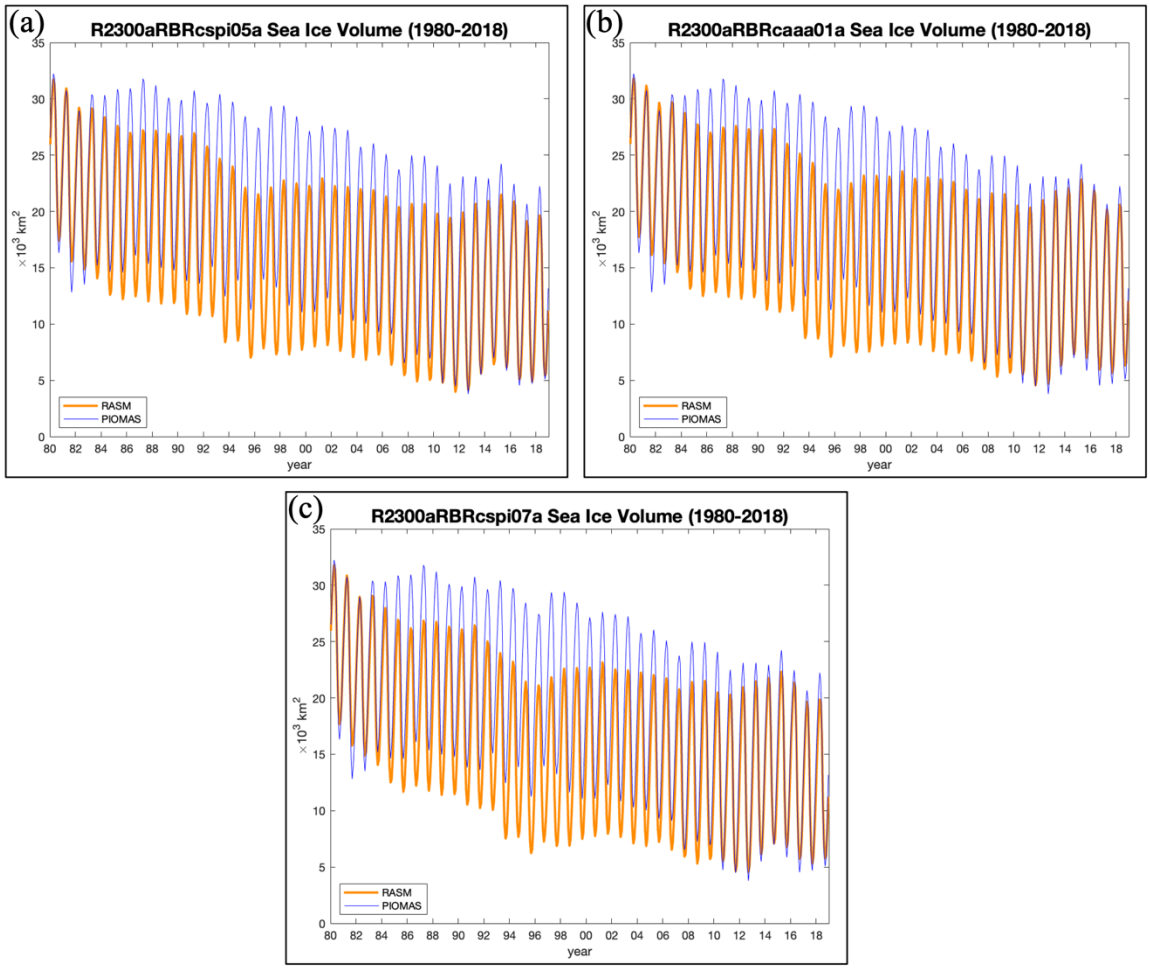

Figure 12 is the monthly time series of pan-Arctic sea ice volume in RASM simulations for the (a) No Flow (b) Control Run and (c) 2X Flow cases. The blue line included in each graphic is the NSIDC monthly time series of pan-Arctic sea ice volume.

Figure 12. Monthly Time Series of Pan-Arctic Sea Ice Volume (1980–2018)

From a pan-Arctic viewpoint, the flow variability through the Bering Strait has a small effect on sea ice, but not as significant of an effect as one would expect. Figure 13 shows the mean annual cycle of sea ice extent, area, and volume among the three RASM runs; each panel contains the three RASM runs with colors as shown in the legend. There is very little variation among the three runs for the ice variables. The most affected variable is sea ice volume, where the 2X Flow case has a value that is consistently around $2.0\text{x}10^3\text{km}^2$ lower than the Control Run.

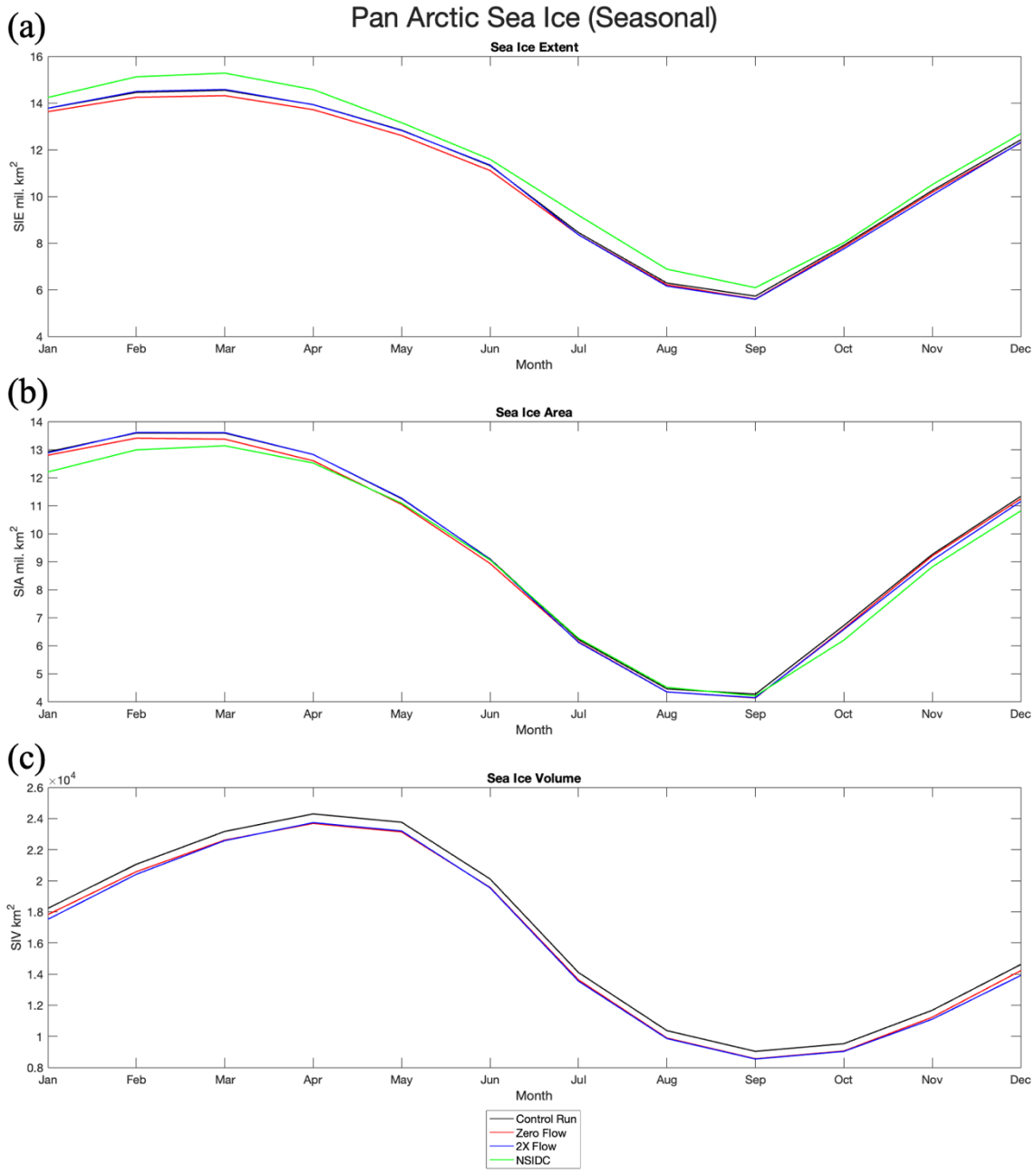

Figure 13 is a pan-Arctic comparison among RASM cases for mean annual cycles of pan-Arctic (a) sea ice extent, (b) sea ice area, and (c) sea ice volume. The black line is the Control Run, the red line is the Zero Flow, the blue line is the 2X Flow, and the green line is NSIDC data.

Figure 13. Mean Annual Cycle of Pan-Arctic Sea Ice Extent (SIE), Area (SIA), and Volume (SIV) from the RASM Cases

2. Freshwater Content

Increases in freshwater content (FWC) in the Beaufort Gyre are apparent in a comparison between 1982 and 2018 for the month of September. As shown in Figure 14, the 2X Flow run has the most dramatic increase, which should be expected due to the influx of relatively fresh Pacific water and the increased anti-cyclonic motion of the Beaufort Gyre in recent decades (Proshutinsky et al. 2019), which RASM has modeled appropriately.

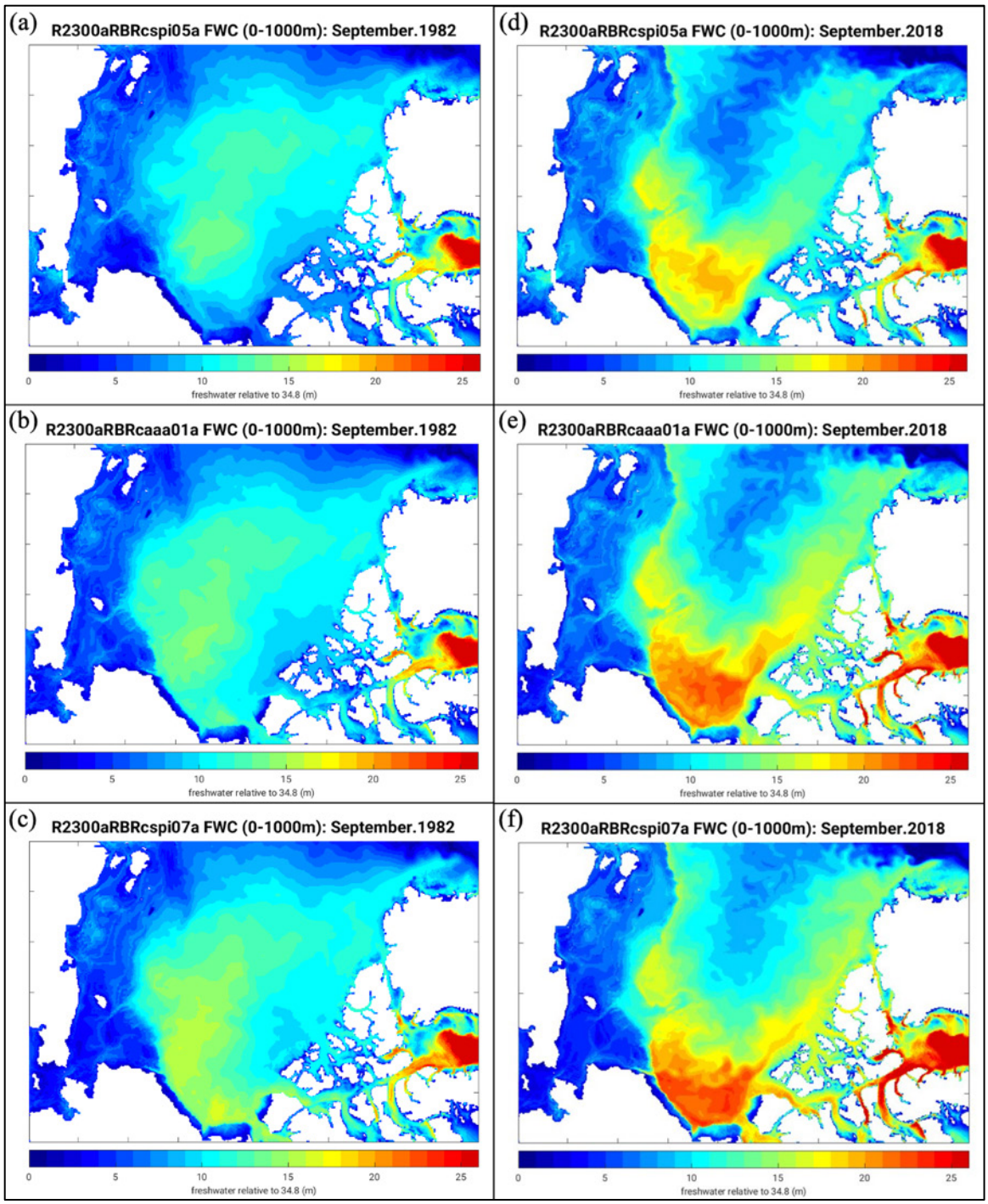

Freshwater content comparisons for September of 1982 (a-c) and 2018 (d-f). The No Flow case is shown on plots (a) and (d), Control Run is (b) and (e), and the 2X Flow is (c) and (f).

Figure 14. Comparison of Pan-Arctic Freshwater Content in September 1982 and 2018

3. Surface Velocities

For surface velocities (0–50m), we compared the same months and years as the FWC in the previous section to see if there were any relationships. The increase in surface velocity from 1982 to 2018 is apparent for both the winter and summer (Figures 15 and 16). The Zero Flow case produces the strongest and most organized Beaufort Gyre in March 2018. Multiple eddies are present in the Beaufort Gyre in September for all cases, especially during 2018.

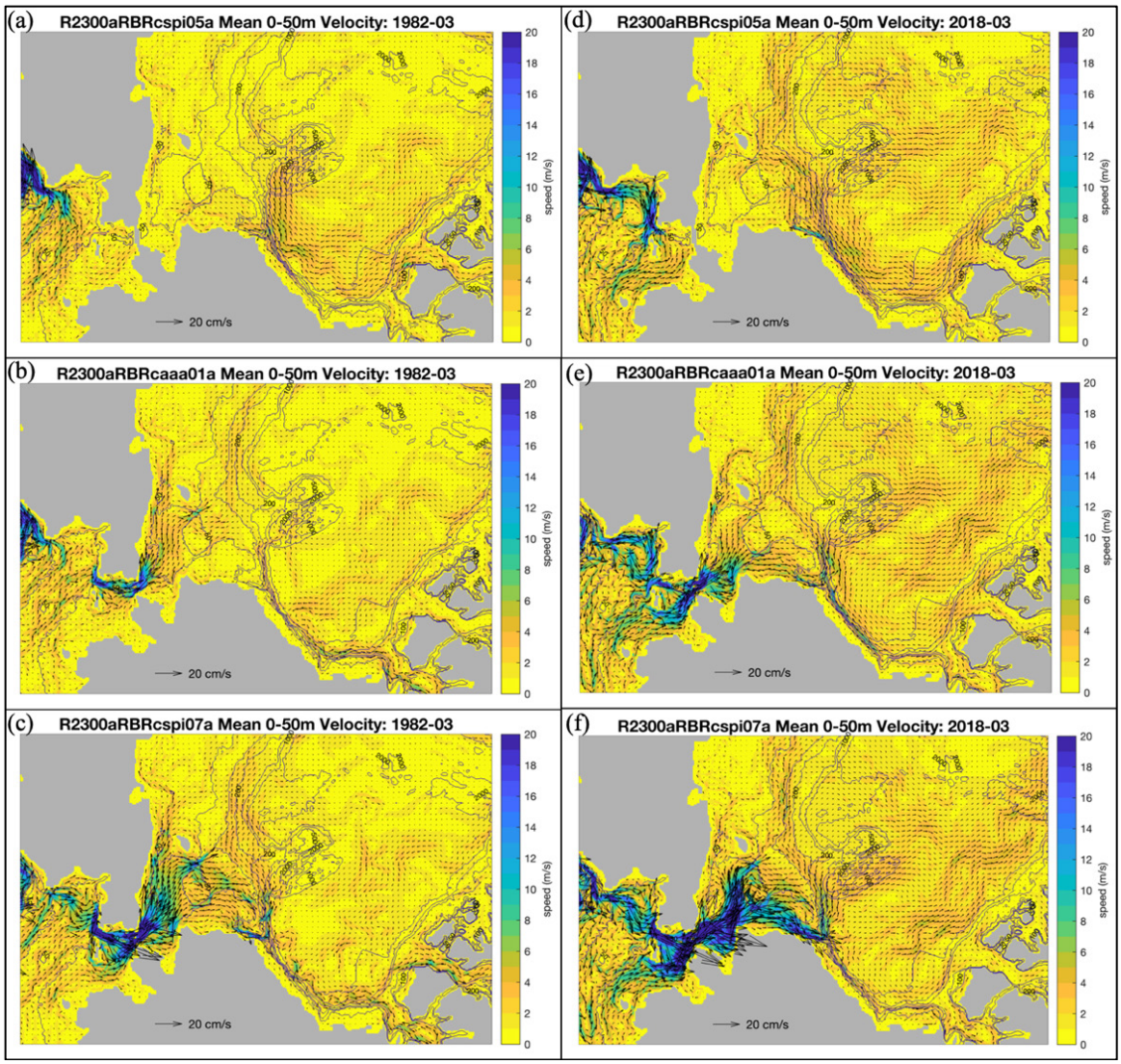

Surface velocity field comparisons for March of 1982 (a-c) and 2018 (d-f). The No Flow case is shown on plots (a) and (d), Control Run is (b) and (e), and the 2X Flow is (c) and (f). The black arrows are the direction and magnitude of the local velocity fields, and the color contours show velocity field magnitudes.

Figure 15. Comparison of Upper 50m Mean Velocity Fields in March, 1982 and 2018

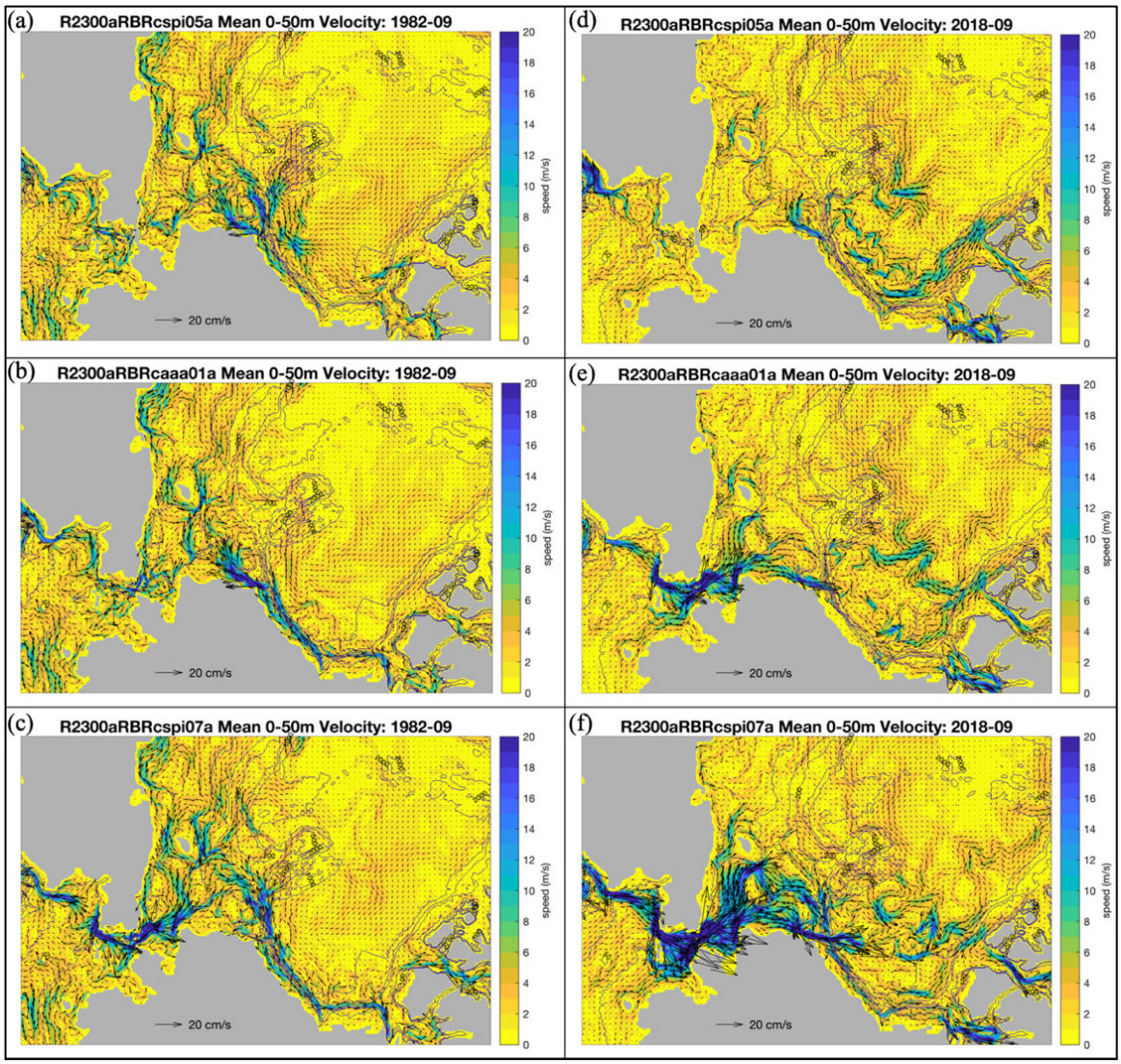

Surface velocity field comparisons for September of 1982 (a-c) and 2018 (d-f). The No Flow case is shown on plots (a) and (d), Control Run is (b) and (e), and the 2X Flow is (c) and (f). The black arrows are the direction and magnitude of the local velocity fields, and the color contours show velocity field magnitudes.

Figure 16. Comparison of Upper 50m Mean Velocity Fields in September, 1982 and 2018

4. Surface Heat Flux

Unlike sea ice extent and volume, the surface heat flux appears to increase overall in the winter (March) from 1982 to 2018 (Figure 17) with stronger negative values, indicating a greater heat release to the atmosphere. This is to be expected due to the decreases in sea ice concentration and thickness and increase in open water. North of the

Fram Strait, there is a significant decrease in surface heat flux, most notably in the Norwegian and Barents seas.

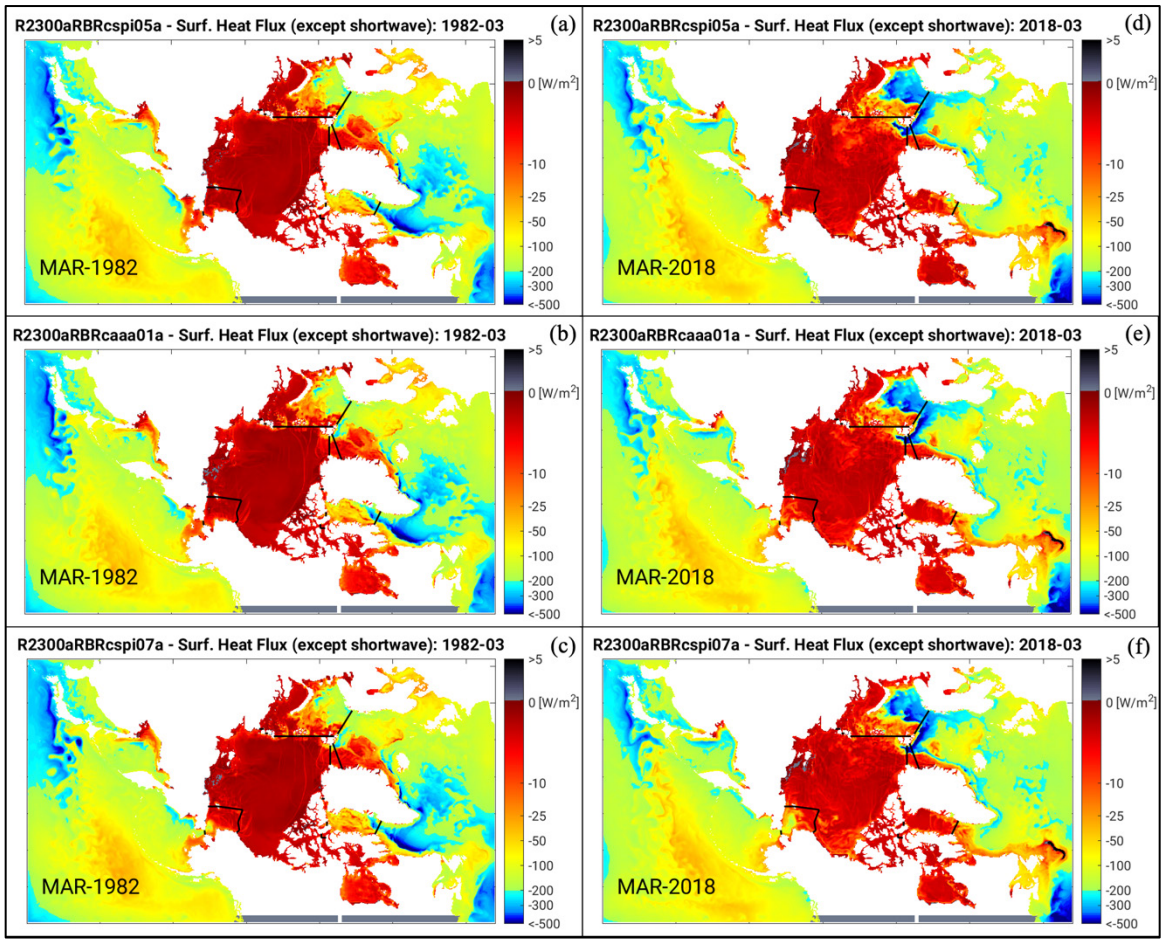

Surface heat flux comparisons for March of 1982 (a-c) and 2018 (d-f). The No Flow case is shown on plots (a) and (d), Control Run is (b) and (e), and the 2X Flow is (c) and (f).

Figure 17. Comparison of Monthly Mean Surface Heat Flux (W/m^2) except Shortwave in March 1982 and 2018

Like March, the surface heat flux increases from 1982 to 2018 at the end of summer as well (Figure 18). The increase is more noticeable in the 2X Flow case, but is present in all three runs. As was the case with March, values of the surface heat flux in the Norwegian and Barents seas become more strongly negative, indicating more heat release to the atmosphere.

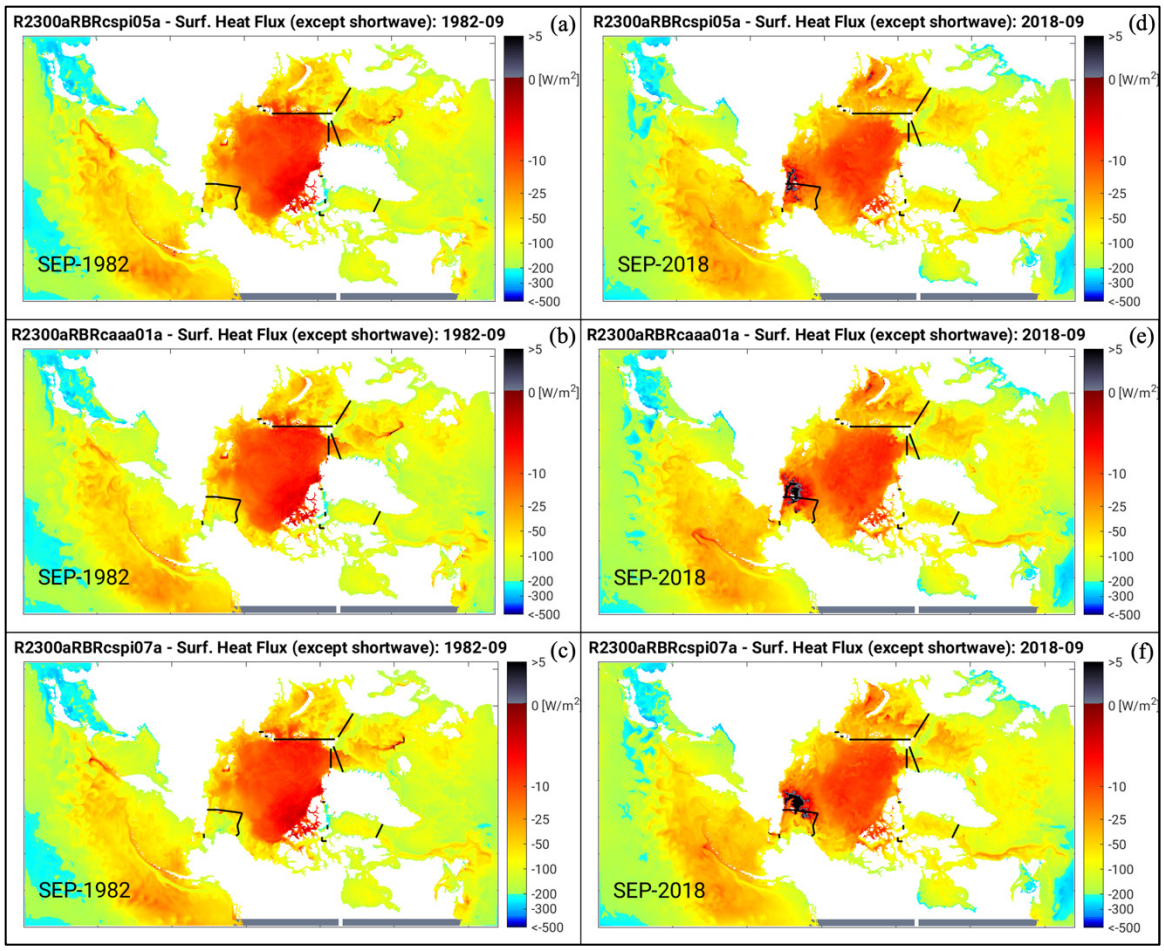

Surface heat flux comparisons for March of 1982 (a-c) and 2018 (d-f). The No Flow case is shown on plots (a) and (d), Control Run is (b) and (e), and the 2X Flow is (c) and (f).

Figure 18. Comparison of Monthly Mean Surface Heat Flux (W/m^2) in September 1982 and 2018

Pan-Arctic heat convergence for all three runs is shown in Figure 19. The mean net flux for the No Flow run is 108.99 TW, the Control run is 106.32 TW, and the 2X Flow run is 115.47 TW. Note the net flux for the Control Run is less than the Zero Flow run.

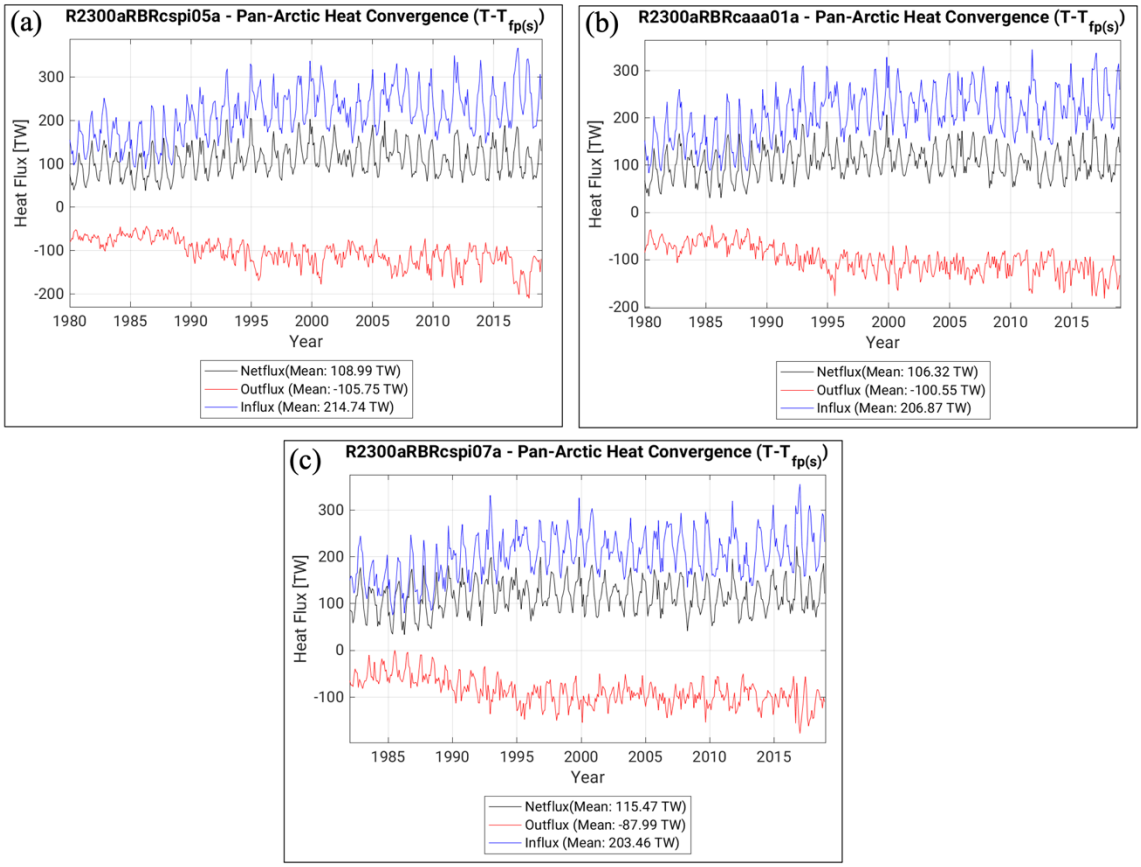

Figure 19 shows the monthly Pan-Arctic heat convergence for the (a) No Flow, (b) Control Run, and (c) 2X Flow cases. Heat convergence is calculated based on the freezing point.

Figure 19. Monthly Time Series of Pan-Arctic Heat Convergence (TW) in the RASM

C. WESTERN ARCTIC

For the purposes of this thesis, the "Western Arctic" is defined as the Chukchi, Beaufort, and East Siberian seas. Figure 20 shows the boundaries for each area used for post-processing, which approximate the 200m depth contour.

The area towards the top of the figure is the East Siberian Sea, below is the Chukchi Sea, and the thin region above Alaska and extending toward the Canada Arctic Archipelago is the Beaufort Sea.

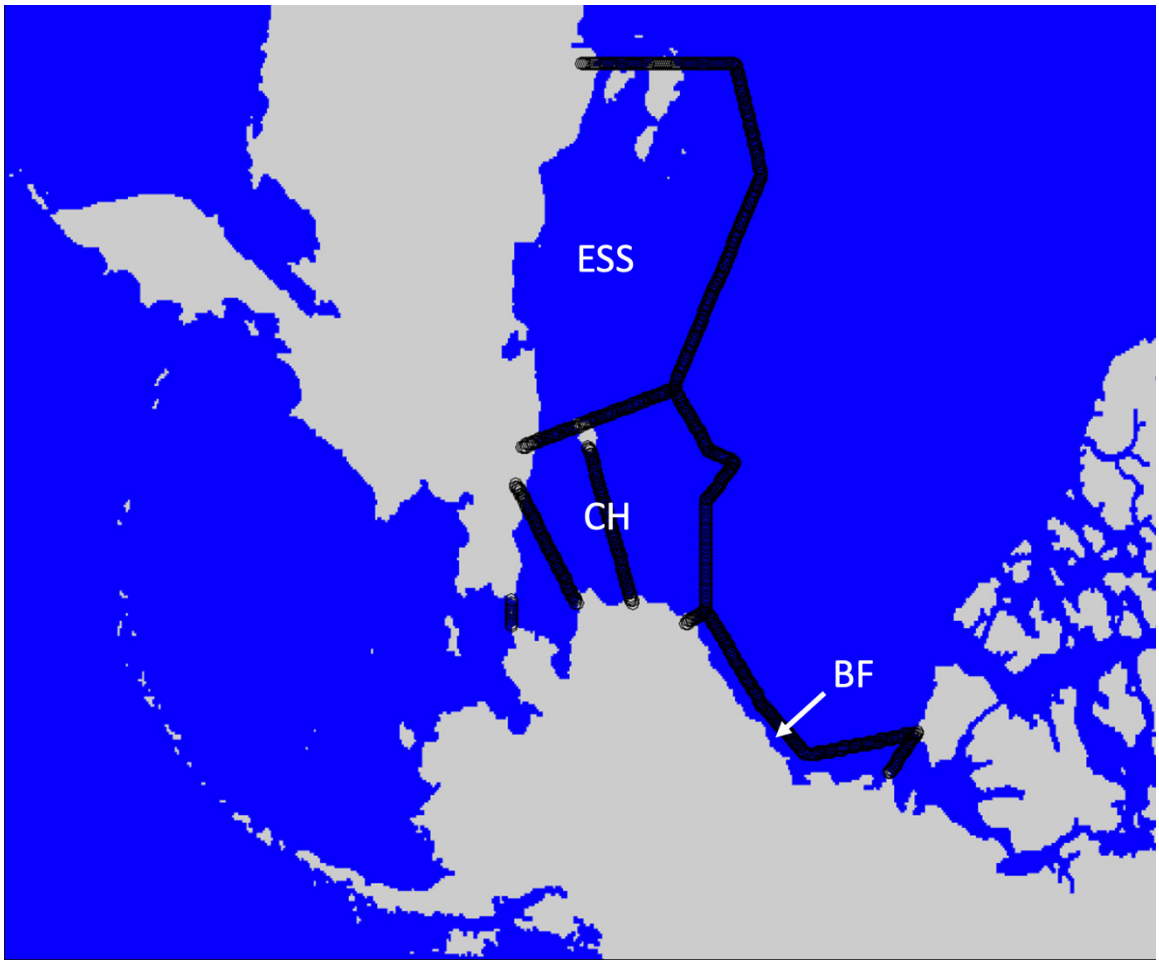

The areas outlined in black were used to specify western Arctic regions for post-processing. Boundaries near the Arctic Basin approximate the 200m depth contour. "CH" is the Chukchi Sea, "BF" is the Beaufort Sea, and "ESS" is the East Siberian Sea.

Figure 20. Western Arctic Sections Used for Post-Processing

1. Sea Ice

This section discusses the differences between sea ice extent, area, and volume in the western Arctic for the three RASM cases.

a. Sea Ice Extent

All three runs have similar values of sea ice extent in the western Arctic, with the major exception being the Chukchi in the 1980s (Figure 21). During this period, the 2X Flow run has noticeably lower sea ice extent in the summer months than the Control and Zero Flow runs. The 1980s had larger values of sea ice extent in the summer months than

in the recent years, with at least some ice remaining on the Chukchi shelf year-round. It is possible that increased Bering Strait flow had a more significant impact on sea ice melt in those earlier years.

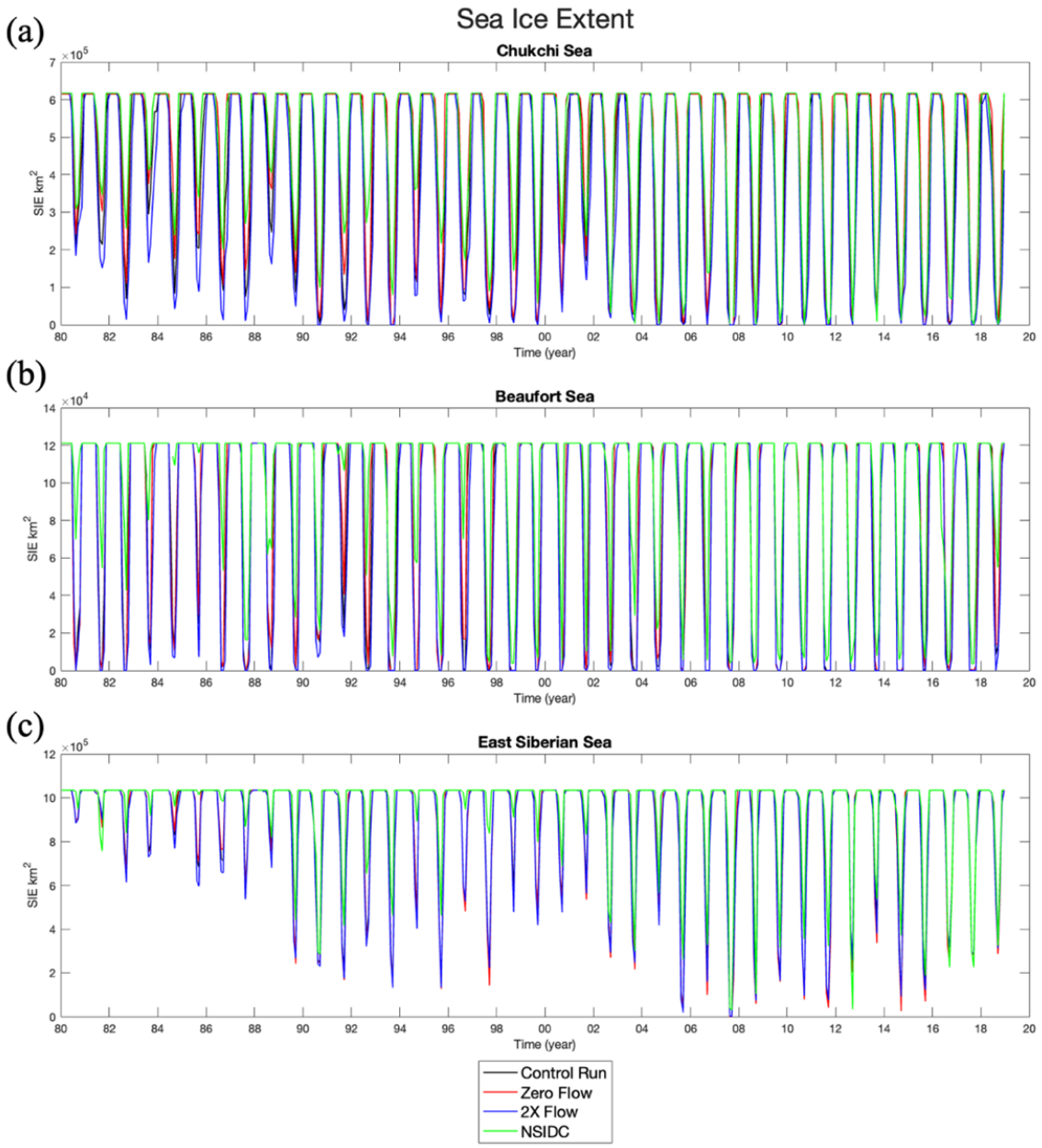

Monthly sea ice extent comparison for the (a) Chukchi, (b) Beaufort, and (c) East Siberian seas. The black line is the Control Run, the red line is the Zero Flow, the blue line is the 2X Flow, and the green line is NSIDC data.

Figure 21. Comparison of Monthly Sea Ice Extent in the Western Arctic Regions

The seasonal sea ice extent shown in Figure 22 illustrates a very clear seasonal trend for the spring and summer months among all three cases. Ice melt begins to occur in mid to late March and reaches its lowest level in September. Except for the Chukchi

Sea, NSIDC values are greater in the western Arctic during spring and summer months compared to all three RASM runs.

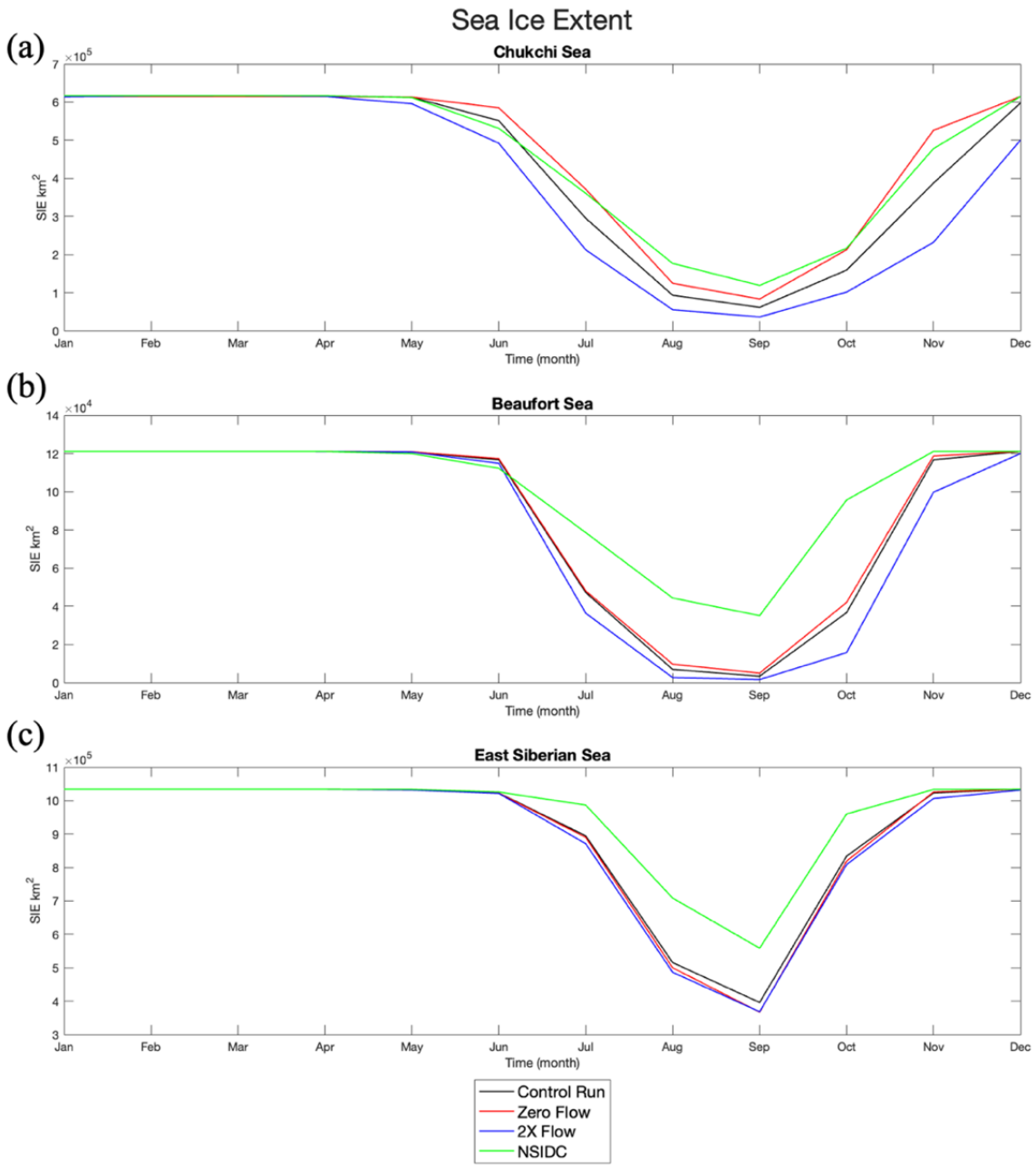

Mean annual cycle sea ice extent comparison for the (a) Chukchi, (b) Beaufort, and (c) East Siberian seas. The black line is the Control Run, the red line is the Zero Flow, the blue line is the 2X Flow, and the green line is NSIDC data.

Figure 22. Comparison of Sea Ice Extent Mean Annual Cycle for Chukchi, Beaufort, and East Siberian Seas

2. Ocean Heat Content

Ocean heat content (OHC) was broken down into the three regions of the western Arctic as shown in Figure 23. Each region was then analyzed at a depth of 0–50m, which was considered adequate for analyzing the effects of heat on sea ice, as anything deeper would be unlikely to affect sea ice melt/growth.

For this layer, there is a positive trend for each RASM run throughout the 39-year period. Every region increases in overall heat content as well.

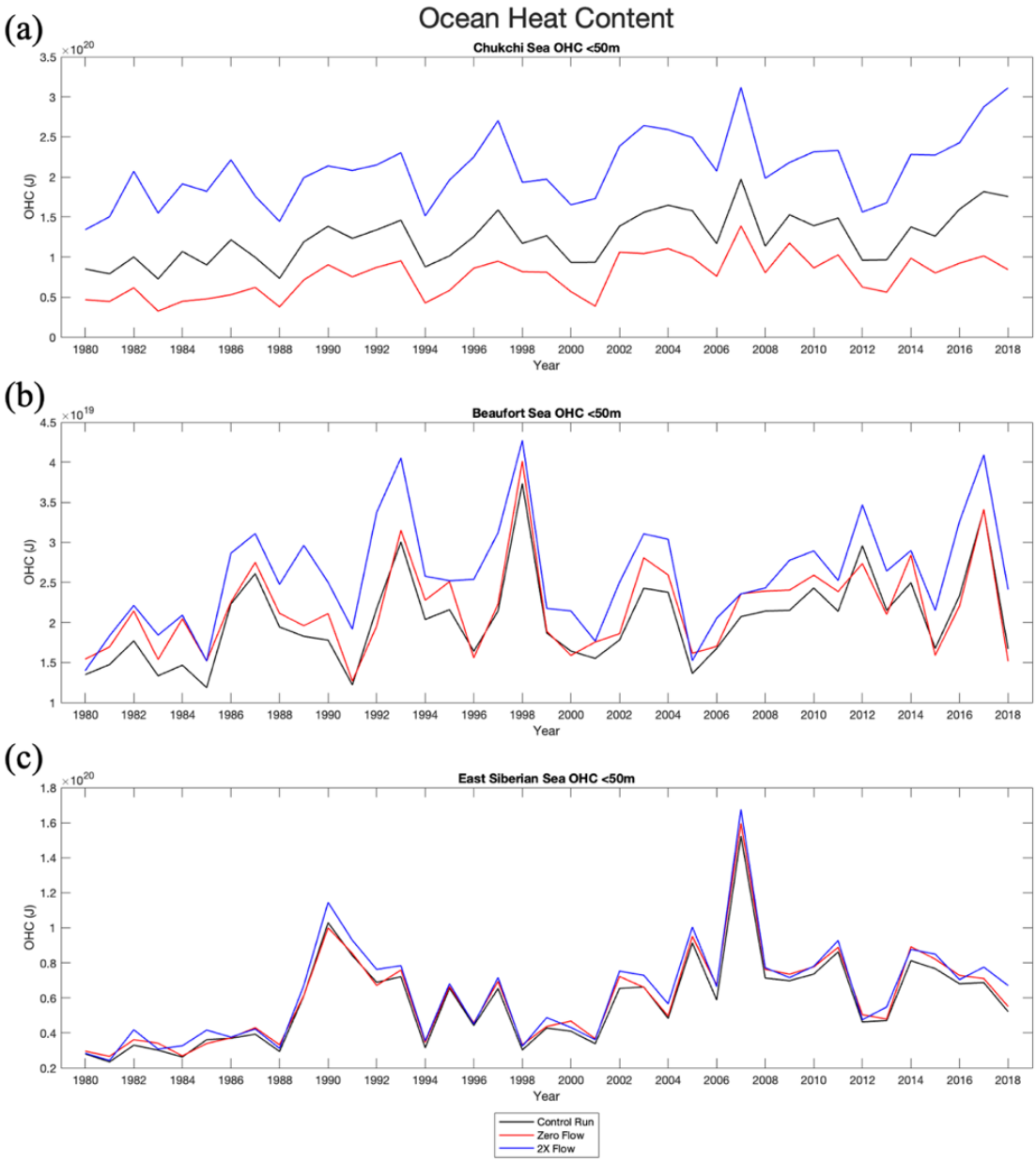

Monthly ocean heat content comparison for the (a) Chukchi, (b) Beaufort, and (c) East Siberian seas. The black line is the Control Run, the red line is the Zero Flow, and the blue line is the 2X Flow.

Figure 23. Ocean Heat Content Comparison at 0–50m in the Western Arctic Regions

The seasonal trends for OHC in the 0–50m layer correspond to seasonal heating and cooling in the western Arctic region (Figure 24). The largest amount of OHC occurs in the late summer months and peaks in September.

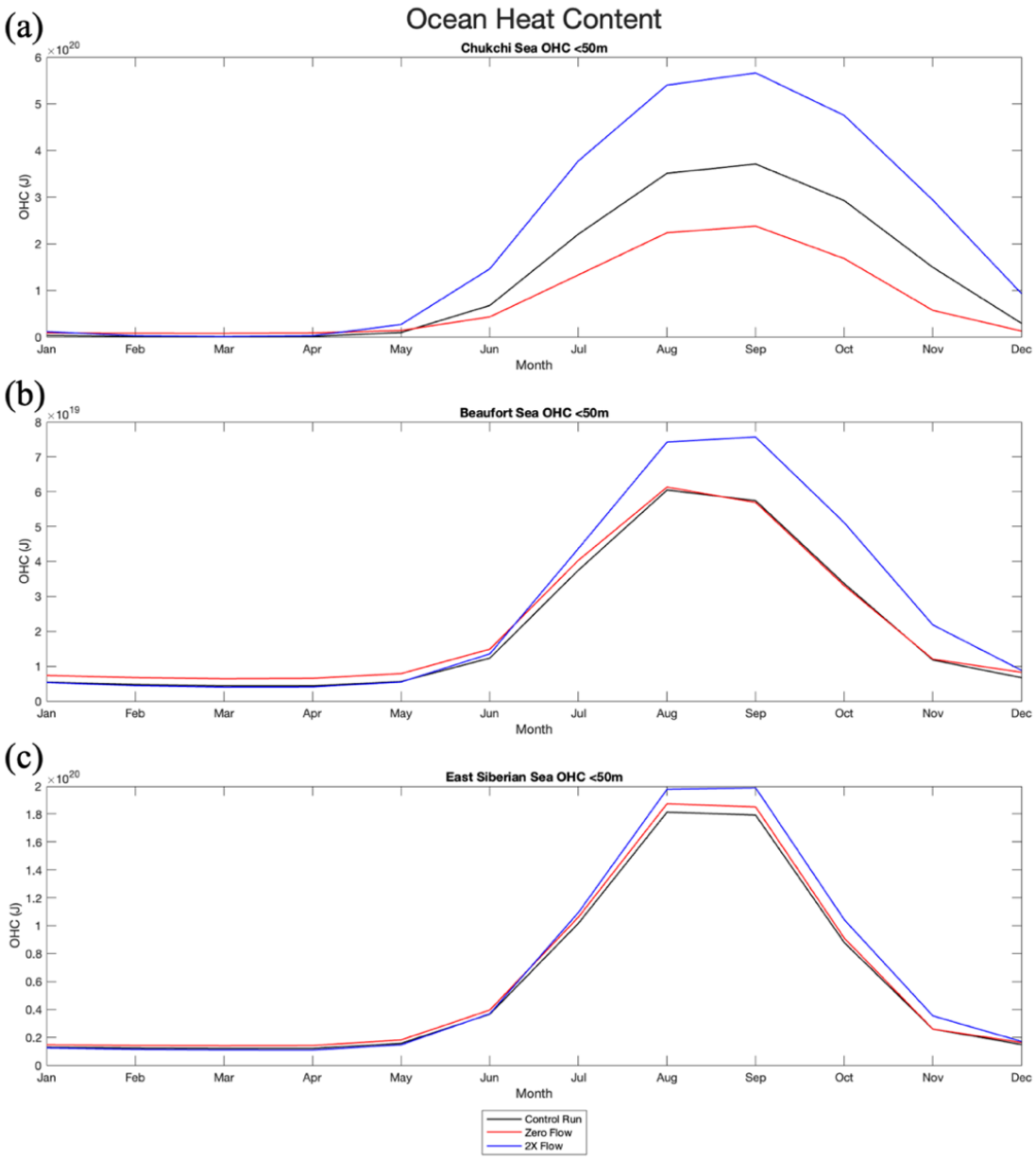

Annual cycle of monthly ocean heat content for the (a) Chukchi, (b) Beaufort, and (c) East Siberian seas. The black line is the Control Run, the red line is the Zero Flow, and the blue line is the 2X Flow.

Figure 24. Annual Cycle of Monthly Ocean Heat Content at 0–50m in the Western Arctic Regions

3. Temperature

Annual mean trends for temperature follow relatively closely with OHC annual trends in all three cases (Figure 25).

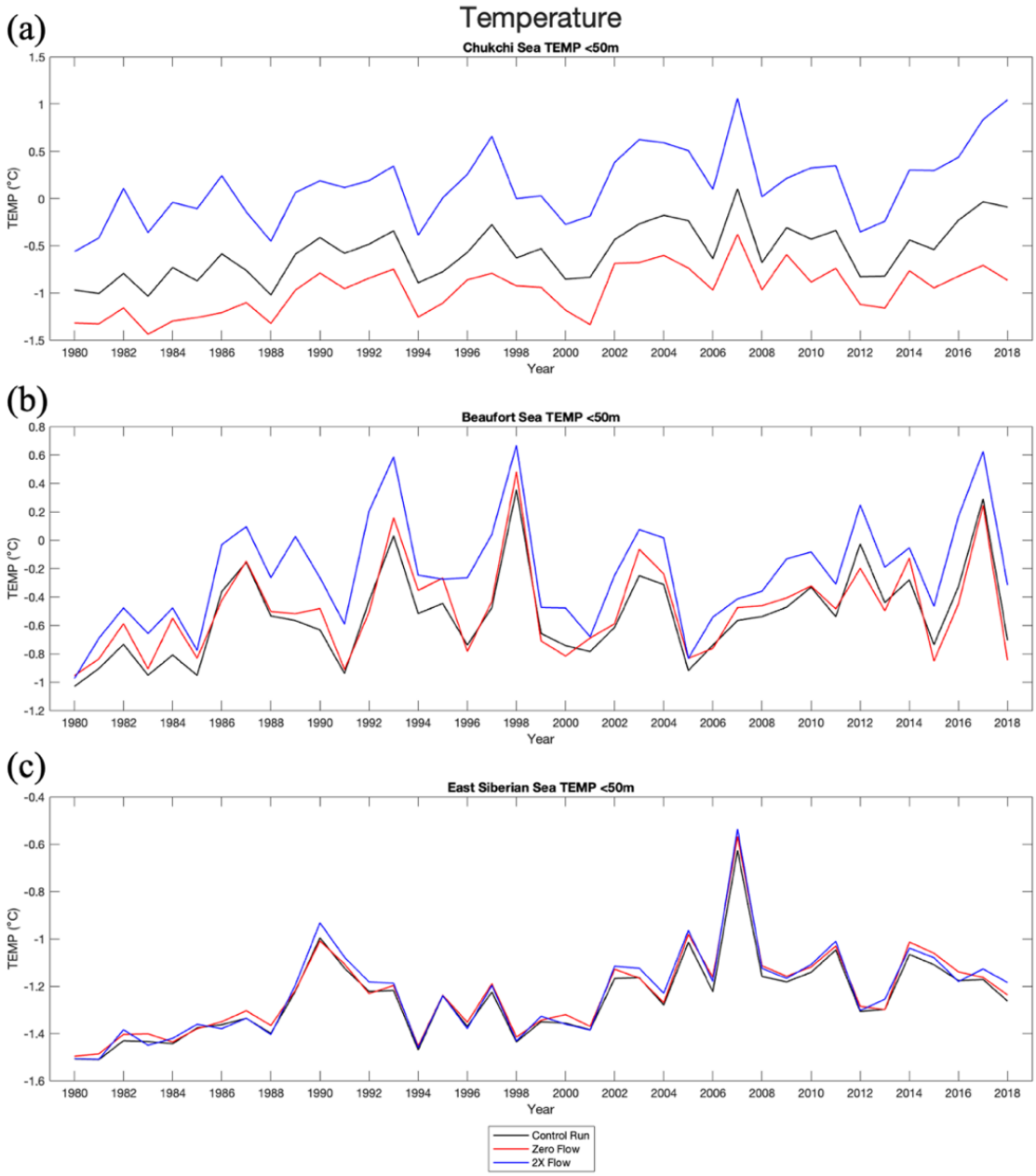

Monthly temperature comparison at depths of 0–50m for the (a) Chukchi, (b) Beaufort, and (c) East Siberian seas. The black line is the Control Run, the red line is the Zero Flow, and the blue line is the 2X Flow.

Figure 25. Temperature Comparison at 0–50m in the Western Arctic Regions

Monthly mean temperature values closely resemble those that were obtained for the monthly mean OHC values (Figure 26).

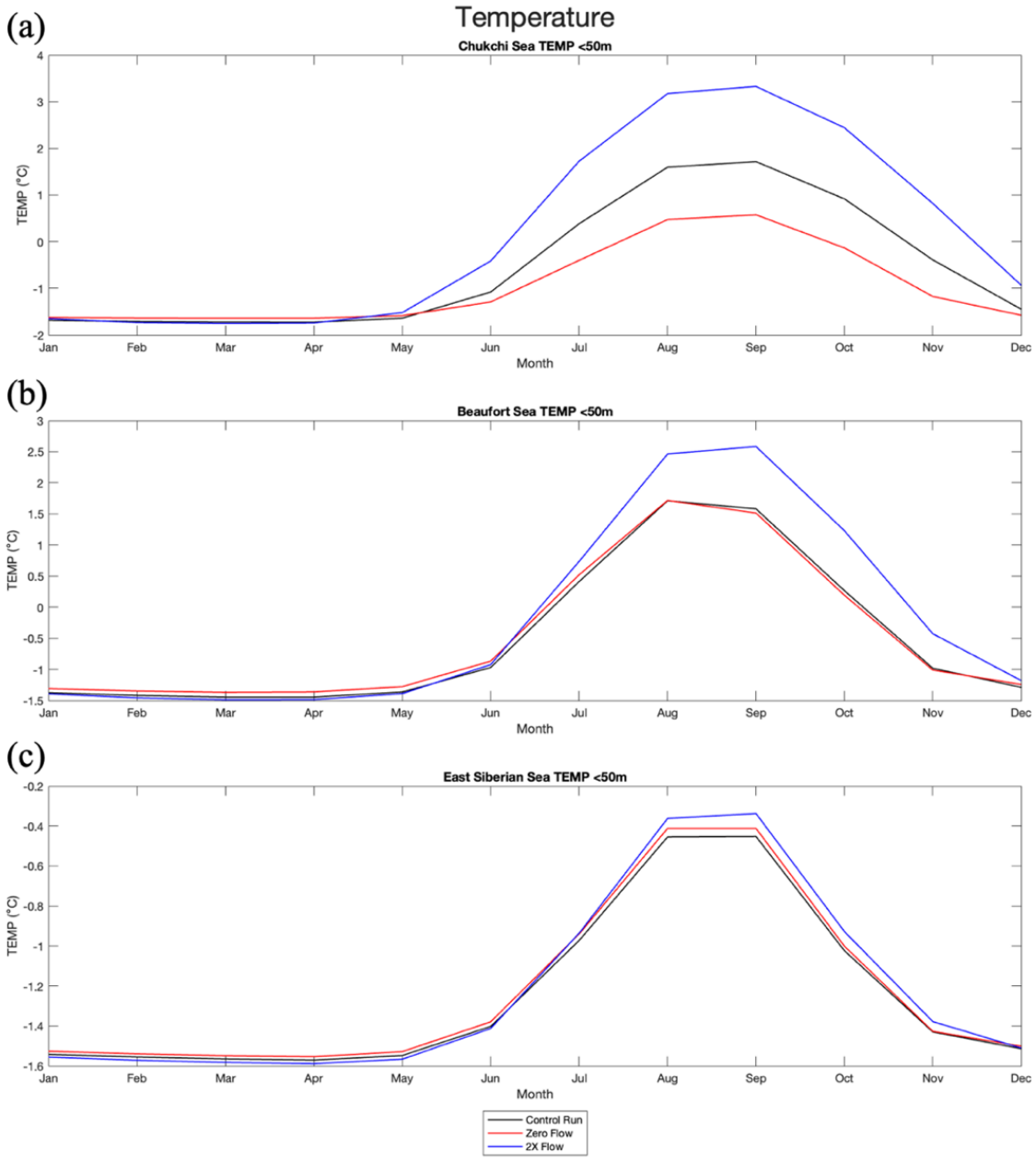

Annual cycle of monthly temperature at depths of 0–50m for the (a) Chukchi, (b) Beaufort, and (c) East Siberian seas. The black line is the Control Run, the red line is the Zero Flow, and the blue line is the 2X Flow.

Figure 26. Annual Cycle of Monthly Temperature at 0–50m in the Western Arctic Regions

4. Salinity

Salinity in the western Arctic (Figures 27 and 28) shows fresher water in the Zero Flow case for the Chukchi Sea, but not for the Beaufort and East Siberian seas. Figure 14 also shows this spatially, indicating how flow through the Bering Strait likely plays an important role in transporting freshwater off the western Arctic shelf.

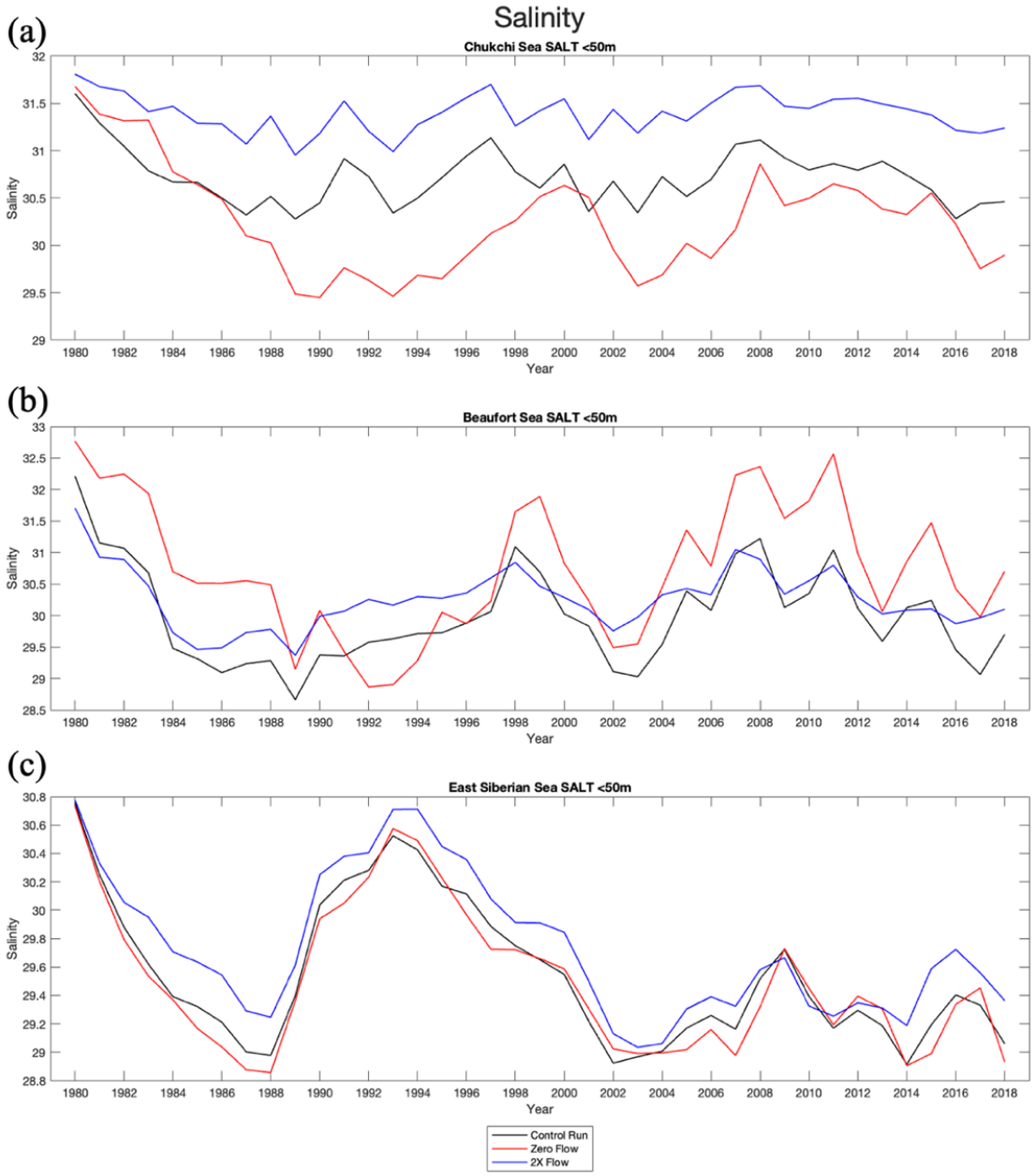

Monthly salinity comparison at depths of 0–50m for the (a) Chukchi, (b) Beaufort, and (c) East Siberian seas. The black line is the Control Run, the red line is the Zero Flow, and the blue line is the 2X Flow.

Figure 27. Salinity Comparison at 0–50m in the Western Arctic Regions

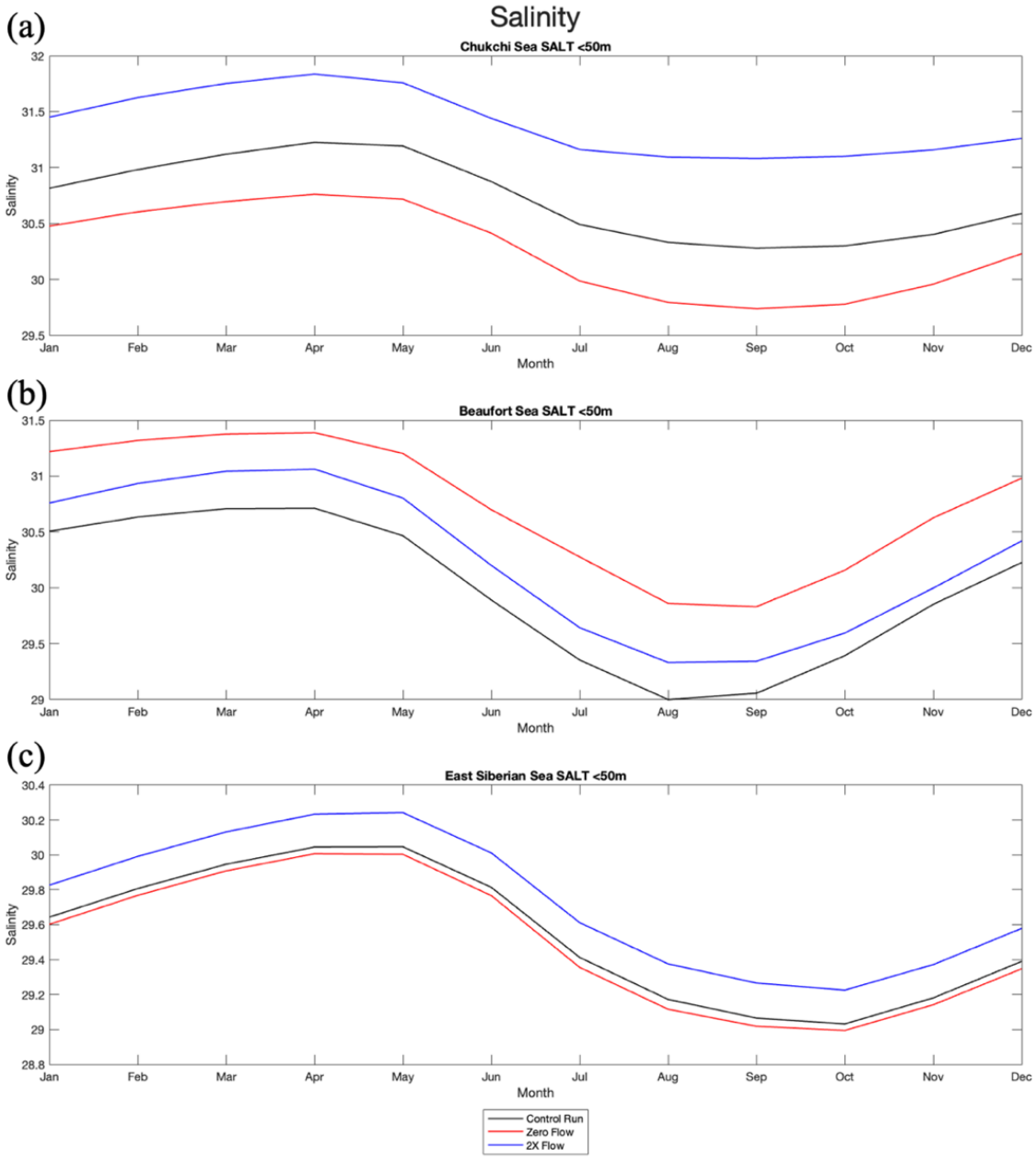

Annual cycle of monthly salinity at depths of 0–50m for the (a) Chukchi, (b) Beaufort, and (c) East Siberian seas. The black line is the Control Run, the red line is the Zero Flow, and the blue line is the 2X Flow.

Figure 28. Annual Cycle of Monthly Salinity at 0–50m in the Western Arctic Regions

5. Heat Convergence

Ocean heat convergence monthly mean timeseries and mean annual cycles are shown in Figures 29 and 30, respectively, and long term mean values are provided in Table 3. As shown, the greatest heat convergence occurs in the Chukchi region by a large margin. The 2X Flow case has nearly three times the heat convergence of the Control Run, and the Zero Flow hovers around zero terawatts (TW) for the total mean. There is not a noticeable increase over time in the heat transport for any region and interestingly, the 2X Flow case has more heat leaving the Beaufort and East Siberian Sea than the Zero Flow case.

When analyzing the mean annual cycle values for heat convergence (Figure 30), the largest amount of heat is transported into the Chukchi during the 2X Flow run. Within the Beaufort, the 2X Flow case has more heat entering the region in the summer months, but much less heat in the winter months than that from the Zero Flow case. Though the Zero Flow case does not have the peaks and valleys of the 2X Flow case, it does have a steady amount of heat entering the region during each month of the year.

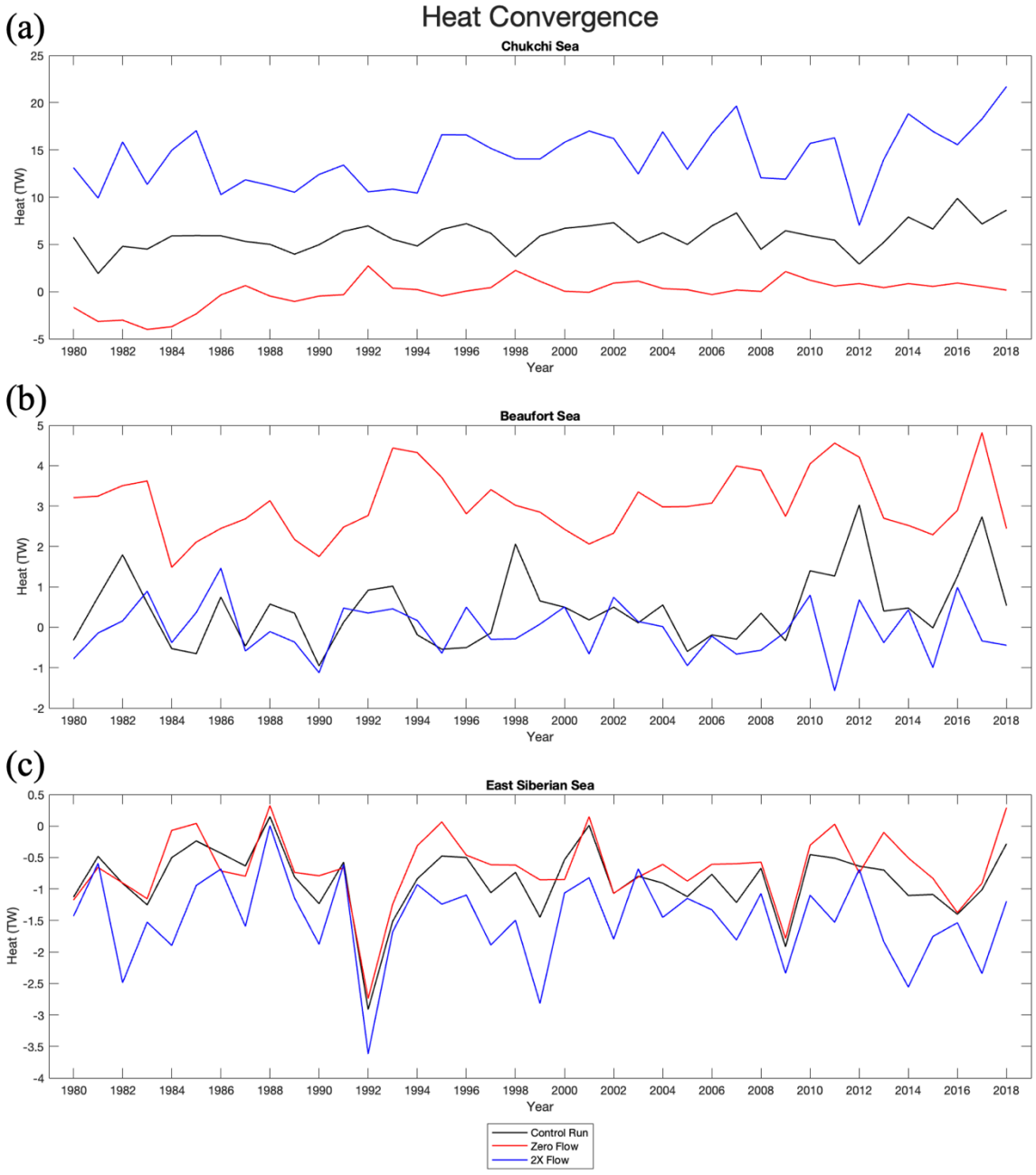

Monthly heat convergence comparison for the (a) Chukchi, (b) Beaufort, and (c) East Siberian seas. The black line is the Control Run, the red line is the Zero Flow, and the blue line is the 2X Flow.

Figure 29. Monthly Mean Ocean Heat Convergence (TW) in the Western Arctic Regions

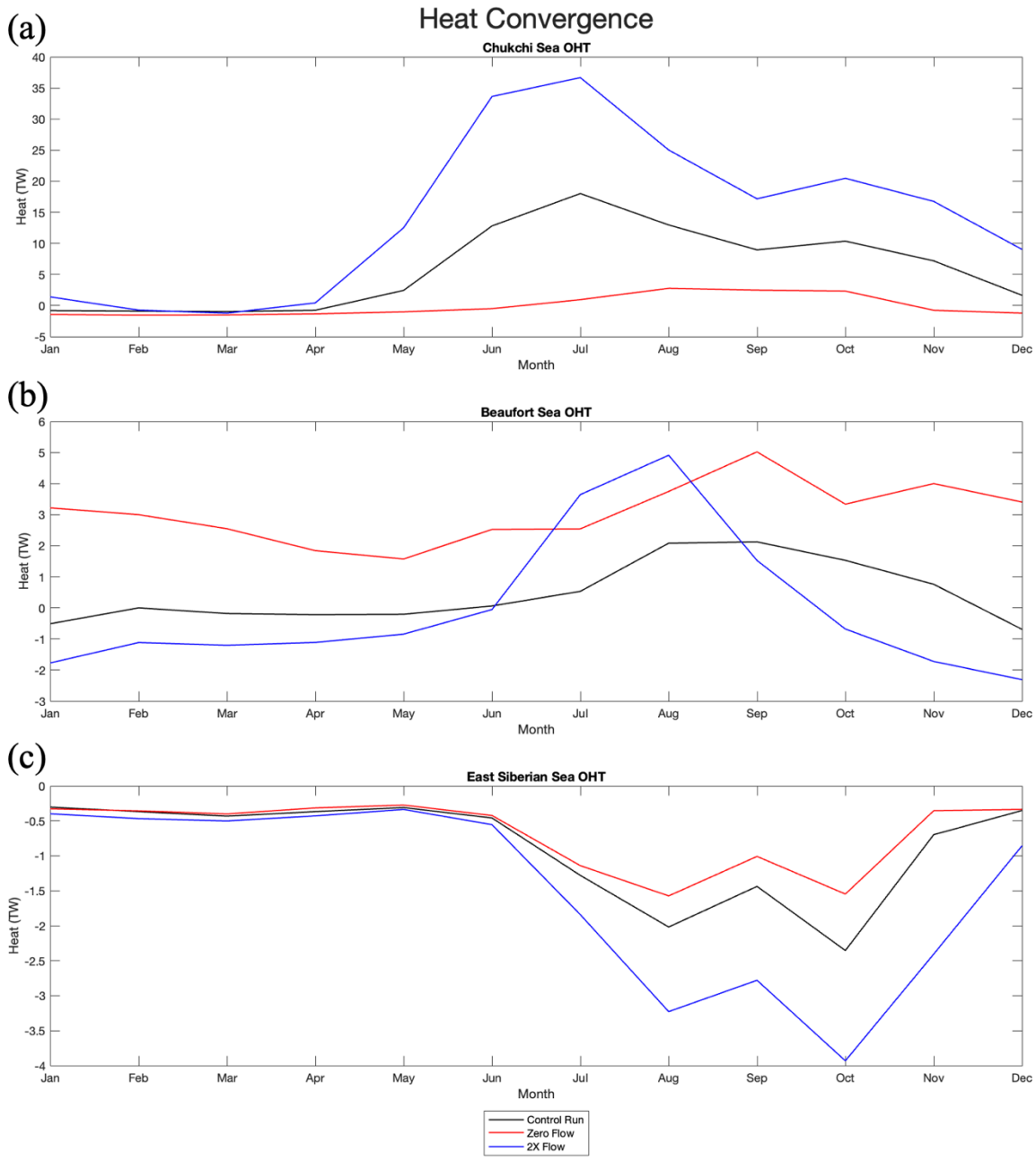

Mean annual cycle of heat convergence for the (a) Chukchi, (b) Beaufort, and (c) East Siberian seas. The black line is the Control Run, the red line is the Zero Flow, and the blue line is the 2X Flow.

Figure 30. Mean Annual Cycle of Ocean Heat Convergence (TW) in the Western Arctic Regions

Table 3. Long-term Mean (1980–2018) of Ocean Heat Convergence (TW) in the Western Arctic Regions

Ocean Heat Convergence (TW)		Zero Flow	Control Run	2X Flow Run
Chukchi Sea	Incoming	0.7238	7.5462	21.4177
	Outgoing	0.9903	1.9667	7.499
	Net	-0.2665	5.5795	13.9187
Beaufort Sea	Incoming	0.1212	0.1867	0.1408
	Outgoing	0.4916	0.3639	-0.1134
	Net	-0.3704	-0.1772	0.2542
East Siberian Sea	Incoming	1.4934	0.881	5.3382
	Outgoing	0.2612	1.3112	5.0448
	Net	1.2322	-0.4302	0.2934

6. Ice Melt Terms

There are three ice melt terms that were analyzed for each RASM run: top melt, bottom melt, and lateral melt.

a. Top Melt

The top melting terms for both monthly mean (Figure 31) and mean annual cycle (Figure 32) timeseries show the most variability among the RASM cases in the Chukchi Sea. The values for all three runs are the largest in the summer months and the Zero Flow case has greater values of top melt than the Control and 2X Flow runs. The Beaufort Sea has some variation during the summer months, but generally the three cases all agree with each other. There is little variation of top melt terms in the East Siberian Sea.

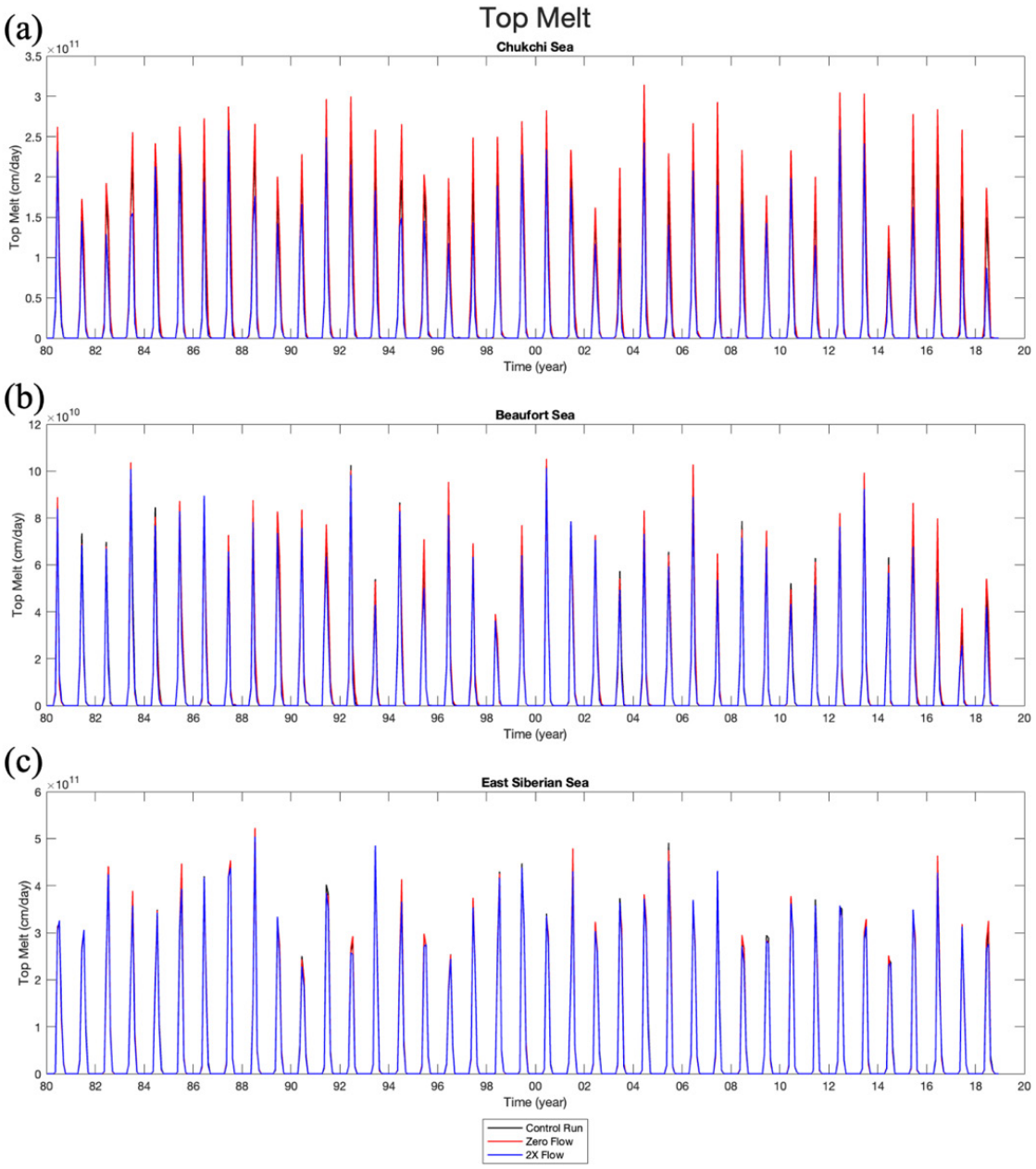

Monthly top melt comparison (cm/day) for the (a) Chukchi, (b) Beaufort, and (c) East Siberian seas. The black line is the Control Run, the red line is the Zero Flow, and the blue line is the 2X Flow.

Figure 31. Monthly Time Series of Top Melt in the Western Arctic Regions

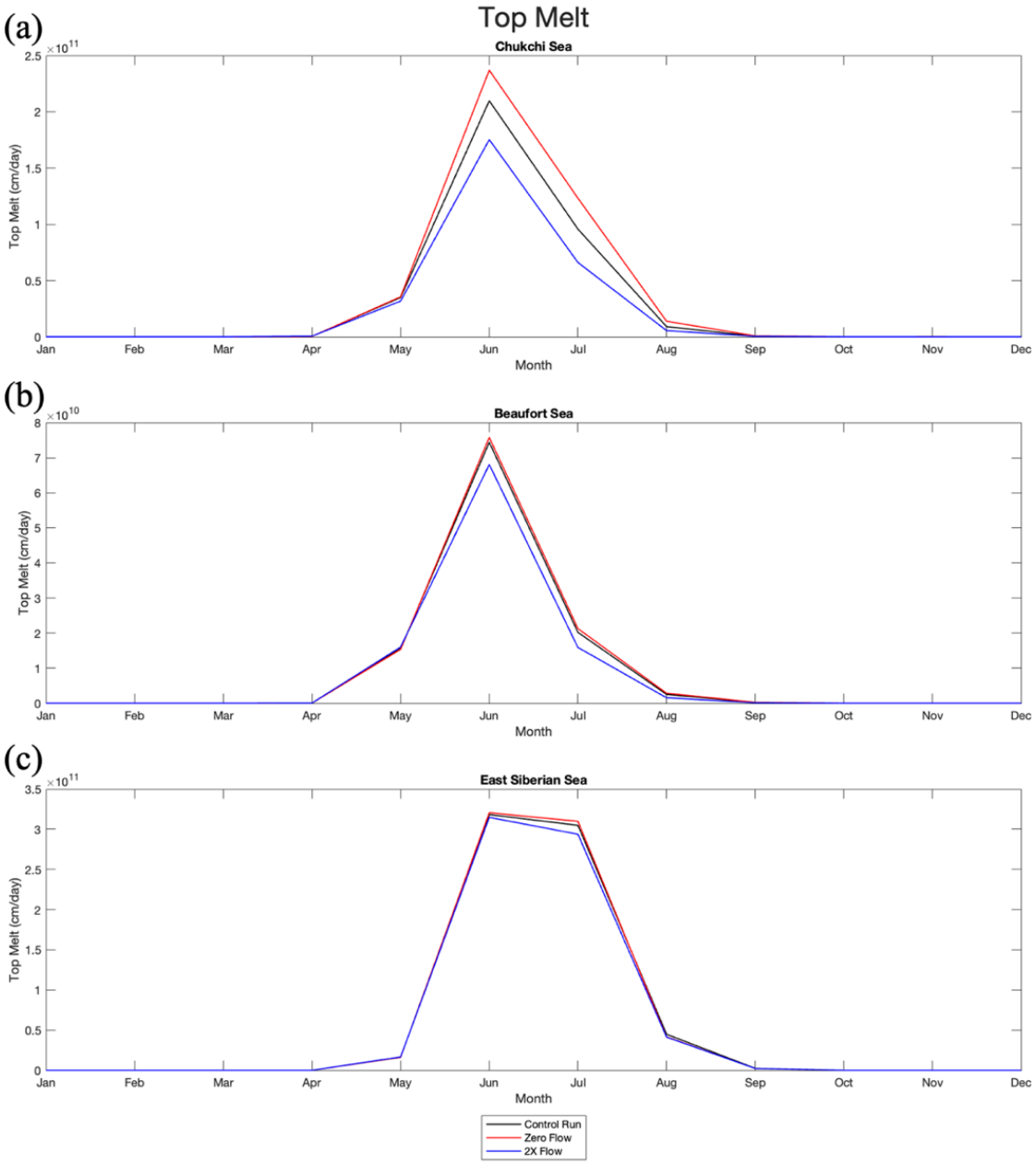

Mean annual cycle of top melt for the (a) Chukchi, (b) Beaufort, and (c) East Siberian seas. The black line is the Control Run, the red line is the Zero Flow, and the blue line is the 2X Flow.

Figure 32. Mean Annual Cycle of Top Melt in the Western Arctic Regions

b. Bottom Melt

The bottom melt terms are similar in magnitude to top melt, though they peak at different times of the year in the Chukchi Sea. The Zero Flow case still generates the largest values in the Chukchi, and all three cases are almost identical for the Beaufort and East Siberian Sea. An interesting observation for the bottom melt monthly mean timeseries is the "secondary peaks" occurring between the larger peaks. This implies there is bottom melting occurring in the late fall/early winter months, which is indicated in Figures 33 and 34.

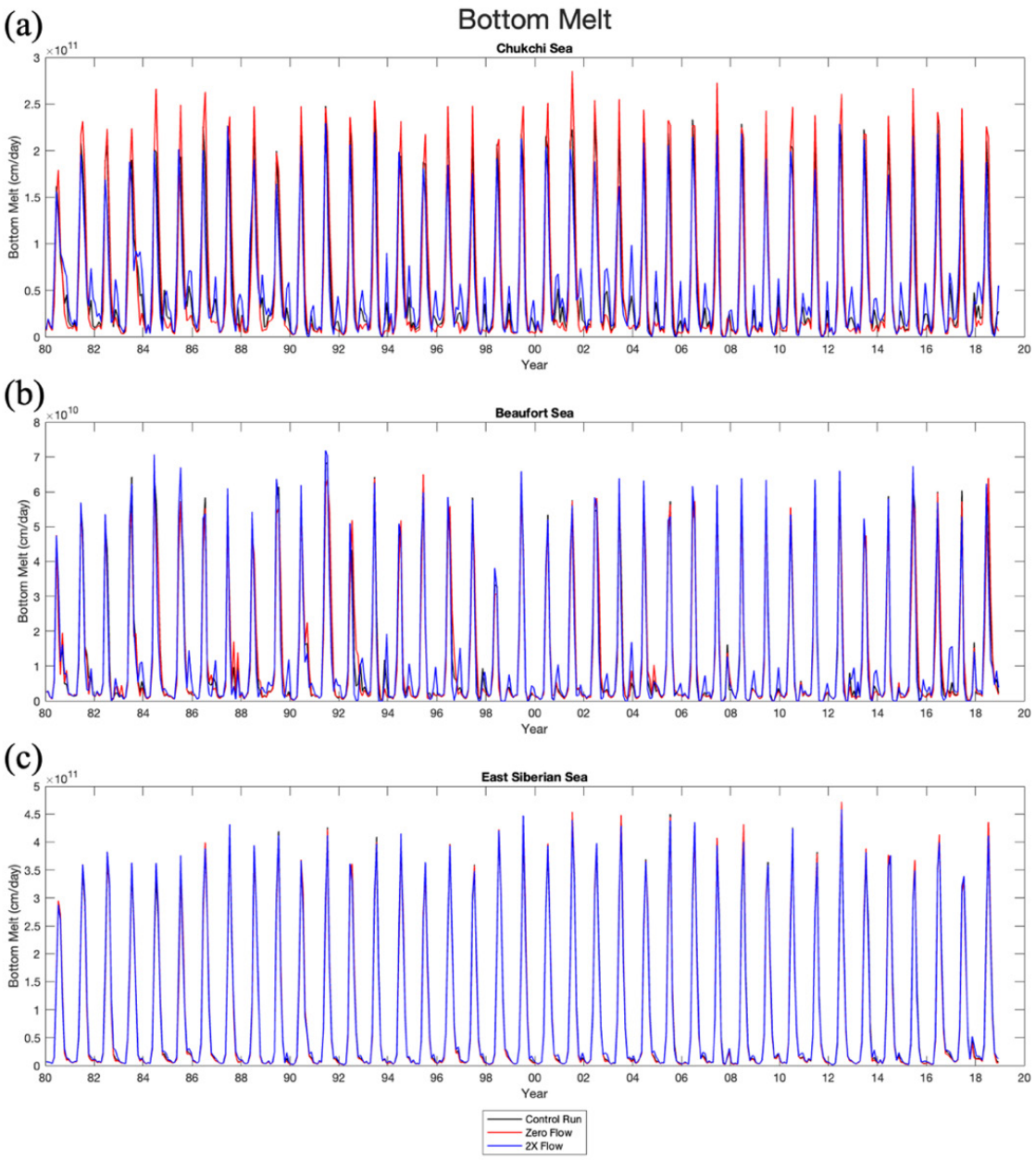

Monthly bottom melt for the (a) Chukchi, (b) Beaufort, and (c) East Siberian seas. The black line is the Control Run, the red line is the Zero Flow, and the blue line is the 2X Flow.

Figure 33. Monthly Time Series of Bottom Melt in the Western Arctic Regions

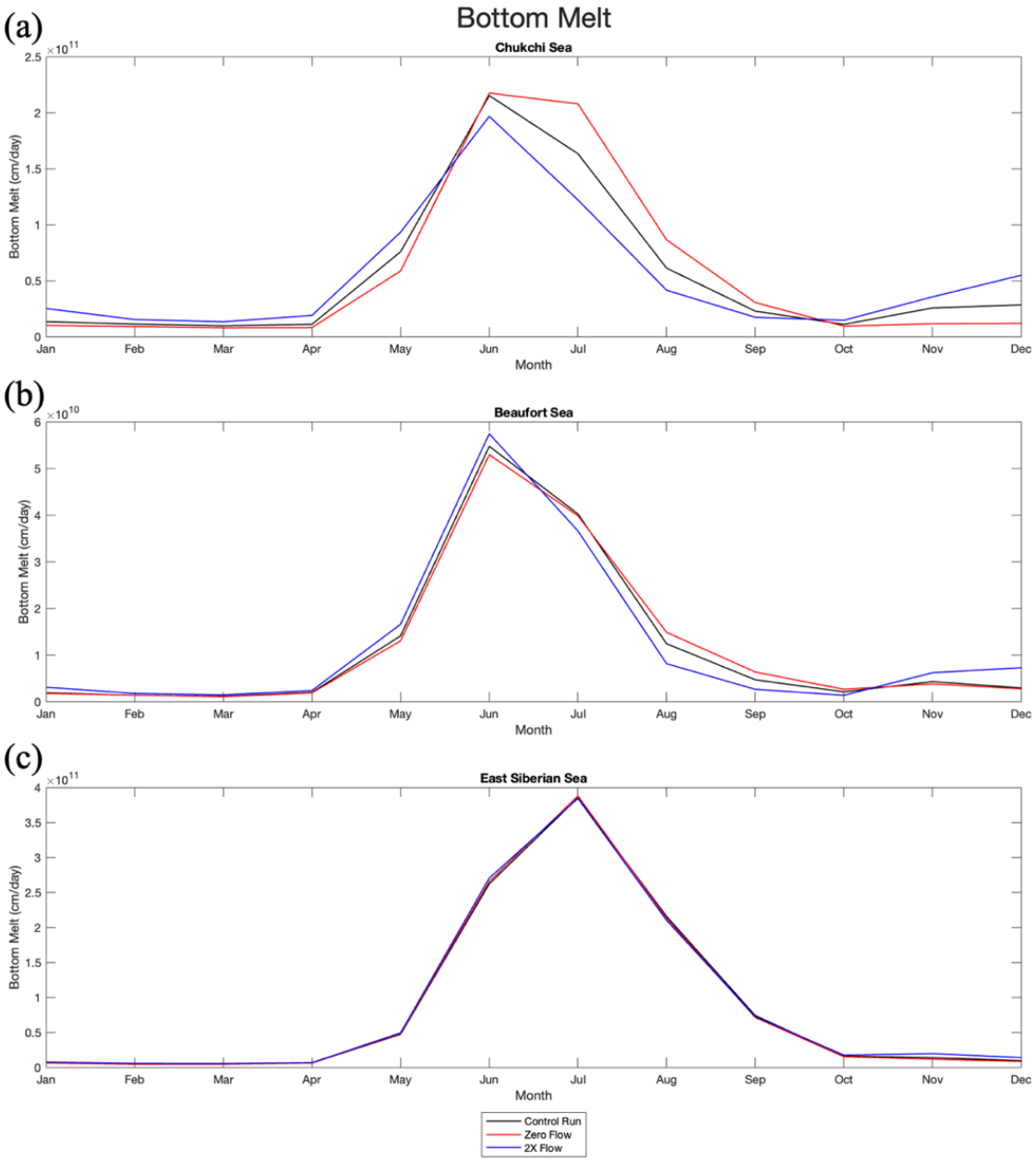

Mean annual cycle of bottom melt for the (a) Chukchi, (b) Beaufort, and (c) East Siberian seas. The black line is the Control Run, the red line is the Zero Flow, and the blue line is the 2X Flow.

Figure 34. Mean Annual Cycle of Bottom Melt in the Western Arctic Regions

c. Lateral Melt

As was the case for the top and bottom melt, the lateral melt has the most variability in the Chukchi Sea among the three runs, with the Zero Flow case being the

largest (Figures 35 and 36). There is very little difference in the Beaufort and East Siberian Sea values.

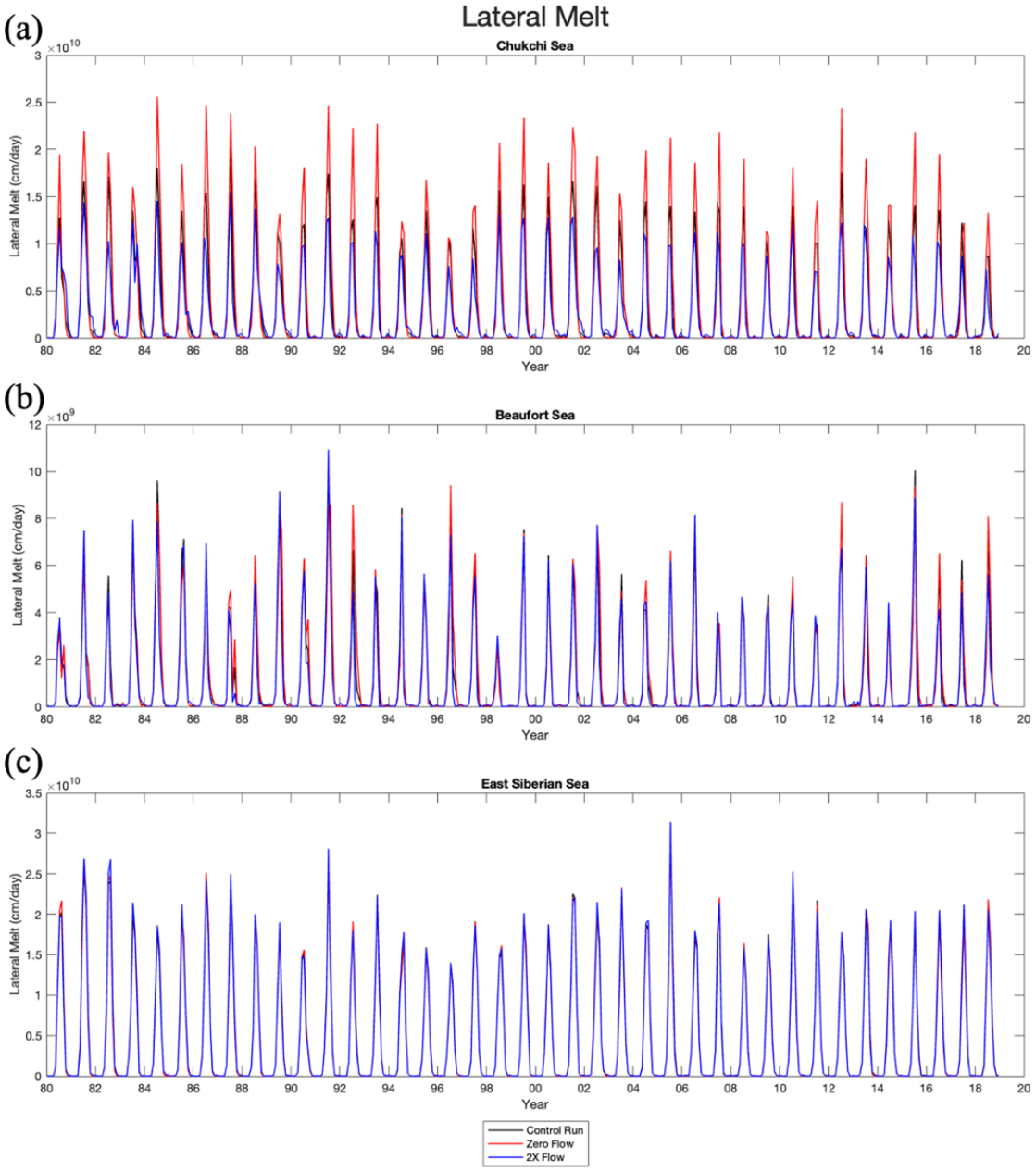

Monthly lateral melt for the (a) Chukchi, (b) Beaufort, and (c) East Siberian seas. The black line is the Control Run, the red line is the Zero Flow, and the blue line is the 2X Flow.

Figure 35. Monthly Time Series of Lateral Melt in the Western Arctic Regions

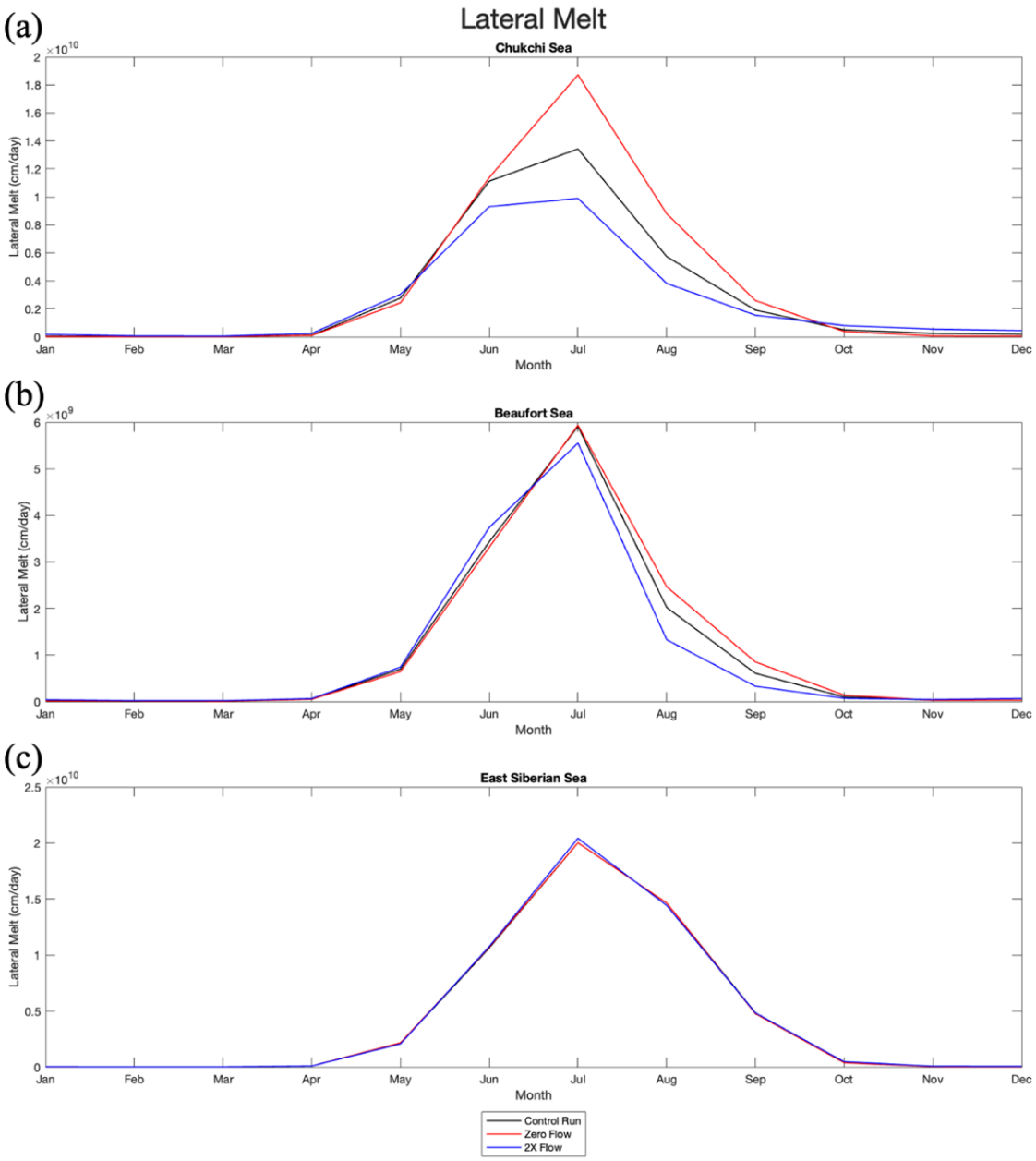

Mean annual cycle of lateral melt for the (a) Chukchi, (b) Beaufort, and (c) East Siberian seas. The black line is the Control Run, the red line is the Zero Flow, and the blue line is the 2X Flow.

Figure 36. Mean Annual Cycle of Lateral Melt in the Western Arctic Regions

7. Ice Growth Terms

There are two ice growth terms that were analyzed: basal growth and frazil growth.

a. Basal Growth

Basal growth shows a large range in the Chukchi Sea during November through January, with a spread of over $9x10^{10}$ cm/day among the cases in November (Figure 37 and 38). At this time, the Zero Flow case has the highest basal growth and the 2X Flow case has the lowest. The Beaufort and East Siberian seas show much smaller differences among the cases than the Chukchi Sea.

b. Frazil Growth

The frazil growth term shows little variation among runs except in the Chukchi Sea during November to January, with a spread of up to $3x10^{10}$ cm/day in November (Figures 39 and 40).

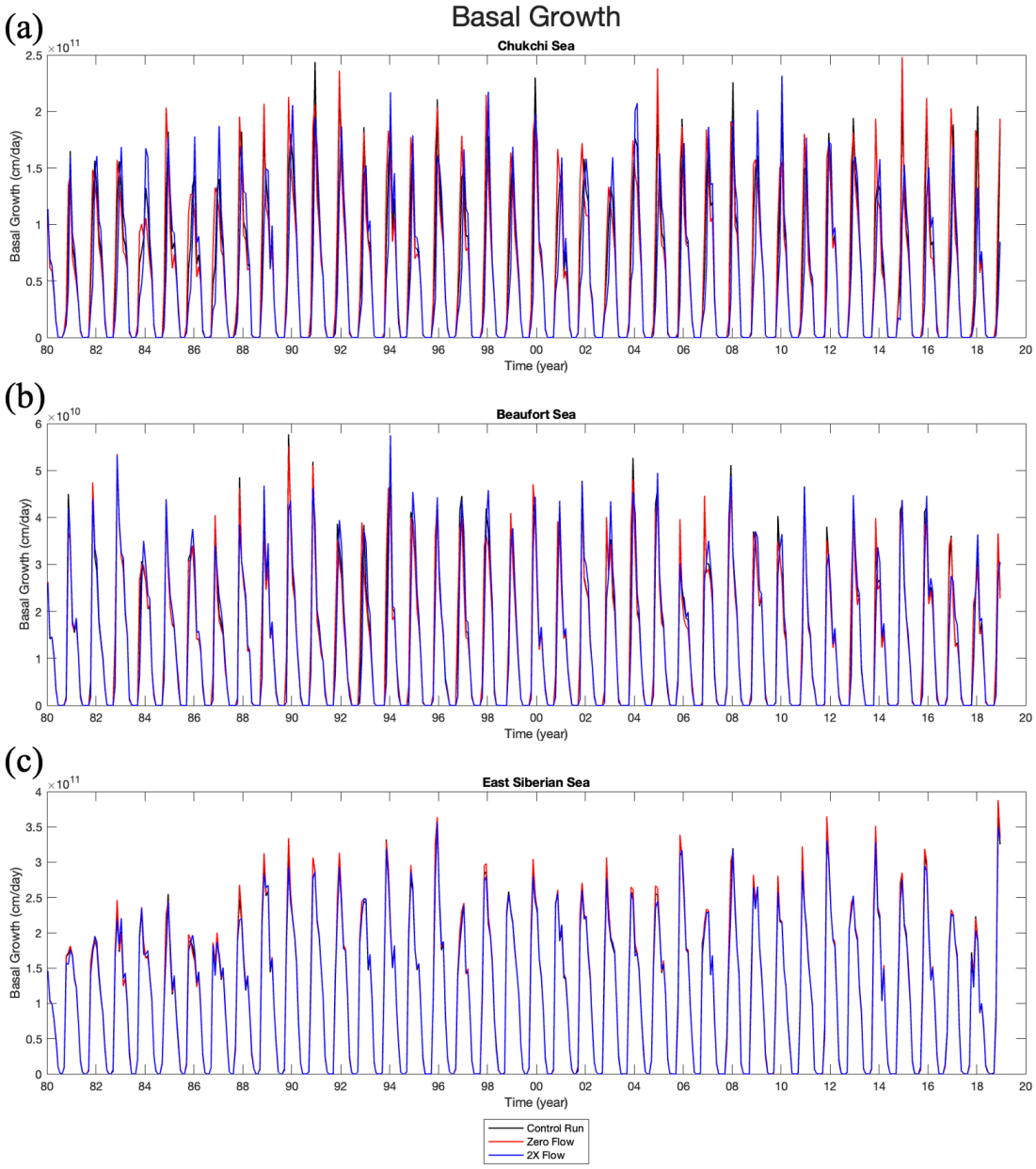

Monthly basal growth for the (a) Chukchi, (b) Beaufort, and (c) East Siberian seas. The black line is the Control Run, the red line is the Zero Flow, and the blue line is the 2X Flow.

Figure 37. Monthly Time Series of Basal Growth in the Western Arctic Regions

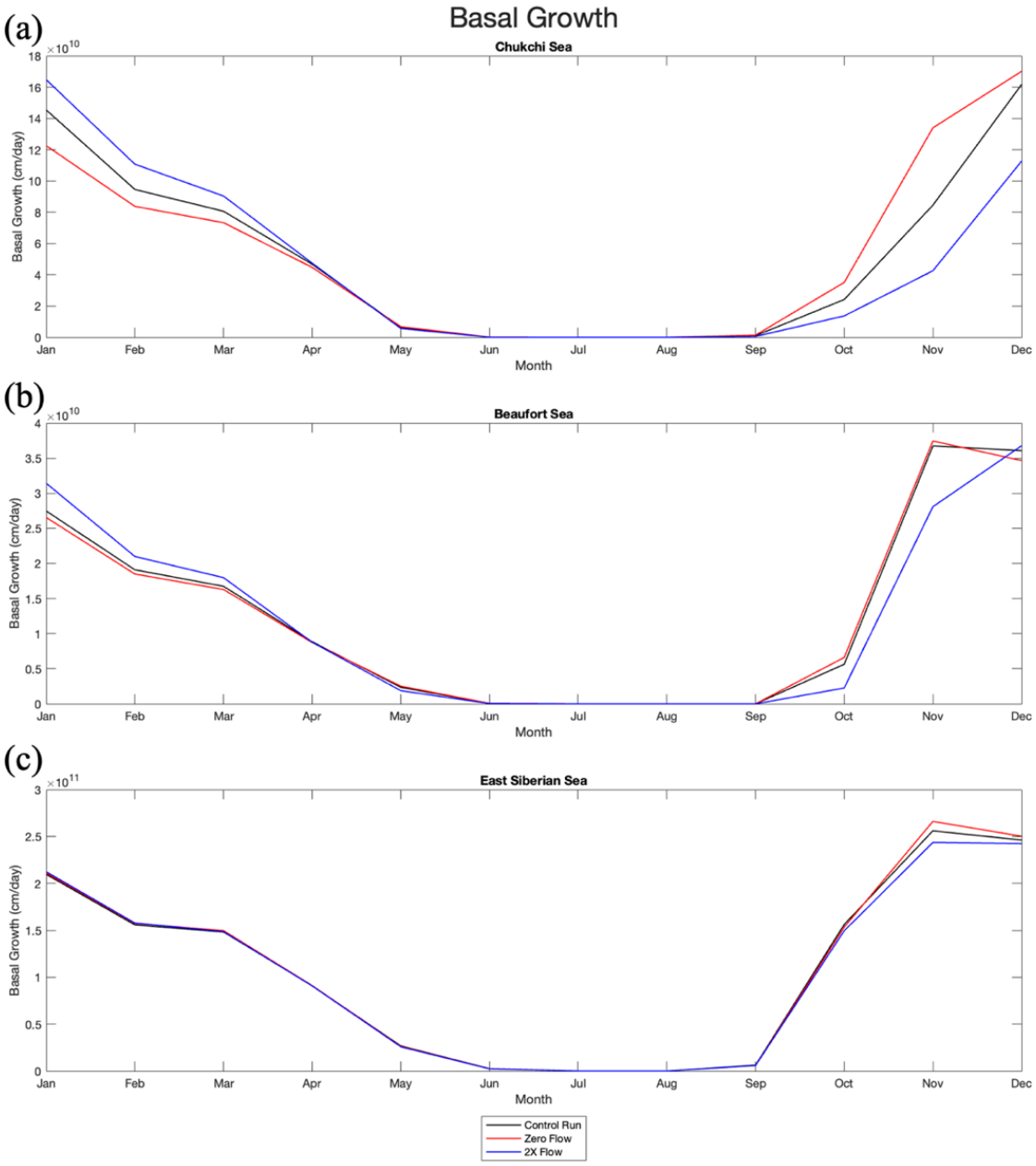

Mean annual cycle of basal growth for the (a) Chukchi, (b) Beaufort, and (c) East Siberian seas. The black line is the Control Run, the red line is the Zero Flow, and the blue line is the 2X Flow.

Figure 38. Mean Annual Cycle of Basal Growth in the Western Arctic Regions

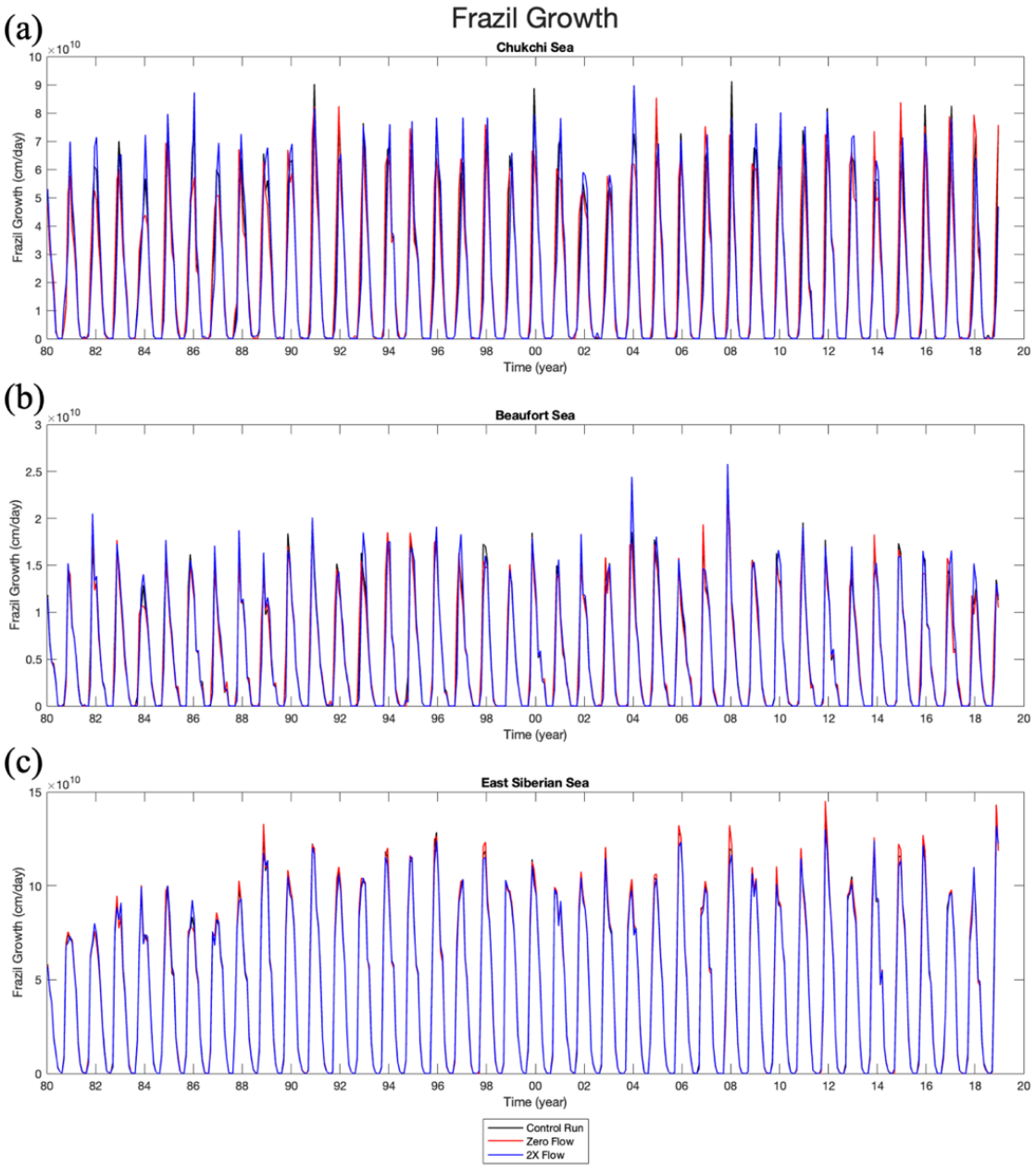

Monthly frazil growth for the (a) Chukchi, (b) Beaufort, and (c) East Siberian seas. The black line is the Control Run, the red line is the Zero Flow, and the blue line is the 2X Flow.

Figure 39. Monthly Time Series of Frazil Growth in the Western Arctic Regions

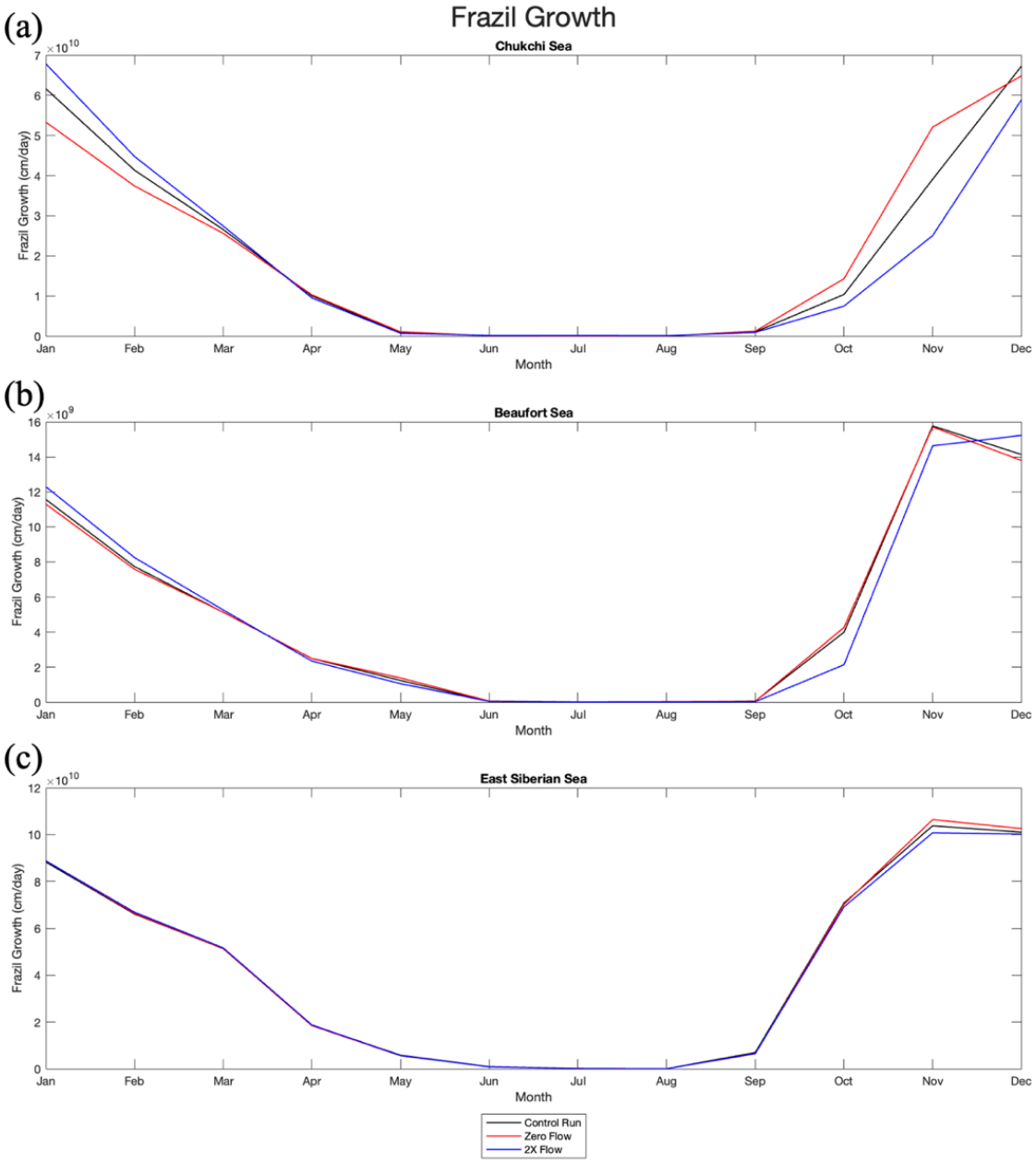

Mean annual cycle of frazil growth for the (a) Chukchi, (b) Beaufort, and (c) East Siberian seas. The black line is the Control Run, the red line is the Zero Flow, and the blue line is the 2X Flow.

Figure 40. Mean Annual Cycle of Frazil Growth in the Western Arctic Regions

8. Turbulent Heat Flux

Turbulent heat flux is broken down into two separate terms; latent heat and sensible heat for the ocean surface, both of which were analyzed. For easier heat comparisons, the latent and sensible heat flux terms were converted from W/m^2 to terawatts (TW) by multiplying the heat flux terms by their respective areas (i.e., our defined areas for the Chukchi, Beaufort, and East Siberian seas).

a. Latent Heat

Of all three cases, the 2X Flow case had the highest amount of latent heat lost from the ocean to the atmosphere (Figures 41 and 42). For the Chukchi Sea, some heat is transferred from the atmosphere to the ocean during the summer months, which coincides with the time frame following ice melt. Even higher values of latent heat loss to the atmosphere occur in autumn, with the greatest loss occurring in the 2X Flow case in November.

In the Beaufort Sea, the annual cycles do not have the same amount of separation among values in the three cases as is seen in the Chukchi and East Siberian seas. The 2X Flow case still has the largest magnitude of heat lost, which seasonally peaks in October.

For the East Siberian, the three cases seem to stay relatively close to each other both annually and seasonally for the entire 39-year run duration. Long term mean latent heat values for all western Arctic regions are listed in Table 4.

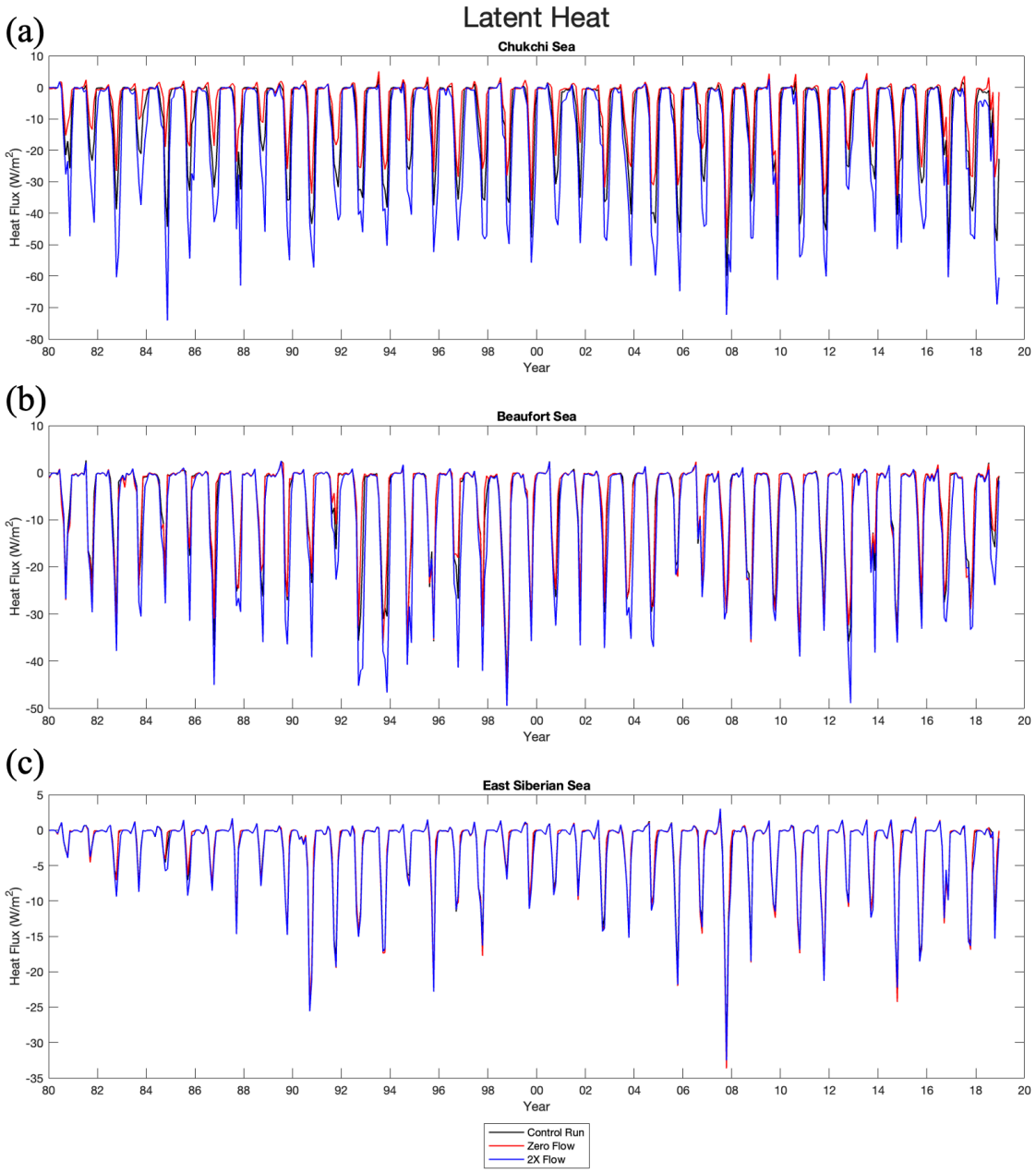

Monthly time series of latent heat for the (a) Chukchi, (b) Beaufort, and (c) East Siberian seas. The black line is the Control Run, the red line is the Zero Flow, and the blue line is the 2X Flow.

Figure 41. Monthly Time Series of Latent Heat in the Western Arctic Regions

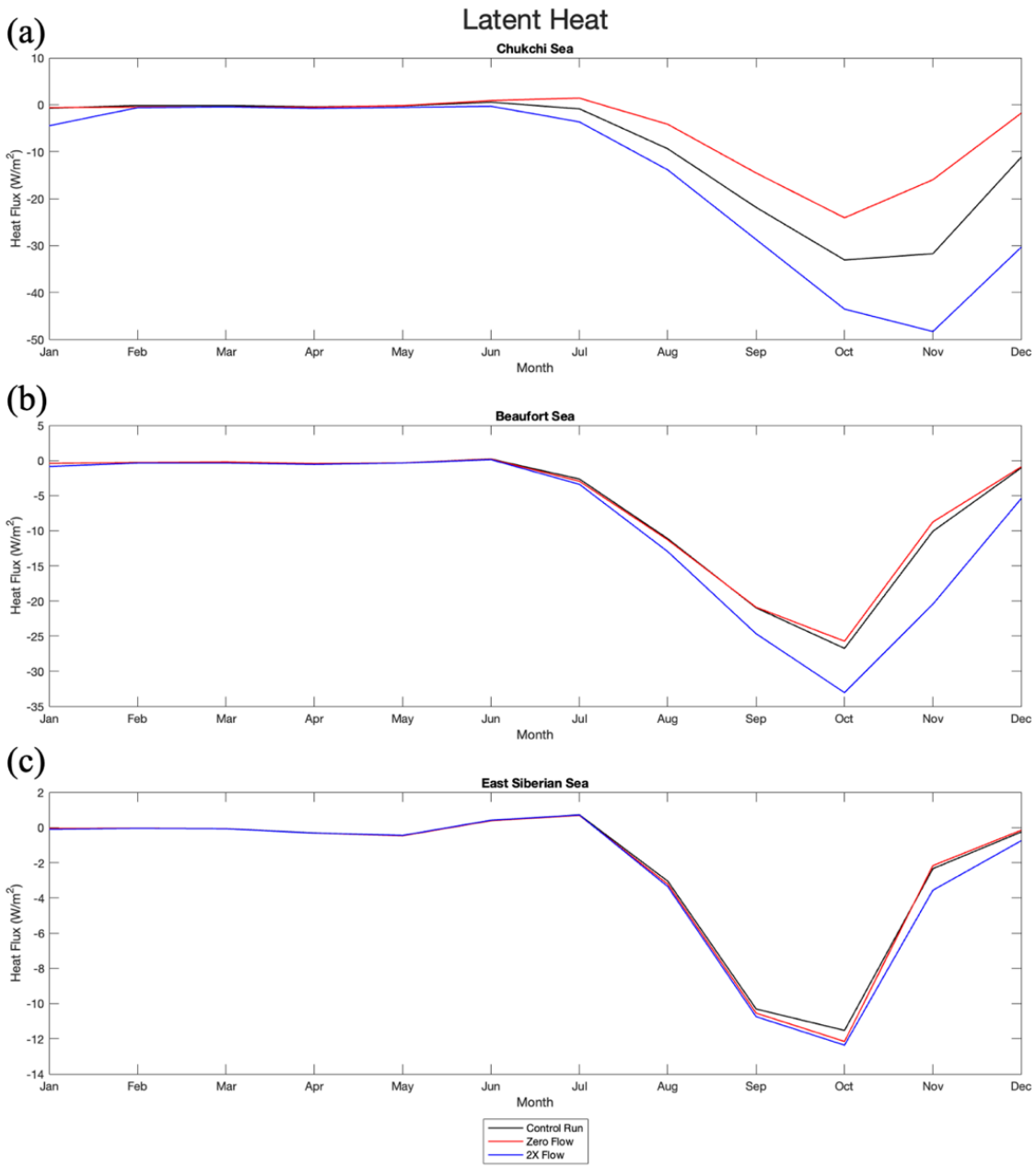

Mean annual cycle of latent heat for the (a) Chukchi, (b) Beaufort, and (c) East Siberian seas. The black line is the Control Run, the red line is the Zero Flow, and the blue line is the 2X Flow.

Figure 42. Mean Annual Cycle of Latent Heat in the Western Arctic Regions

Table 4. Long-Term Mean (1980–2018) Latent Heat in the Western Arctic

Latent Heat (TW)	Zero Flow	Control Run	2X Flow Run
Chukchi Sea	-3.10	-5.60	-9.01
Beaufort Sea	-0.73	-0.75	-1.03
East Siberian Sea	-2.42	-2.35	-2.64

b. Sensible Heat

Figures 43 and 44 show sensible heat following a similar pattern to the latent heat. The Chukchi Sea produces the highest sensible heat loss, and the East Siberian Sea has little variation among the three cases. Long term mean sensible heat values are listed in Table 5.

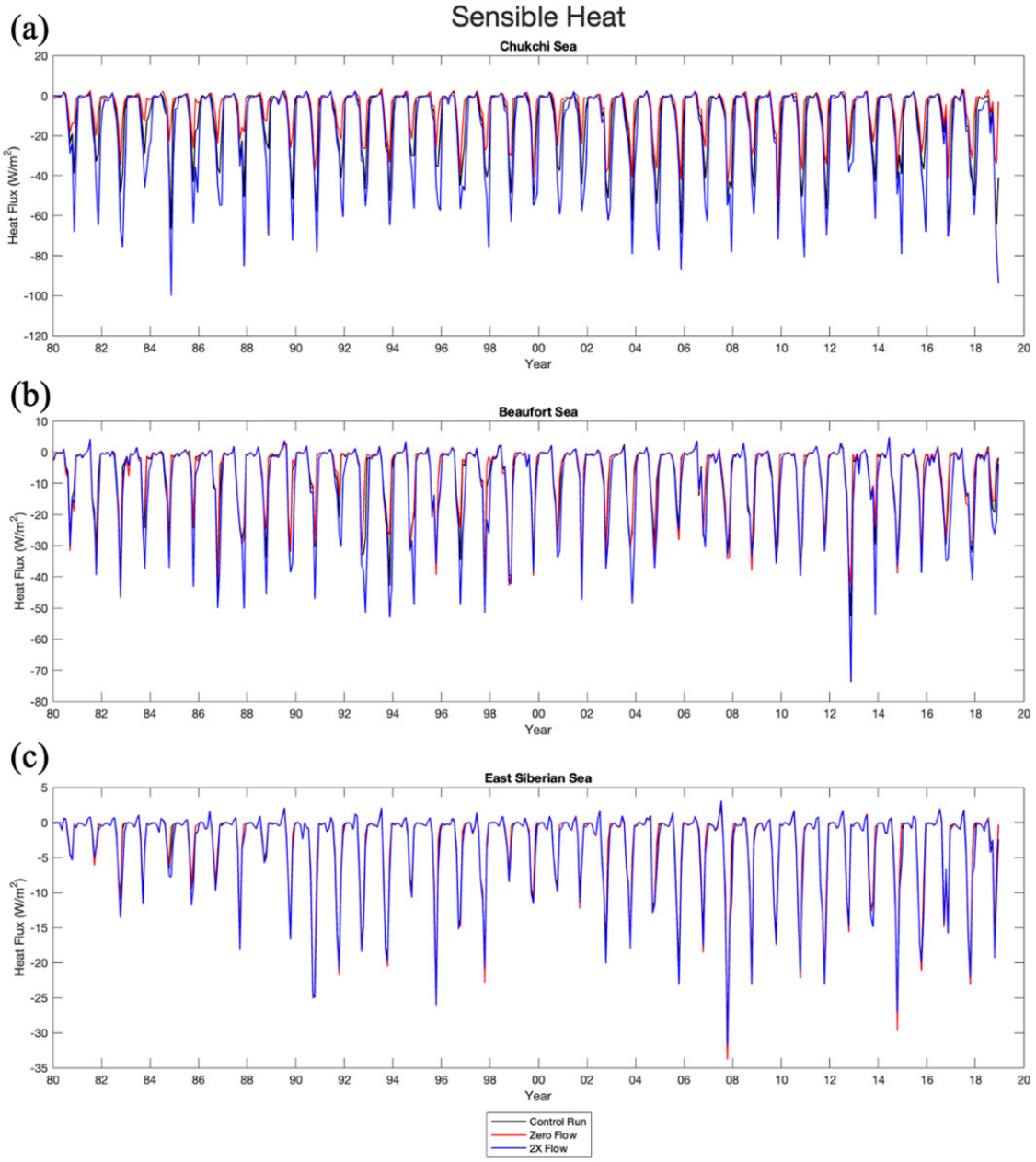

Monthly time series of sensible heat for the (a) Chukchi, (b) Beaufort, and (c) East Siberian seas. The black line is the Control Run, the red line is the Zero Flow, and the blue line is the 2X Flow.

Figure 43. Monthly Time Series of Sensible Heat in the Western Arctic Regions

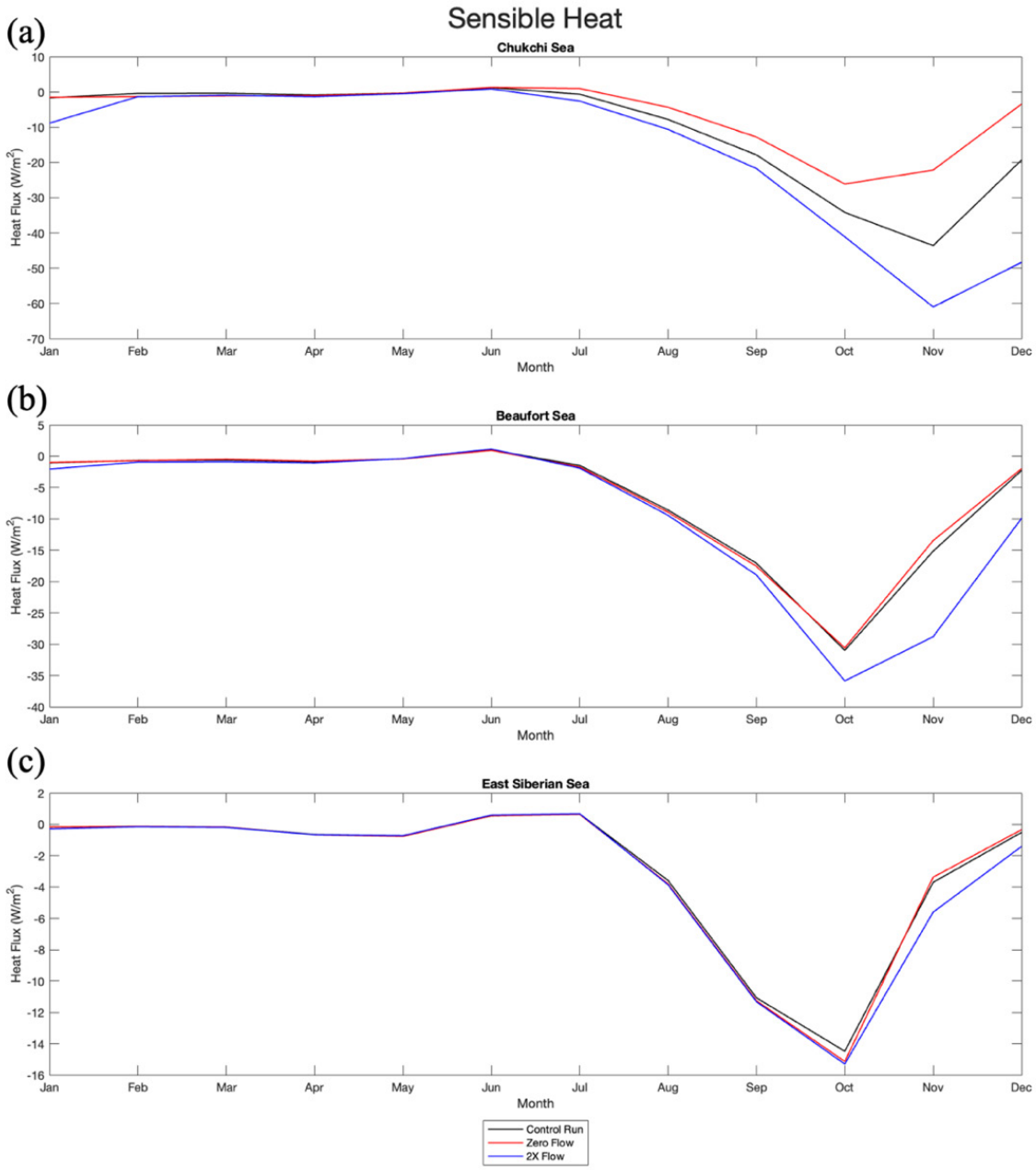

Mean annual cycle of sensible heat for the (a) Chukchi, (b) Beaufort, and (c) East Siberian seas. The black line is the Control Run, the red line is the Zero Flow, and the blue line is the 2X Flow.

Figure 44. Mean Annual Cycle of Sensible Heat in the Western Arctic Regions

Table 5. Long-Term Mean (1980–2018) Sensible Heat in the Western Arctic Regions

Sensible Heat (TW)	Zero Flow	Control Run	2X Flow Run
Chukchi Sea	-3.67	-6.44	-10.10
Beaufort Sea	-0.77	-0.79	-1.10
East Siberian Sea	-2.98	-2.93	-3.29

9. Radiative Heat Flux

To get a better representation of what is occurring in the western Arctic from a heating perspective, we analyzed the incoming and outgoing radiative heat for the ocean surface. Both short and longwave data was extracted from the RASM flux coupler and converted to watts using the same process as for latent and sensible heat.

a. Shortwave Heat

Figures 45 and 46 show the monthly time series and mean annual cycle of shortwave heat in the Chukchi, Beaufort, and East Siberian seas. Table 6 lists the long term mean values for shortwave radiation in the western Arctic.

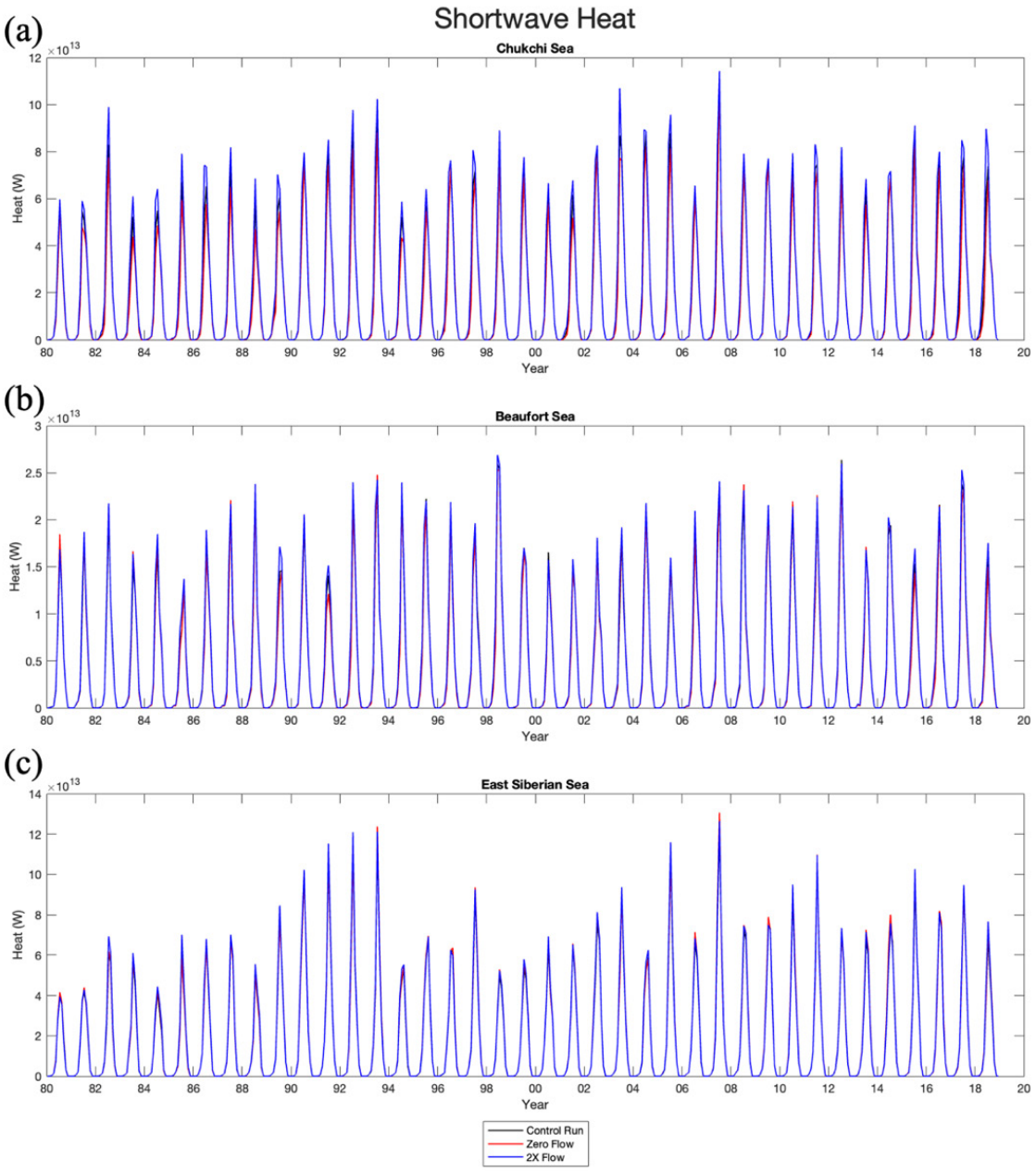

Monthly time series of shortwave heat for the (a) Chukchi, (b) Beaufort, and (c) East Siberian seas. The black line is the Control Run, the red line is the Zero Flow, and the blue line is the 2X Flow.

Figure 45. Monthly Time Series of Shortwave Heat in the Western Arctic Regions

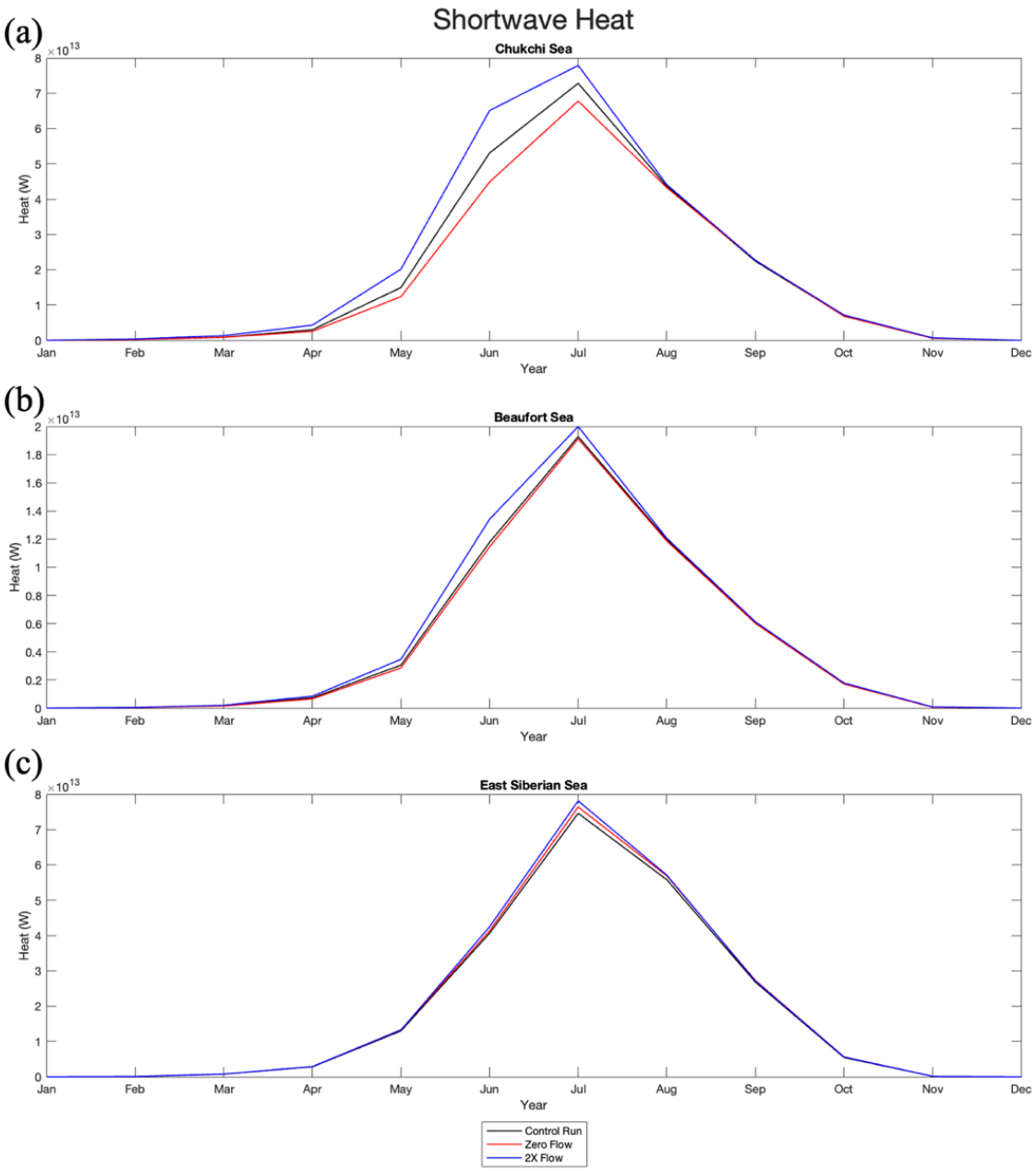

Mean annual cycle of monthly shortwave heat for the (a) Chukchi, (b) Beaufort, and (c) East Siberian seas. The black line is the Control Run, the red line is the Zero Flow, and the blue line is the 2X Flow.

Figure 46. Mean Annual Cycle of Monthly Shortwave Heat in the Western Arctic Regions

Table 6. Long-Term Mean (1980–2018) of Shortwave Radiation in the Western Arctic Regions

Shortwave Radiation (TW)	Zero Flow	Control Run	2X Flow Run
Chukchi Sea	16.8	18.2	20.3
Beaufort Sea	4.50	4.58	4.84
East Siberian Sea	18.7	18.3	18.9

b. Longwave Heat

Figures 47 and 48 show the monthly time series and mean annual cycle of longwave heat in the Chukchi, Beaufort, and East Siberian seas. Table 7 lists the long term mean values for shortwave radiation in the western Arctic. There were some erroneous values for the 2X Flow case in the summer months of 2011, the cause of which is still undetermined. Those values have been neglected in the time series, mean annual cycle, and long term mean calculations.

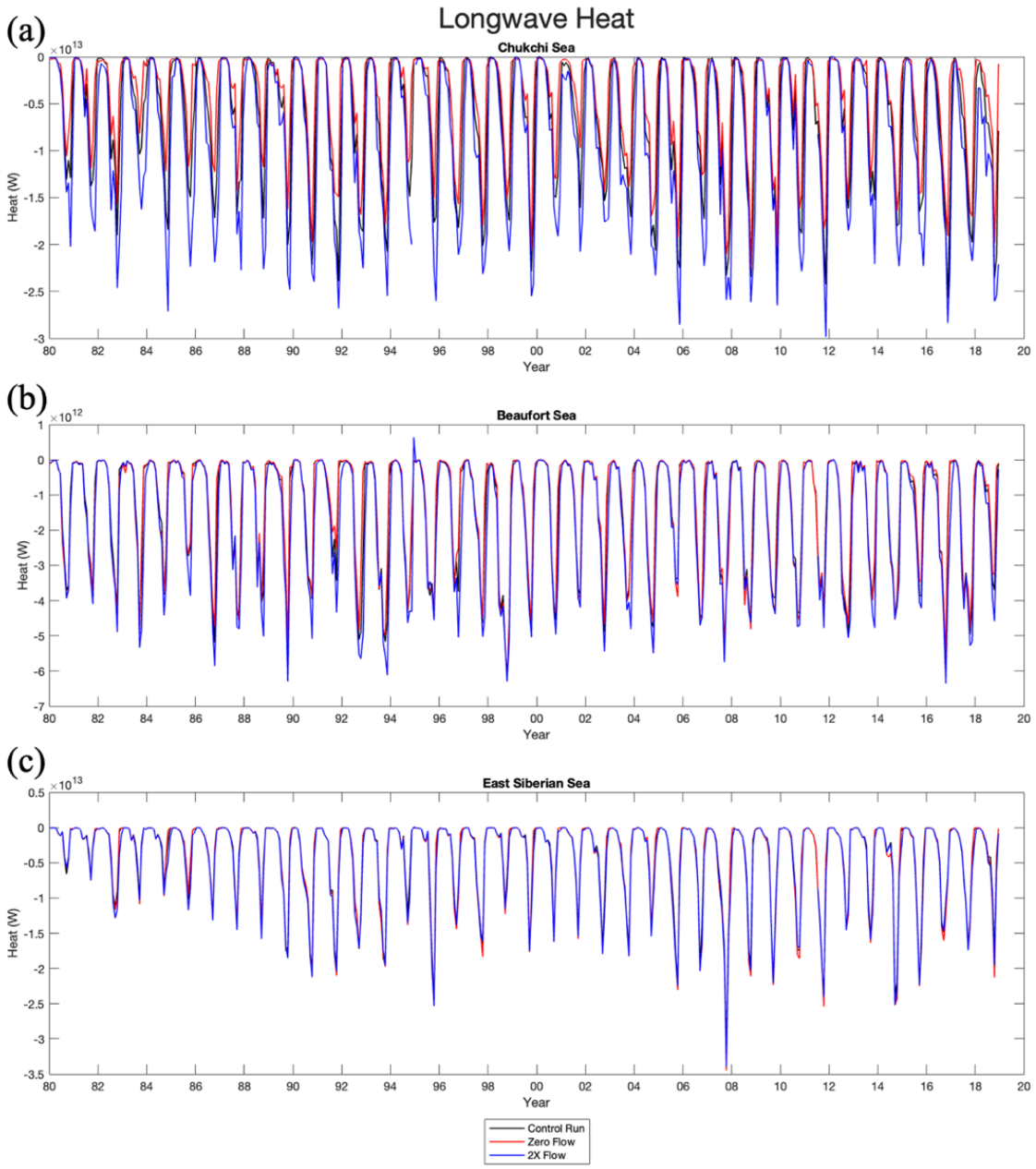

Monthly time series of longwave heat for the (a) Chukchi, (b) Beaufort, and (c) East Siberian seas. The black line is the Control Run, the red line is the Zero Flow, and the blue line is the 2X Flow.

Figure 47. Monthly Time Series of Longwave Heat in the Western Arctic Regions

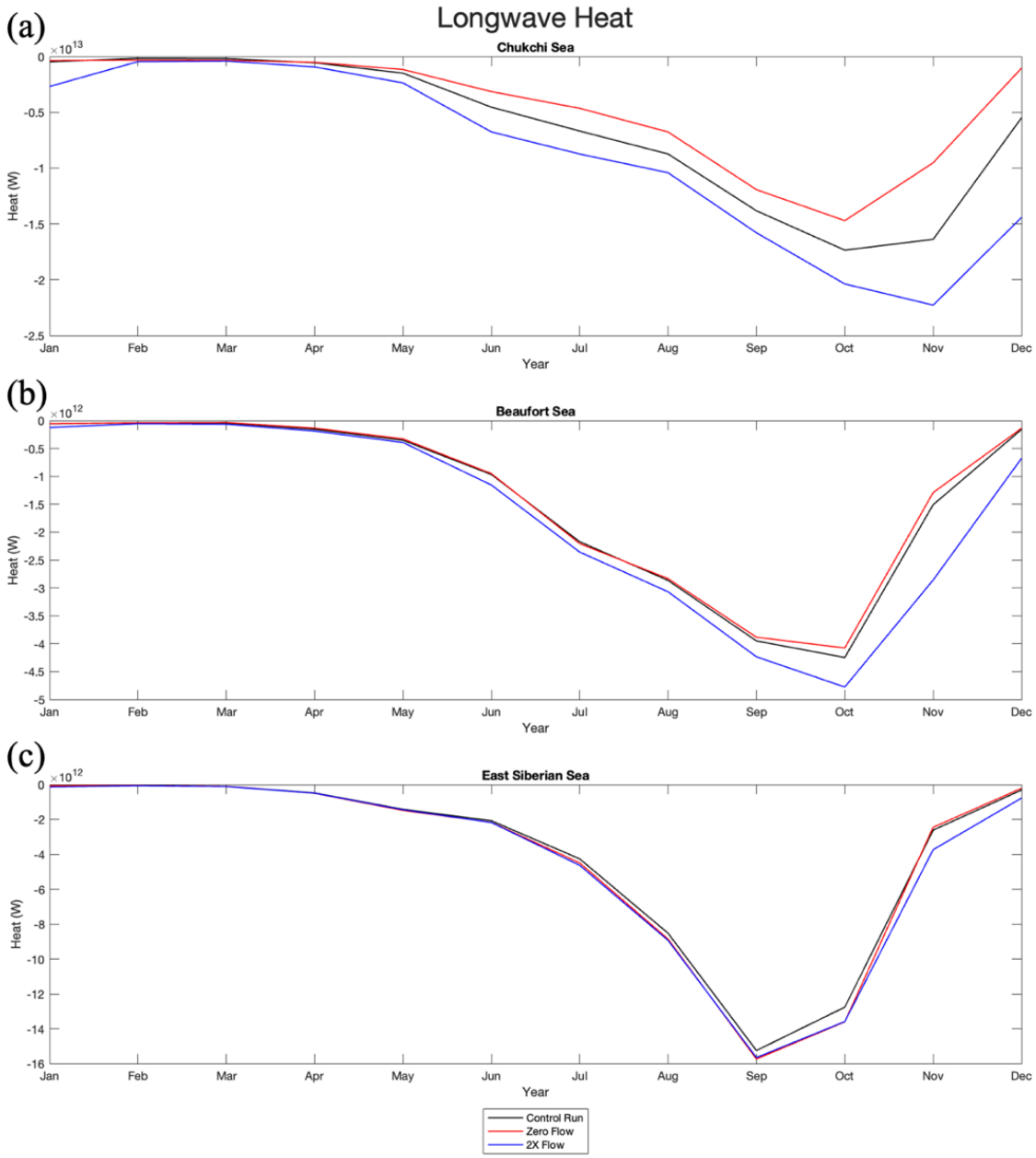

Mean annual cycle of monthly longwave heat for the (a) Chukchi, (b) Beaufort, and (c) East Siberian seas. The black line is the Control Run, the red line is the Zero Flow, and the blue line is the 2X Flow.

Figure 48. Mean Annual Cycle of Monthly Longwave Heat in the Western Arctic Regions

Table 7. Long Term Mean (1980–2018) of Longwave Radiation in the Western Arctic Regions

Longwave Radiation (TW)	Zero Flow	Control Run	2X Flow Run
Chukchi Sea	-4.53	-6.32	-8.43
Beaufort Sea	-1.33	-1.38	-1.62
East Siberian Sea	-4.14	-3.99	-4.16

10. Combining the Heat Parameters

The mean turbulent heat values (latent and sensible) for each region are listed separately and combined in Table 8. To get a better idea of the net heat content in the western Arctic Ocean from all the dynamic and thermodynamic processes, the individual terms from each source are listed for each region and for the entire western Arctic in Table 9. Next, all the heat terms were converted to TW (if not done already) and added together to find the net heat remaining within each of our defined regions in the western Arctic. These values are also listed in Table 9.

Table 8. Turbulent Heat Fluxes in the Western Arctic Regions

Turbulent Heat (Latent + Sensible) (TW)		Zero Flow	Control Run	2X Flow Run
Chukchi Sea	Latent	-3.10	-5.60	-9.01
	Sensible	-3.67	-6.44	-10.10
	Net	**-6.77**	**-12.04**	**-19.10**
Beaufort Sea	Latent	-0.73	-0.75	-1.03
	Sensible	-0.77	-0.79	-1.10
	Net	**-1.50**	**-1.54**	**-2.13**
East Siberian Sea	Latent	-2.42	-2.35	-2.64
	Sensible	-2.98	-2.93	-3.29
	Net	**-5.40**	**-5.28**	**-5.93**

Table 9. Total Heat Content in the Western Arctic Regions

Region / Heat Flux (TW)		Zero Flow	Control Run	2X Flow Run
Chukchi Sea	Radiative	12.30	11.90	11.88
	OHT	-0.27	5.58	13.92
	Turbulent	-6.77	-12.04	-19.13
	Net	**5.26**	**5.44**	**6.67**
Beaufort Sea	Radiative	3.17	3.20	3.22
	OHT	1.23	-0.43	0.29
	Turbulent	-1.50	-1.54	-2.13
	Net	**2.90**	**1.24**	**1.38**
East Siberian Sea	Radiative	14.57	14.34	14.78
	OHT	-0.37	-0.18	-0.25
	Turbulent	-5.40	-5.28	-5.93
	Net	**8.80**	**8.88**	**9.11**
Western Arctic (all three seas)	**Total Net**	**16.96**	**15.56**	**17.16**

11. Results Summary

In summary, Chapter III showcases the results derived from the application of RASM to explore the interactions between Bering Strait flow variability and sea ice dynamics and thermodynamics. By illuminating the modeled variations in Bering Strait flow and their effects on sea ice, this chapter forms a critical bridge between the methodology and the subsequent discussion in Chapter IV, which further elaborates on the results, implications, and broader significance of the findings from Chapter III.

IV. DISCUSSION

The findings of this study illuminate the relationship between Bering Strait flow magnitudes, sea ice, and ocean properties in the Arctic, with particular attention focused on the Chukchi, Beaufort, and East Siberian seas. As anticipated, the Bering Strait emerges as a pivotal gateway in shaping the Arctic environment, though our findings reveal nuanced dynamics that diverge from initial expectations.

A. WESTERN ARCTIC EFFECTS

1. Sea Ice Extent

Initial assumptions regarding the Bering Strait flow's direct and pronounced influence on sea ice extent are partially confirmed. Variations in Bering Strait throughflow impact sea ice conditions, but the degree of this influence appears to be more moderate than initially hypothesized. The sea ice extent appears to be most affected by Bering Strait flow variations in the Chukchi Sea, most notably in the 1980s. This effect is likely due to heavier ice cover in the Chukchi Sea during that decade.

This analysis demonstrates that differing Bering Strait flow magnitudes contribute to sea ice extent variability, particularly during periods of increased flow, which can lead to an increase in the transport of warmer Pacific waters into the Arctic Ocean. However, this impact does not manifest as significantly as initially postulated. The complex interplay of numerous factors influencing sea ice extent, including atmospheric circulation, temperature gradients, and ice-albedo feedback, underscores the intricacies of the Arctic climate system.

2. Ocean Heat Convergence

One of the most significant revelations of this study pertains to the role of ocean heat transport and temperatures in ice-melt processes. Examining ocean properties indicates that ocean heat convergence, particularly within the upper ocean layers, would appear to exert a less substantial influence than previously recognized. The observed increase in heat convergence in the upper ocean layers is closely aligned with the

enhanced inflow of warmer waters from the Pacific Ocean through the Bering Strait. This warming effect, coupled with prolonged exposure to solar radiation during the ice-free summer months, should accelerate the melt of Arctic sea ice, particularly in the Chukchi Sea. However, this does not seem to be the case.

3. Ice Melt

Before analyzing long-term ice trends, it is useful to compare bottom and top ice melt terms to provide a more encompassing picture of what was happening below and above the ocean surface. The ice bottom melt monthly mean time series (Figure 33) shows secondary peaks occurring between major ones for the Control Run and 2X Flow cases, indicating secondary periods of ice melt. The bottom melt mean annual cycle (Figure 34) shows an increase in bottom melt reaching a minimum in October and then rising until December. This indicates the increased levels of ocean heat being transported through the Bering Strait (and the solar warming that occurs on the shelf) have lingering effects on sea ice bottom melt, resulting in later onset ice growth.

Top ice melt does not have these same seasonal spikes, but the No Flow case has the largest annual and monthly mean values for all three cases in the entire western Arctic.

Interestingly, long-term mean ice melt and ice growth terms show the Zero Flow case has the largest values for all ice terms of all RASM runs in the Chukchi Sea and the largest net melting for the entire western Arctic Ocean. Recall that the No Flow case also had the largest long-term mean values for sea ice extent in the Chukchi Sea, listed in Table 2. This indicates that the No Flow case has the most amount of ice melt, ice growth, and sea ice extent of all three RASM runs in the Chukchi Sea. If this is true, then it points to the fact that the larger quantities of heat being transported through the Bering Strait in the Control Run and 2X Flow cases are being utilized for something other than ice melt.

4. Heat Fluxes

Up to this point, it has been shown that variations in Bering Strait flow magnitudes do not cause widely differing values of pan-Arctic and western Arctic sea ice extent, and ice melting terms seem to favor the RASM case with the least amount of oceanic heat convergence. It was then investigated whether RASM had produced similar Bering Strait heat fluxes among the runs, which could explain why sea ice extent values did not greatly diverge. Instead, it was found the 2X Flow case transported warm Pacific Waters through the Bering Strait with a heat flux value nearly three times that of the Control Run (Table 3). If the heat flux through the Bering Strait varied so greatly among the RASM cases, why were the sea ice extent and melting terms so similar?

The suspected reason for the lack of differentiation was the turbulent heat flux, so it was necessary to examine all the incoming, outgoing, and advective heat sources for the western Arctic regions. Longwave and shortwave radiation, ocean heat convergence, and turbulent heat flux were calculated and combined to find the net amount of heat remaining in the Chukchi, Beaufort, and East Siberian seas.

a. Radiation

Longwave and shortwave radiation values were obtained using RASM Coupler data and integrated over the RASM regions defined in Figures 2 and 3. The values for shortwave and longwave radiation are listed in Tables 6 and 7. When viewing the total radiative heat (longwave plus shortwave), the values for all three cases in all three regions are similar. This would make sense as the atmospheric component for each case should be roughly the same. Upon closer inspection, however, we find the longwave heat magnitude increases as the Bering Strait throughflow increases. As longwave heat increases, the shortwave heat value rises as well, bringing the net atmospheric heat to near identical values among the three runs. This would imply that as more longwave radiative heat departs from the Chukchi or Beaufort seas, the incoming short-rave radiative heat counteracts the loss by increasing in magnitude. This could be from more ocean-to-atmosphere exposure from ice melting, but it is not readily apparent from the numbers alone.

b. Ocean Heat Convergence

To compute ocean heat convergence, the directional volumetric flow was computed between the gates that were set up for each region (Figure 20). Then the volumetric flow values and directions were used to find the corresponding incoming and outgoing heat values passing through each of the gates (Table 3). These represent the advective heat terms for each region. Unsurprisingly, the Chukchi Sea has the largest amount of variation among the three cases.

c. Turbulent Heat

To examine the turbulent heat, we extracted ocean-to-atmosphere latent and sensible heat flux terms from RASM Coupler data. These fluxes were then converted into watts by multiplying the values with the area of their respective region (i.e., Chukchi, Beaufort, and East Siberian seas), which are listed in Tables 4 and 5. The latent and sensible heat fluxes are all negative, corresponding to a release of heat from the ocean to the atmosphere.

The turbulent heat flux explains why the 2X Flow case did not have a significantly higher sea ice retreat in the western Arctic compared to the other RASM runs.

d. Net Heat Content

Finally, all the heat flux values were combined within the western Arctic to see the total oceanic heat remaining within each sea. These values are shown in Table 9. As flow and heat flux increase through the Bering Strait, the amount of heat released to the atmosphere within the Chukchi Sea increases as well. The Beaufort Sea does not follow this pattern, but it is worth noting that the Zero Flow case has almost double the amount of heat in the Beaufort Sea compared to the Control Run and 2X Flow cases. Turbulent heat values for the East Siberian Sea in all three cases were within 10 percent of each other.

Comparing these values with the images of ice thickness in the western Arctic provides a reasonable explanation for the absence of significant differentiation in sea ice

extent among the three RASM runs, as both the western Arctic sea ice extent and the net heat remaining values for all three RASM runs are within 10 percent of each other. What is unclear, however, is how the remaining heat was utilized in the western Arctic since temperature increase, ice-melt, and ocean heat transport co-occurred throughout the RASM 39-year run. The excess heat was likely used in multiple types of processes, but the specific proportions of the various mechanisms were not investigated in this thesis.

B. PAN-ARCTIC EFFECTS

While the effects of various Bering Strait flow magnitudes are more easily distinguishable in the western Arctic region, they are less noticeable when viewed from the pan-Arctic perspective. The sea ice extent and volume time series (Figures 9 and 12) show very little difference among the three RASM cases. This is also the case with overall pan-Arctic ice thickness, surface heat flux, and the strength of the Beaufort Gyre. However, two properties underwent some unique changes: the freshwater content (FWC) of the Beaufort Gyre and the sea ice extent in the eastern Arctic Ocean.

For FWC, the Zero Flow case has the least freshwater in the Beaufort Gyre and the most freshwater content on the Chukchi shelf. This is due to the closed Bering Strait, which allows for the freshwater to remain on the shelf due to the altered circulation pattern (Figure 14). The 2X Flow and Control Runs have the more typical circulation pattern that allows freshwater to move off the shelf and into the Beaufort Gyre. The FWC is more prominent in the 2X Flow case due to the increase in relatively fresher water from the Bering Sea being transported through the Bering Strait and later into the Beaufort Sea. The Beaufort Gyre has been predominantly positive (anti-cyclonic rotation) for roughly the past 15 years (Proshutinsky et al. 2019), consistently increasing the FWC volume within the gyre. RASM was able to accurately model this, though the Bering Strait flow appeared to have little to no effect on the Beaufort Gyre's direction of rotation.

The outcomes of this research accentuate the importance of acknowledging the intricate climate feedback mechanisms within the Arctic. It is evident that changes in the Arctic environment are not isolated events but are part of a dynamic system influenced by

multiple interacting components. The interplay between Bering Strait flow, sea ice extent, ocean temperatures, and atmospheric conditions requires comprehensive climate modeling.

This investigation of Bering Strait flow variability and its impacts on sea ice extent and ocean properties underscores the complexities inherent in the Arctic environment. Although a local impact is seen in the sea ice of the Chukchi Sea, the influence of the Bering Strait flow does not have a strong impact on the pan-Arctic sea ice. Instead of having a strong impact on melting sea ice in the western Arctic, much of the oceanic heat moving northward via Bering Strait is released to the atmosphere as it crosses the broad, shallow shelf of the Chukchi Sea. These findings agree with a study conducted by Aylmer et al. (2022) that used CMIP6 model outputs to investigate the impact of ocean heat transport on sea ice. Though their focus was on the eastern Arctic, they found that increased oceanic heat transport from the Atlantic produced greater ocean convergence along the Atlantic sea ice edge. These strong localized heat fluxes drove atmospheric moist-static energy convergence, which resulted in a reduction of sea ice thickness (Aylmer et al. 2022). Our findings produced similar results for the western Arctic Ocean, showing that an increase in ocean heat transport near the sea ice edges produces an increase in atmospheric heat flux.

V. CONCLUSION

The Arctic, a region of breathtaking beauty and significance, stands at the forefront of climate change research due to its susceptibility to environmental shifts and capacity to influence global climate dynamics. This thesis has delved into the intricate web of relationships within the Arctic environment, explicitly focusing on Bering Strait flow variability and its consequences on sea ice extent and ocean heat transport. Through thoroughly examining the Bering Strait as a pivotal gateway connecting the Pacific and Arctic Oceans, a nuanced narrative of its effect on the Arctic has been unveiled.

A. BERING STRAIT FLOW MAGNITUDE AND ITS IMPACT

Increasing the Bering Strait flow contributed to an increase in the transport of warmer Pacific waters into the Arctic Ocean. The increase in the oceanic heat transport through Bering Strait was greater (by a factor of 3) than the increase imposed on the volume transport (a factor of 2). This investigation has shown that Bering Strait flow significantly influences the Arctic, particularly the Chukchi, Beaufort, and East Siberian seas. While the immediate effects on sea ice extent do not manifest at the levels initially postulated, the 2X flow case shows the greatest difference in the Chukchi and Beaufort seas, with delayed sea ice freeze-up and accelerated melt, with the strongest impacts occurring in the 1980s. This nuanced influence on sea ice extent called for a comprehensive approach to understanding the factors shaping the Arctic climate system.

B. OCEAN HEAT TRANSPORT

Of paramount importance in this research is the revelation of the pivotal role of ocean heat transport in the Arctic climate system. Transporting warmer waters from the Pacific Ocean to the Arctic through the Bering Strait introduces a significant heat source, which is increasing according to observations (Woodgate and Peralta-Ferriz 2021). Although not investigated here, this warming effect has the potential to impact atmospheric circulation and ecosystem dynamics. Furthermore, these findings point to the influence of the Bering Strait flow on releasing heat into the atmosphere as a significant contributor to the Arctic's total heat budget.

C. IMPLICATIONS AND IMPACTS

The implications of our findings stretch far beyond the boundaries of scientific inquiry. The Arctic, often considered a sentinel of global climate change, is transforming rapidly. The consequences of these changes ripple across the planet, influencing weather patterns, sea level rise, and global climate dynamics (Berner et al. 2005). The subtle interplay of Bering Strait flow variability and ocean heat transport underscores the need for comprehensive regional and global climate models and an integrated approach to understanding climate feedback loops.

While the study contributes valuable insights, there remain avenues for further exploration that build upon the foundation laid by this study. Potential areas of investigation could include an enhanced understanding of specific feedback mechanisms, a more detailed exploration of ecosystem responses, and incorporating socio-economic factors into modeling approaches.

As this thesis concludes, I cannot overemphasize the urgency of informed decision-making and proactive measures to address the challenges posed by the evolving Arctic environment. Indigenous communities are already struggling to deal with coastal erosion, an issue that will only accelerate as Bering Strait flow temperature and velocity continue to increase (Nielsen et al. 2022). Fragile Arctic ecosystems and global climate patterns are intricately tied to the fate of the Arctic, and we must acknowledge the importance of the Bering Strait as a focal point of change within this environment to move toward sustainable resource management, climate adaptation, and conservation efforts.

In a world where the Arctic is both an indicator of climate change and an amplifier of its effects, this thesis underscores the importance of continued research and collaboration to safeguard the Arctic's delicate balance. It is a call to action, a recognition of the need for informed policies, and a commitment to understanding the Arctic's evolving role in the broader context of our changing planet. As we venture into a future of climate uncertainty, the Arctic beckons as a sentinel and a source of invaluable knowledge deserving of our continued exploration and conservation.

LIST OF REFERENCES

Aagaard, K., and L. K. Coachman, 1975: Toward an ice-free Arctic Ocean. *EoS Transactions*, **56**, 484–486, https://doi.org/10.1029/EO056i007p00484.

Aylmer, J., D. Ferreira, and D. Feltham, 2022: Different mechanisms of Arctic and Antarctic sea ice response to ocean heat transport. *Clim. Dyn.*, **59**, 315–329, https://doi.org/10.1007/s00382-021-06131-x.

Berner, J., C. Symon, L. Arris, O. W. Heal, Arctic Climate Impact Assessment, National Science Foundation (U.S.), and United States, eds., 2005: *Arctic Climate Impact Assessment*. Cambridge University Press, 1042 pp.

Blackport, R., and J. A. Screen, 2020: Insignificant effect of Arctic amplification on the amplitude of midlatitude atmospheric waves. *Sci. Adv.*, **6**, eaay2880, https://doi.org/10.1126/sciadv.aay2880.

Cassano, J. J., and Coauthors, 2017: Development of the Regional Arctic System Model (RASM): Near-surface atmospheric climate sensitivity. *J. Climate*, **30**, 5729–5753, https://doi.org/10.1175/JCLI-D-15-0775.1.

Clement Kinney, J., and Coauthors, 2014: On the flow through Bering Strait: A synthesis of model results and observations. *The Pacific Arctic Region*, J.M. Grebmeier and W. Maslowski, Eds., Springer Netherlands, 167–198.

Clement Kinney, J., W. Maslowski, R. Osinski, M. Jin, M. Frants, N. Jeffery, and Y. J. Lee, 2020: Hidden Production: On the Importance of Pelagic Phytoplankton Blooms Beneath Arctic Sea Ice. *JGR Oceans*, **125**, e2020JC016211, https://doi.org/10.1029/2020JC016211.

Craig, A. P., M. Vertenstein, and R. Jacob, 2012: A New Flexible Coupler for Earth System Modeling Developed for CCSM4 and CESM1. *The International Journal of High Performance Computing Applications*, **26**, 31–42, https://doi.org/10.1177/1094342011428141.

Grebmeier, J. M., 2012: Shifting Patterns of Life in the Pacific Arctic and Sub-Arctic Seas. *Annu. Rev. Mar. Sci.*, **4**, 63–78, https://doi.org/10.1146/annurev-marine-120710-100926.

Hamman, J., B. Nijssen, A. Roberts, A. Craig, W. Maslowski, and R. Osinski, 2017: The coastal streamflow flux in the Regional Arctic System Model. *JGR Oceans*, **122**, 1683–1701, https://doi.org/10.1002/2016JC012323.

Hamman, J. J., B. Nijssen, T. J. Bohn, D. R. Gergel, and Y. Mao, 2018: The Variable Infiltration Capacity Model Version 5 (VIC-5): Infrastructure improvements for

new applications and reproducibility. *Geosci. Model Dev.*, **11**, 3481–3496, https://doi.org/10.5194/gmd-11-3481-2018.

Hayden, E. E., and L. W. O'Neill, 2023: Processes contributing to Bering Sea temperature variability in the late 20th and early 21st century. *J. Climate*, https://doi.org/10.1175/JCLI-D-23-0331.1.

Jakobsson, M., and Coauthors, 2020: The International Bathymetric Chart of the Arctic Ocean Version 4.0. *Sci. Data*, **7**, 176, https://doi.org/10.1038/s41597-020-0520-9.

Kwok, R., and D. A. Rothrock, 2009: Decline in Arctic Sea Ice thickness from submarine and ICESat records: 1958–2008: Arctic sea ice thickness. *Geophys. Res. Lett.*, **36**, https://doi.org/10.1029/2009GL039035.

Lindsay, R. W., and J. Zhang, 2005: The thinning of Arctic sea ice, 1988–2003: Have we passed a tipping point? *J. Climate*, **18**, 4879–4894, https://doi.org/10.1175/JCLI3587.1.

Maslowski, W., D. Marble, W. Walczowski, U. Schauer, J. L. Clement, and A. J. Semtner, 2004: On Climatological Mass, Heat, and Salt Transports Through the Barents Sea and Fram Strait from a Pan-Arctic Coupled Ice-Ocean Model Simulation. *J. Geophys. Res.*, **109**, 2001JC001039, https://doi.org/10.1029/2001JC001039.

Nielsen, D. M., P. Pieper, A. Barkhordarian, P. Overduin, T. Ilyina, V. Brovkin, J. Baehr, and M. Dobrynin, 2022: Increase in Arctic Coastal Erosion and its Sensitivity to Warming in the Twenty-First Century. *Nat. Clim. Chang.*, **12**, 263–270, https://doi.org/10.1038/s41558-022-01281-0.

Notz, D., and S. Community, 2020: Arctic Sea Ice in CMIP6. *Geophys. Res. Lett.*, **47**, e2019GL086749, https://doi.org/10.1029/2019GL086749.

Proshutinsky, A., and Coauthors, 2019: Analysis of the Beaufort Gyre freshwater content in 2003–2018. *JGR Oceans*, **124**, 9658–9689, https://doi.org/10.1029/2019JC015281.

Schweiger, A., R. Lindsay, J. Zhang, M. Steele, H. Stern, and R. Kwok, 2011: Uncertainty in modeled Arctic sea ice volume. *J. Geophys. Res.*, **116**, C00D06, https://doi.org/10.1029/2011JC007084.

Serreze, M. C., A. P. Barrett, A. G. Slater, M. Steele, J. Zhang, and K. E. Trenberth, 2007: The large-scale energy budget of the Arctic. *J. Geophys. Res.*, **112**, 2006JD008230, https://doi.org/10.1029/2006JD008230.

Wang, M., and J. E. Overland, 2012: A sea ice free summer Arctic within 30 years: An update from CMIP5 models: summer Arctic sea ice. *Geophys. Res. Lett.*, **39**, https://doi.org/10.1029/2012GL052868.

Woodgate, R. A., 2018: Increases in the Pacific inflow to the Arctic from 1990 to 2015, and insights into seasonal trends and driving mechanisms from year-round Bering Strait mooring data. *Prog. Oceanogr.*, **160**, 124–154, https://doi.org/10.1016/j.pocean.2017.12.007.

Woodgate, R. A., K. Aagaard, and T. J. Weingartner, 2005: Monthly temperature, salinity, and transport variability of the Bering Strait through flow: Bering Strait through flow. *Geophys. Res. Lett.*, **32**, L04601, https://doi.org/10.1029/2004GL021880.

Woodgate, R. A., and C. Peralta-Ferriz, 2021: Warming and freshening of the Pacific inflow to the Arctic from 1990–2019 implying dramatic shoaling in Pacific Winter Water ventilation of the Arctic water column. *Geophys. Res. Lett.*, **48**, e2021GL092528, https://doi.org/10.1029/2021GL092528.

Woodgate, R. A., T. J. Weingartner, and R. Lindsay, 2012: Observed increases in Bering Strait oceanic fluxes from the Pacific to the Arctic from 2001 to 2011 and their impacts on the Arctic Ocean water column. *Geophys. Res. Lett.*, **39**, 2012GL054092, https://doi.org/10.1029/2012GL054092.

Zhang, J., and D. A. Rothrock, 2003: Modeling global sea ice with a thickness and enthalpy distribution model in generalized curvilinear coordinates. *Mon. Wea. Rev.*, **131**, 845–861, https://doi.org/10.1175/1520-0493(2003)131<0845:MGSIWA>2.0.CO;2.

THIS PAGE INTENTIONALLY LEFT BLANK

INITIAL DISTRIBUTION LIST

1. Defense Technical Information Center
   Fort Belvoir, Virginia

2. Dudley Knox Library
   Naval Postgraduate School
   Monterey, California